



GPO PRICE \$ _____

CSFTI PRICE(S) \$ _____

Hard copy (HC) 3.00

Microfiche (MF) .65

ff 653 July 65

N 68-29983

(ACCESSION NUMBER)

(THRU)

132

1

(PAGES)

(CODE)

CR-72426

33

(NASA CR OR TMX OR AD NUMBER)

(CATEGORY)

FACILITY FORM 602

Nonlinear Aspects of Combustion Instability in Liquid Propellant Rocket Motors

by

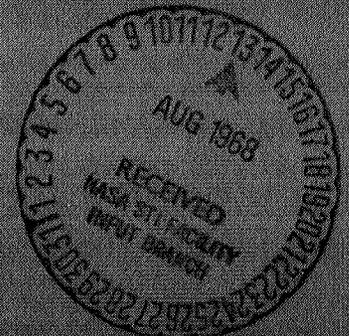
L. Crocco, D.T. Harrje, W.A. Sirignano
F.V. Bracco, J.B. Elgin, R.M. Lloyd, P.K. Tang
T.S. Tonon, A.K. Varma, J.S. Wood and G.F. Zaic

prepared for

NATIONAL AERONAUTICS AND SPACE ADMINISTRATION
Contract NASr 217

June 1968

Department of Aerospace
and Mechanical Sciences
PRINCETON UNIVERSITY



NOTICE

This report was prepared as an account of Government sponsored work. Neither the United States, nor the National Aeronautics and Space Administration (NASA), nor any person acting on behalf of NASA:

- A.) Makes any warranty or representation, expressed or implied, with respect to the accuracy, completeness, or usefulness of the information contained in this report, or that the use of any information, apparatus, method, or process disclosed in this report may not infringe privately owned rights; or
- B.) Assumes any liabilities with respect to the use of, or for damages resulting from the use of any information, apparatus, method or process disclosed in this report.

As used above, "person acting on behalf of NASA" includes any employee or contractor of NASA, or employee of such contractor, to the extent that such employee or contractor of NASA, or employee of such contractor prepares, disseminates, or provides access to, any information pursuant to his employment or contract with NASA, or his employment with such contractor.

Requests for copies of this report should be referred to

National Aeronautics and Space Administration
Office of Scientific and Technical Information
Attention: AFSS-A
Washington, D. C. 20546

STATUS REPORT
(Eighth Yearly Report for the Period
1 June 1967 to 31 May 1968)

NONLINEAR ASPECTS OF COMBUSTION INSTABILITY
IN LIQUID PROPELLANT ROCKET MOTORS

by

L. Crocco, D.T. Harrje, W.A. Sirignano
F.V. Bracco, J.B. Elgin, R.M. Lloyd, P.K. Tang
T.S. Tonon, A.K. Varma, J.S. Wood and G.F. Zaic

prepared for

NATIONAL AERONAUTICS AND SPACE ADMINISTRATION

June 1968

CONTRACT NASr-217

Technical Management
NASA Lewis Research Center
Cleveland, Ohio
Chemistry and Energy Conversion Division
Marcus F. Heidmann

Guggenheim Laboratories for the Aerospace Propulsion Sciences
Department of Aerospace and Mechanical Sciences
PRINCETON UNIVERSITY
Princeton, New Jersey

TABLE OF CONTENTS

	Page
TITLE PAGE	1
TABLE OF CONTENTS	2
I. <u>SUMMARY</u>	3
II. <u>INTRODUCTION</u>	5
III. <u>DAMPING DEVICES</u>	
A. Theoretical Studies of Acoustic Liners	8
B. Liner Acoustic Admittance	32
C. Placement of Damping Devices	42
D. Damping of Shock-Type Waves	45
IV. <u>ENERGY SOURCES</u>	
A. Use of Shock Waves to Study Combustion Parameters	59
B. Chemical Kinetics as a Driving Mechanism for Liquid Propellant Rocket Combustion Instability	75
V. <u>EXTENSIONS TO THE THEORY</u>	
A. Theory of Nonlinear Transverse Instability	92
B. New Expansion Technique for the Case $v' \ll \bar{u} - \bar{u}_e$	107
REFERENCES	125
DISTRIBUTION LIST	

I. SUMMARY

The analysis of the acoustic liner which was presented in the Sixth Yearly Report has been extended to higher order and the effect of chamber flow is considered. The analysis is divided into two parts: one for a near-resonant situation and another away-from resonance. The second-order analysis of the latter part is presented in detail in this report (Section III-A). Also a short discussion of the approach used in the analysis of the near-resonant case is presented. The chamber flow, including both the mean flow and oscillatory flow is shown to modify the equations which determine the cavity pressure and orifice velocity oscillations. Calculations are presently being performed so that the precise effect of the chamber flow as well as the cavity orifice geometry will be determined.

Based on a numerical approach, the acoustic admittance has been calculated for a number of liner design conditions in an attempt to find possible simplifications in the representation of the flow field by this means (Section III-B). The merits of this approach, as well as the problems involved, are discussed.

A series of tests performed in a rocket chamber environment to determine the optimum circumferential placement of acoustic dampers is described in Section III-C. Because this hot environment proved unacceptable as a test bed, a cold flow approach is now being pursued and is proving quite fruitful.

In another cold flow simulation study of liner behavior, shock-type waves are being generated and damped (Section III-D). This study is providing insight to not only the damping efficiency with regard to non-linear waves; but, via use of shadow photography, is providing a visual history of the events that take place in the cavity e.g., the jet-like flow, vortices and turbulent phenomena.

In the energy source study of steady and unsteady combustion based upon the use of a shock wave passing through the combustion zone, two sets of equations have been generated for the steady-state (Section IV-A). Although complete experimental data have not been collected,

preliminary experimental data falls in the expected calculated range. Further experimental results are currently being obtained to allow a complete solution of the steady-state problem. The unsteady problem now is receiving increased attention.

In another area dealing with energy sources, the effect of tangential spin direction is being investigated as a chemical kinetic effect (Section IV-B). LOX/liquid methane testing is described which yields interesting extensions to the previous LOX/ALC and LOX/RP-1 data. Reaction rate data from associated experiments (gas rocket and kinetic flow reactor) are also discussed in relation to this problem.

Several analyses of nonlinear transverse oscillations with shock waves in annular chambers have been performed. The Priem-Heidmann vaporization model provides the combustion rate-controlling mechanism in the theoretical model. Droplet drag is neglected. An important ratio is that of the transverse velocity perturbation to the relative steady-state axial velocity between droplet and gas. In a paper to be presented at the Twelfth International Combustion Symposium by Professor Crocco, it has been shown that for small absolute values of this ratio, instability can only be possible when triggered by finite amplitude disturbances. However, no time-lag effect occurs due to the particular order-of-magnitude analysis which has been employed. In Section V-B, progress on another perturbation scheme which retains the time-lag effect to the order of interest is presented.

Also considered in Section V-A is the case when the transverse velocity perturbation is large compared to the steady-state relative velocity. Here, it is shown that all oscillations decay with time. However, the analysis becomes invalid when the velocity ratio is of order unity. The small velocity ratio and large velocity ratio results combine to indicate that a stable periodic solution can exist when the velocity ratio is of order unity.

II. INTRODUCTION

This is the Eighth Yearly Report on the research at Princeton University on the problem of combustion instability in liquid propellant rocket motors. These investigations are being sponsored by the National Aeronautics and Space Administration under NASA Contract NASr-217 and, in the past, under NASA Grant NsG-99-60. The nonlinear aspects of the problem have been emphasized in both the theoretical and experimental portions of the program. Presently, the theoretical research is concentrating on studies of possible mechanisms of combustion instability such as droplet burning, the nonlinear gasdynamic oscillations associated with combustion instability involving shock-type waves in both the tangential and longitudinal modes, the effect of damping devices on stability with particular emphasis on nonlinear effects associated with acoustic liners, and fundamental studies of the basic energy sources. In connection with the theoretical program, an experimental program of equally broad range is being conducted. This program includes basic experiments with rocket motors and "cold" chambers which have been designed to study various phases of the combustion process and/or the instability phenomena to provide understanding which would prove useful in the construction of theoretical models. It also includes studies of the effects of exhaust nozzles and damping devices upon the instability as well as controlled testing of liquid rocket motors with parametric variations intended to determine the factors which strongly influence the incidence of nonlinear combustion instability.

In the theoretical study of mechanisms of combustion instability, the greatest difficulty involves the construction of the model or models which contain the essential physical aspects of the phenomena. In this respect the basic experiments are extremely useful. The theoretical study of the nonlinear gasdynamic oscillations presents another type of difficulty. Generally, mathematical techniques for the treatment of nonlinear partial differential equations are not well-developed and, in most cases, they are undeveloped. Therefore, the theoretician must develop techniques as he works with the physical problem.

As is the norm for any status report, a considerable amount of the material discussed herein is in the state of active investigation. Thus, only tentative conclusions or observations are sometimes possible. At least a mention of one example of each type of work being conducted has been made so that this report would prove to be of maximum benefit to those readers working in similar areas.

During the past year the following technical reports, papers and book have been published:

"Axial Mode Shockwave Combustion Instability in Liquid Propellant Rocket Engines", C. E. Mitchell, NASA CR-72259 (Princeton University AMS TR 798), July 1967.

"A Preliminary Study of the Effects of Vaporization and Transverse Oscillations of Jet Breakup", J. A. Newman, NASA CR-72258 (Princeton University AMS TR 785), July 1967.

"Nonlinear Wave Phenomena in Liquid Rocket Combustion Chambers", L. Crocco, C. E. Mitchell and W. A. Sirignano, presented at the Colloquia on Gas Dynamics of Explosions, Brussels, Belgium, September 1967.

"Behavior of Supercritical Nozzles Under Three-Dimensional Oscillatory Conditions", L. Crocco and W. A. Sirignano, AGARDograph 117, 1967.

"Flow Behavior With Acoustic Liners", D. T. Harrje, W. A. Stinger and W. A. Sirignano, ICRPG 4th Combustion Conference, CPIA Publication No. 162, December 1967, pg 103.

"Nonlinear Transversal Instability with a Simplified Droplet Evaporization Model", L. Crocco, Ibid, pg. 159.

"Axial and Transversal Instability Using the n, γ Model", C. E. Mitchell, L. Crocco, Ibid, pg. 169.

"Simulation of Droplet Vaporization and Jet Breakup in a Tangential Mode Environment", J. A. Newman, G. L. Waring and D. T. Harrje, Ibid, pg. 249.

"Mixture Ratio Survey Technique Based on Propellant Temperature Differences", G. R. Black and D. T. Harrje, Ibid, pg. 281.

"Experimental Investigations of Liquid Propellant Combustion Processes Using Streak Photography", R. M. Williams, Jr., NASA CR-72371 (Princeton University AMS TR 800), February 1968.

In addition, two papers relating to this research will be presented at the 12th International Symposium on Combustion at Poitiers, France, July 15-19, 1968.

"Research in Combustion Instability in Liquid Propellant Rocket Motors", L. Crocco.

"A Theory of Axial-Mode Shock Wave Oscillations in a Solid Rocket Combustor", W. A. Sirignano

Additional background and history of the research on combustion instability at Princeton University may be found in the partial list of References 1 - 12. In addition, Reference 13 represents the final report in an extensive series of reports on earlier work primarily concerned with the linear type of combustion instability (i.e., spontaneous buildup from steady-state operation).

It should be acknowledged that this work made use of computer facilities supported in part by National Science Foundation Grant NSF-GP579.

III. DAMPING DEVICES

A. THEORETICAL STUDIES OF ACOUSTIC LINERS

In this section, an analytical study of the flow field associated with an acoustic liner is presented. This particular theoretical approach had been initiated by Sirignano, whose work can be found in this group's Sixth Yearly Report.² The model used in the study presented here is much the same as the one developed by Sirignano. The basic assumptions used in the previous work are made use of here except that the assumption of no flow in the combustion chamber is now relaxed, viscous effects are omitted, and the effects of all harmonics in the chamber pressure are now considered. The assumed representation of the chamber conditions is done in such a way so as to represent any combustion instability type commonly experienced in liquid propellant rocket thrust chambers. In considering a chamber flow within this model, a clearer insight can be gained as to its effects on dissipation than that gained by the current empirical approach. A computer program has been developed to perform calculations in an attempt to correlate the theoretical predictions with experimental studies; however, the results of these calculations are inconclusive at this time and will not be presented here.

Model

Aside from the detailed justifications which could be found in the work by Sirignano, the basic description of the assumed flow field is as follows.

Each orifice (hole) in the liner is considered separately along with its own individual backing volume. The system then geometrically constitutes a Helmholtz resonator. The low amplitude regime of potential flow is neglected so that there will exist a jet on the side(s) of the orifice in which flow is away from the orifice. No mean flow exists in the orifice, but both a mean flow and perturbed flow exist within the combustion chamber. For flow into the orifice, the flow just outside the orifice is considered to be quasi-steady. On the chamber side, when

the flow is away from the orifice, the pressure that the jet experiences will be some average pressure (defined in terms of a pressure coefficient) which is not necessarily the chamber static or stagnation values because of the presence of flow within the chamber passing over this jet. When the flow is into the resonator cavity (backing volume), it is assumed that the pressure across the jet at exit is equal to the static pressure within the cavity. Within the orifice itself, it is assumed that the flow is one-dimensional, isentropic, and unchoked.

With this assumed model, the mechanisms for dissipation will be the following:

- 1) the jet breakup produced on both sides of the orifice
- 2) the eddies produced in the chamber flow due to the interaction of the chamber flow with the jet.

The kinetic energy lost in the jet can be calculated directly from the analytical results. The interaction between the jet on the chamber side and the chamber flow produces a more difficult problem and a solution has not yet been attempted in connection with this work. It would be expected, however, that the second mechanism is not as important as the first since it occurs only during half of the cycle and since the jet velocities usually are higher than the chamber velocities.

Formulation

The mathematical formulation of the above model is now presented. The nomenclature used is defined in the table found at the end of this section. All quantities are non-dimensionalized with respect to the mean chamber state properties, the mean chamber speed of sound, and the orifice length. The problem will be first cast into a form convenient for the calculation of orifice velocity and orifice density.

The governing equations for the orifice flow are the continuity and momentum equations with the isentropic relation replacing the energy equation. Thus, the following two equations describe the flow within the orifice

$$\rho_t + (\rho u)_x = 0 \quad (1)$$

$$u_t + u u_x + \rho^{\gamma-2} \rho_x = 0 \quad (2)$$

For flow into the orifice on the chamber side,

$$P_0 = \frac{P_I}{(1 - W_I^2)^{\frac{\gamma}{\gamma-1}}} = \frac{P_I}{(1 - W_I^2)^{\frac{\gamma}{\gamma-1}}}$$

where

$$W_I^2 = \frac{U_I^2}{2 C_p T_0} = \left[\frac{\frac{\gamma-1}{2} U_I^2 / P_I^{\frac{\gamma-1}{\gamma}}}{1 + \left(\frac{\gamma-1}{2}\right) U_I^2 / P_I^{\frac{\gamma-1}{\gamma}}} \right]$$

$$W_I^2 = \frac{u_I^2}{2 C_p T_0} = \left[\frac{\frac{\gamma-1}{2} u_I^2 / P_I^{\frac{\gamma-1}{\gamma}}}{1 + \left(\frac{\gamma-1}{2}\right) U_I^2 / P_I^{\frac{\gamma-1}{\gamma}}} \right]$$

Now from the isentropic relation

$$\rho_1 = P_I^{\frac{1}{\gamma}}$$

so that the above could be written

$$\rho_1 = P_I^{\frac{1}{\gamma}} \left[\frac{1 - W_I^2}{1 - W_I^2} \right]^{\frac{1}{\gamma-1}} \quad (3)$$

For the cavity side, when there is flow into the orifice

$$P_{II} = \frac{P_2}{(1 - W_2^2)^{\frac{\gamma}{\gamma-1}}}$$

where

$$W_2^2 = \frac{u_2^2}{2 C_p T_{II}} = \frac{\frac{\gamma-1}{2} u_2^2 / P_{II}^{\frac{\gamma-1}{\gamma}}}{1 + \left(\frac{\gamma-1}{2}\right) u_2^2 / P_{II}^{\frac{\gamma-1}{\gamma}}}$$

Since

$$\rho_2 = P_2^{\frac{1}{\gamma}}$$

there results

$$\rho_2 = P_{II}^{\frac{1}{\gamma}} (1 - W_2^2)^{\frac{1}{\gamma-1}} \quad (4)$$

For the cavity side when there is flow away from the orifice

$$P_2 = P_I$$

For flow away from the orifice on the chamber side, some average exit pressure must be used as mentioned before. This is done by making use of a pressure coefficient, defined as (in dimensional form)

$$C_{P,\theta} = (P_\theta - P_I) / \frac{1}{2} \rho_I U_I^2$$

where P_θ is the static pressure at a point on the surface of the jet. Since the surface of the jet will be ill-defined and the jet will be distorted, this pressure coefficient will not in general be the same as the familiar one obtained for a circular solid cylinder in cross flow. It is also true that this coefficient will vary with time due to the unsteady nature of the flow field; however, since its effect will be seen to be of second order, for a second order result; both a time averaged and circumferentially averaged coefficient can be used to obtain the average pressure. Thus

$$P_i = \frac{1}{2} \gamma \rho_I U_I^2 \bar{C}_P + P_I$$

Then for the chamber side with flow away from the orifice

$$\rho_i = \left[\frac{1}{2} \gamma \rho_I^{\frac{1}{2}} U_I^2 \bar{C}_P + P_I \right]^{\frac{1}{\gamma}} \quad (5)$$

Equations (1) and (2) contain two unknowns whereas the above conditions in the cavity side contain an additional unknown, P_I . The continuity equation written for the cavity is used to eliminate this additional variable. For the cavity then

$$\rho_2 u_2 = \frac{V}{A l} \frac{d(P_I)}{dt} \quad (6)$$

For flow from the orifice to the cavity, since

$$p_2 = p_2^{\frac{1}{\gamma}} = p_H^{\frac{1}{\gamma}} = p_H$$

the above becomes

$$\frac{d p_2}{d t} - \frac{A l}{V} p_2 u_2 = 0 \quad (7)$$

For flow from the cavity into the orifice, the isentropic relation (Eq. (4)) together with Eq. (6) yields

$$\begin{aligned} \frac{1}{\gamma-1} \left[p_2^{\gamma-1} + \frac{\gamma-1}{2} u_2^2 \right]^{\frac{\gamma}{\gamma-1}} \left[(\gamma-1) p_2^{\gamma-2} \frac{d p_2}{d t} + (\gamma-1) u_2 \frac{d u_2}{d t} \right] \\ - \frac{A l}{V} p_2 u_2 = 0 \end{aligned} \quad (8)$$

The formulation of this problem then consists of the two governing relations (1) and (2) together with the above boundary conditions which are summarized below

at $x = 0$

$$p_1 = p_1^{\frac{1}{\gamma}} \left[\frac{1 - W_1^2}{1 - W_2^2} \right]^{\frac{1}{\gamma-1}} \quad + \text{ flow}$$

$$p_1 = \left[\frac{1}{2} \gamma p_1^{\frac{1}{\gamma}} U_1^2 \bar{C}_p + p_1 \right]^{\frac{1}{\gamma}} \quad - \text{ flow}$$

at $x = 1$

$$\frac{d p_2}{d t} - \beta u_2 p_2 = 0 \quad + \text{ flow}$$

$$\begin{aligned} \frac{1}{\gamma-1} \left[p_2^{\gamma-1} + \frac{\gamma-1}{2} u_2^2 \right]^{\frac{\gamma}{\gamma-1}} \left[(\gamma-1) p_2^{\gamma-2} \frac{d p_2}{d t} + (\gamma-1) u_2 \frac{d u_2}{d t} \right] \\ - \beta p_2 u_2 = 0 \quad - \text{ flow} \end{aligned}$$

where

$$\beta = \frac{A l}{V}$$

The boundary conditions at $x = 0$ illustrate the effect of the presence of a chamber flow on the orifice velocity. This effect is one of a modification of chamber static pressure, but this is accomplished in a different manner for the different flow directions. For flow into

the orifice, this effect is clearly a nonlinear one arising because of the modification of the flow field in general. For flow into the chamber, the effect is similar to an aerodynamic one modifying the local static pressure at the jet exit.

Since the governing equations constitute a hyperbolic system, for the formulation to be well-posed mathematically, the boundary conditions must be open and specify both a value and a derivative at every point of the boundary (Cauchy conditions). The boundary conditions are open in the sense of the time variable and the Cauchy conditions are likewise achieved. This latter fact can be easily visualized by replacing u by ρ through the use of the two governing equations and by noting that the condition at $x = 0$ supplies a value for ρ , (the chamber conditions assumed known) and the condition at $x = 1$ supplies a value for the derivative of ρ_2 . The derivative of ρ_1 and the value for ρ_2 could then be found from the relation for ρ which must exist through the orifice.

The method of solution will be one of small perturbations pursuing the periodic solution. In seeking a solution, a distinction must be made between the near-resonance and off-resonance conditions. Both solutions have been obtained, and the off-resonance case is now presented in detail.

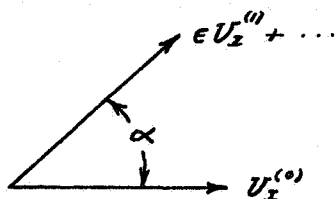
Off-Resonance Solution

The chamber static pressure and velocity are assumed to be given in the following form

$$P_I = 1 + \epsilon P_I^{(1)} + \epsilon^2 P_I^{(2)} + \dots$$
$$U_I = U_I^{(0)} + \epsilon a U_I^{(1)} + \epsilon^2 a^2 U_I^{(2)} + \dots$$

where all quantities are assumed known with the proper ordering as to ϵ , except for $U_I^{(0)}$; the mean flow, constant in time, which is assumed to be of perturbation magnitude. The quantities $P_I^{(i)}$ and $U_I^{(i)}$, $i > 0$ will be functions of time. The angle between the mean flow and the perturbed

flow is assumed known and is defined as



For the case of longitudinal instability $\alpha = 0^\circ$, and for the case of transverse instability $\alpha = 90^\circ$. From the boundary condition, note that the basic solution (solution for $\epsilon \rightarrow 0$) will depend on the manner in which the limiting form is achieved; that is, it depends upon the direction of the flow when $\epsilon \rightarrow 0$. This, of course, is an inconsistency which occurs due to the simplifying assumptions made as to the discontinuous nature of the jet. A jet is defined in terms of the direction, with no regard as to the magnitude of the orifice velocity. It will be explained shortly how this inconsistency is treated.

Substituting the above expansions into the W^2 functions yields formally:

$$W_I^2 = \mathfrak{z} + \epsilon F + \epsilon^2 S + \mathcal{O}(\epsilon^3)$$

where \mathfrak{z} , F , and S are various functions of $U_I^{(0)}$, $P_I^{(1)}$, and other similar terms. The above mentioned inconsistency can be treated so as to produce no mathematical difficulty by making use of the fact that $U_I^{(1)}$ is of perturbation magnitude and ordering with regard to this magnitude. When this is done here and in similar occurrences, the basic solution will formally reduce to the case in which the chamber static conditions prevail throughout the chamber, orifice, and cavity - for either flow direction. Thus, after neglecting small terms

$$W_I^2 = \epsilon^2 \left[\frac{1}{\epsilon^2} \frac{\gamma-1}{2} U_I^{(0)2} + \frac{1}{\epsilon} (\gamma-1) a U_I^{(0)} U_I^{(1)} \cos \alpha + \frac{\gamma-1}{2} a^2 U_I^{(1)2} \right] + \mathcal{O}(\epsilon^3)$$

so that, in effect, W_I^2 contributes only a second order term. One also obtains

$$W_I^2 = \epsilon^2 \left[\frac{\gamma-1}{2} U_I^{(1)2} \right] + \mathcal{O}(\epsilon^3)$$

The boundary conditions could now be expanded, and after neglecting small terms and equating like powers of ϵ , one obtains at $x = 0$

for + flow

$$\rho_1^{(0)} = 1 \quad (9)$$

$$\rho_1^{(1)} = \frac{1}{\gamma} P_I^{(1)} \quad (10)$$

$$\begin{aligned} \rho_1^{(2)} = & \frac{1}{\gamma} P_I^{(2)} - \frac{\gamma-1}{2\gamma^2} P_I^{(1)2} + \frac{1}{2} a^2 U_I^{(1)2} - \frac{1}{2} u_1^{(1)2} \\ & + \frac{1}{\epsilon} a U_I^{(0)} U_I^{(1)} \cos \alpha + \frac{1}{\epsilon^2} \frac{1}{2} U_I^{(0)2} \end{aligned} \quad (11)$$

for - flow

$$\rho_1^{(0)} = 1 \quad (12)$$

$$\rho_1^{(1)} = \frac{1}{\gamma} P_I^{(1)} \quad (13)$$

$$\begin{aligned} \rho_1^{(2)} = & \frac{1}{\gamma} P_I^{(2)} - \frac{\gamma-1}{2\gamma^2} P_I^{(1)2} + \frac{1}{2} \bar{c}_p a^2 U_I^{(1)2} \\ & + \frac{1}{\epsilon} \bar{c}_p a U_I^{(0)} U_I^{(1)} \cos \alpha + \frac{1}{\epsilon^2} \frac{1}{2} \bar{c}_p U_I^{(0)2} \end{aligned} \quad (14)$$

at $x = 1$

for + flow

$$\frac{d\rho_2^{(1)}}{dt} - \beta u_2^{(1)} = 0 \quad (15)$$

$$\frac{d\rho_2^{(2)}}{dt} - \beta \left[u_2^{(2)} + u_2^{(1)} \rho_2^{(1)} \right] = 0 \quad (16)$$

for - flow

$$\frac{d\rho_2^{(1)}}{dt} - \beta u_2^{(1)} = 0 \quad (17)$$

$$\frac{d\rho_2^{(2)}}{dt} - \beta \left[u_2^{(2)} + u_2^{(1)} \rho_2^{(1)} \right] + u_2^{(1)} \frac{du_2^{(1)}}{dt} = 0 \quad (18)$$

Note the occurrence of the term $\frac{1}{2} u^{(1)2}$ ($\frac{d}{dt} [\frac{1}{2} u^{(1)2}]$ for $x=1$) in the second order boundary conditions. This term embodies the second order "jet effect" captured by Sirignano. It is interesting to note how this term corresponds to a jet effect. The origin of the term itself is due to the nonlinear effect of inflow to the orifice, but its significance is enhanced because of the absence of the term upon outflow (jet). If the outflow were also quasi-steady, this term would appear again.

For the purposes of dissipation, the liner system is treated as a jet diffuser with a zero efficiency, that is, none of the kinetic energy of the jet is used in regaining stagnation pressure but is merely dissipated through viscous action. From this consideration, it is reasonable to postulate that the further the system is away from isentropic deceleration of the jet the better. Thus, when $\bar{C}_p = 1$, the exit pressure of the jet is the stagnation pressure in the chamber and this indicates a poor condition. This is illustrated by the second order boundary conditions at $x = 0$, for when $\bar{C}_p = 1$, the equations become the same except for the $u^{(1)2}$ term, and in this case, the action of the discontinuities in the equations for different flow directions as a forcing function is diminished. This interpretation is also conformable to the fact that the smaller the algebraic value of \bar{C}_p , the greater is the pressure difference across the orifice and thus the acceleration of the fluid. From the above reasoning, in practice it may be advantageous to shape the orifice cross sectional area so that the shape of the distorted jet enhances this aerodynamic effect.

The relation between ρ_2 and $\frac{P}{\rho}$ is desired, and upon expansion:

for + flow

$$\rho_2^{(1)} = \frac{1}{\gamma} P_{II}^{(1)} \quad (19)$$

$$\rho_2^{(2)} = \frac{1}{\gamma} \left[P_{II}^{(2)} - \frac{1}{2} \frac{\gamma-1}{\gamma} P_{II}^{(1)2} \right] \quad (20)$$

for - flow

$$\rho_2^{(1)} = \frac{1}{\gamma} P_{II}^{(1)} \quad (21)$$

$$\rho_2^{(2)} = \frac{1}{\gamma} \left[P_{II}^{(2)} - \frac{1}{2} \frac{\gamma-1}{\gamma} P_{II}^{(1)2} \right] - \frac{1}{2} u_2^{(1)2} \quad (22)$$

The expansions of the governing equations become

continuity

$$\rho_t^{(1)} + u_x^{(1)} = 0 \quad (23)$$

$$\rho_t^{(2)} + u_x^{(2)} + (\rho^{(1)} u^{(1)})_x = 0 \quad (24)$$

momentum

$$u_t^{(1)} + \rho_x^{(1)} = 0 \quad (25)$$

$$u_t^{(2)} + \rho_x^{(2)} + u^{(1)} u_x^{(1)} - (2-\gamma) \rho^{(1)} \rho_x^{(1)} = 0 \quad (26)$$

First order solution

Equations (23) and (25) yield the wave equation upon taking partial derivatives and equating mixed derivatives:

$$u_{xx}^{(1)} = u_{tt}^{(1)} \quad (27)$$

$$\rho_{xx}^{(1)} = \rho_{tt}^{(1)} \quad (28)$$

The most general harmonic solution periodic in time is of the form

$$J(x)e^{imt}$$

where $J(x)$ may be complex (solution at different stations may differ in phase), and m is related to the frequency of oscillation. Then, assuming

$$\begin{aligned} u^{(1)} &= [J_1(x) + iJ_2(x)]e^{imt} \\ \rho^{(1)} &= [H_1(x) + iH_2(x)]e^{imt} \end{aligned}$$

Equations (27) and (28) yield

$$\begin{aligned} J_1 &= Ae^{imx} + Be^{-imx} \\ J_2 &= Ce^{imx} + De^{-imx} \\ H_1 &= Ee^{imx} + Fe^{-imx} \\ H_2 &= Ge^{imx} + Ke^{-imx} \end{aligned}$$

Either Eq. (23) or (25) could be used to determine the relations between the arbitrary constants. Doing so yields

$$\begin{aligned} u^{(1)} &= [(Ae^{imx} + Be^{-imx}) + i(Ce^{imx} + De^{-imx})]e^{imt} \\ \rho^{(1)} &= [(-Ae^{imx} + Be^{-imx}) + i(-Ce^{imx} + De^{-imx})]e^{imt} \end{aligned}$$

Expanding and collecting real parts gives

$$u^{(1)} = [M \cos mx - S \sin mx] \cos mt + [-N \cos mx - R \sin mx] \sin mt \quad (29)$$

$$\rho'' = [-R \cos mx + N \sin mx] \cos mt + [S \cos mx + M \sin mx] \sin mt \quad (30)$$

Note that the first order boundary conditions are the same for both + and - flow. Assuming $P_2'' = \cos \omega t$ and using the boundary condition at $x = 0$ to evaluate Equation (30) gives

$$m = \omega, \quad R = -\frac{1}{\gamma}, \quad S = 0 \quad (31)$$

The boundary condition at $x = 1$ together with Equations (29) and (30) yield

$$[R \cos \omega - N \sin \omega] \omega \sin \omega t + \omega M \sin \omega \cos \omega t - \beta [M \cos \omega \cos \omega t - (N \cos \omega + R \sin \omega) \sin \omega t] = 0$$

Thus

$$\left. \begin{aligned} M &= 0 \\ N &= \left[\frac{\omega \cos \omega + \beta \sin \omega}{\omega \sin \omega - \beta \cos \omega} \right] R \end{aligned} \right\} \quad (32)$$

or

$$\left. \begin{aligned} u'' &= \frac{1}{\gamma} [A \cos \omega x + \sin \omega x] \sin \omega t \\ \rho'' &= \frac{1}{\gamma} [-A \sin \omega x + \cos \omega x] \cos \omega t \end{aligned} \right\} \quad (33)$$

where

$$A = \frac{\omega \cos \omega + \beta \sin \omega}{\omega \sin \omega - \beta \cos \omega}$$

$$\text{Now } \omega = 2\pi f l / c = 2\pi l / \lambda$$

so that for $\lambda \gg l$ ω is small, and thus

$$u'' = \frac{1}{\gamma} \left[\frac{\omega(1+\beta)}{\omega^2 - \beta} + \omega x \right] \sin \omega t$$

$$\rho'' = \frac{1}{\gamma} \left[-\frac{\omega(1+\beta)}{\omega^2 - \beta} + 1 \right] \cos \omega t$$

Since the Helmholtz resonating frequency can be expressed as (for negligible end correction)

$$f_0 \equiv (f_{res})_H = \beta^{1/2} c / 2\pi l$$

or

$$\beta = (2\pi f_0 l / c)^2 \equiv \omega_0^2$$

for chamber oscillatory frequencies near this frequency, the above reduces further to (assuming approximate accuracy)

$$u^{(1)} = \frac{1}{\gamma} \frac{\omega}{\omega^2 - \beta} \sin \omega t$$

$$p^{(1)} = \frac{1}{\gamma} \left[-\frac{\omega^2}{\omega^2 - \beta} x + 1 \right] \cos \omega t$$

The last result is the first order result obtained by Sirignano, and note that in this case, the first order velocity is constant throughout the orifice with a linear density (or pressure) gradient

Second Order Solution

Evaluating Equations (24) and (26), taking partial derivatives, and equating mixed derivatives gives the inhomogeneous wave equation for $u^{(2)}$ & $p^{(2)}$:

$$\left. \begin{aligned} u_{tt}^{(2)} - u_{xx}^{(2)} &= [M \sin 2\omega x + N \cos 2\omega x] \sin 2\omega t \\ p_{tt}^{(2)} - p_{xx}^{(2)} &= [-N \sin 2\omega x + M \cos 2\omega x] \cos 2\omega t \\ &\quad + P \sin 2\omega x + Q \cos 2\omega x \end{aligned} \right\} \quad (34)$$

where

$$M = \frac{\omega^2}{2\gamma^2} [(1 + \gamma)(A^2 - 1)]$$

$$N = -\frac{\omega^2}{\gamma^2} [A(1 + \gamma)]$$

$$P = -\frac{\omega^2}{\gamma^2} [A(3 - \gamma)]$$

$$Q = \frac{\omega^2}{2\gamma^2} [(3 - \gamma)(1 - A^2)]$$

These results are of the form

$$u_{tt}^{(2)} - u_{xx}^{(2)} = f_1(2\omega x) \sin 2\omega t$$

$$\rho_{tt}^{(2)} - \rho_{xx}^{(2)} = f_2(2\omega x) + f_3(2\omega x) \cos 2\omega t$$

A particular solution periodic in time can be obtained by separation of variables and is

$$u_p^{(2)} = \left[B_1 \sin 2\omega x + B_2 \cos 2\omega x - \frac{1}{4\omega} N x \sin 2\omega x + \frac{1}{4\omega} M x \cos 2\omega x \right] \sin 2\omega t$$

$$\rho_p^{(2)} = \frac{1}{4\omega^2} [P \sin 2\omega x + Q \cos 2\omega x] + B_3 x + B_4 + \left[B_5 \sin 2\omega x + B_6 \cos 2\omega x - \frac{1}{4\omega} M x \sin 2\omega x - \frac{1}{4\omega} N x \cos 2\omega x \right] \cos 2\omega t$$

where B_1, \dots, B_6 are to be determined such that this is a particular solution of Equations (24) and (26). Substituting the above into either of Equations (24) and (26) will give the required result and is

$$u_p^{(2)} = \frac{1}{4\omega} [M \cos 2\omega x - N \sin 2\omega x] x \sin 2\omega t$$

$$\rho_p^{(2)} = \frac{1}{4\omega^2} [P \sin 2\omega x + Q \cos 2\omega x] + \frac{1}{4\omega} \left[\left(\frac{1}{2\omega} P - M x \right) \sin 2\omega x + \left(\frac{1}{2\omega} Q - N x \right) \cos 2\omega x \right] \cos 2\omega t$$

where any arbitrary constants still remaining from the higher ordered equations have been set equal to zero. The complete solution will consist of the homogeneous solution and the above particular solution with the homogeneous solution adjusted so as to conform to both the particular solution and the boundary conditions. These boundary conditions will now be developed.

The specification of the input functions will first be made

$$P_I^{(2)} = \sum_{n=2}^{\infty} e_{p,n} \cos n\omega t + \sum_{n=1}^{\infty} q_{p,n} \sin n\omega t$$

$$U_I^{(1)} = e_u \cos \omega t + q_u \sin \omega t$$

The boundary conditions change for the different flow directions. If the exact points of flow reversal were known (which in general would differ for each end of the orifice), then a Fourier expansion could be used to obtain a single expression for the boundary conditions valid for both flow directions. Since these points are not known until the solution has been obtained, one method of attack would be to treat these points as unknowns, solve the problem, and then evaluate these unknowns from the solution. A vast simplification can be obtained here by making use of the points in time when the first order velocity goes through zero. This is particularly convenient since the first order velocity goes through zero uniformly in x . The justification of this approach leading to a result accurate to second order is the following. Let A be a point in time in which the first order velocity goes through zero. The actual velocity at $t = A$ will then be of second order in magnitude. Since the slope of the velocity curve vs. time is of first order, the error incurred in the time of actual flow reversal will be of first order; that is, the actual time of reversal will be $A + \mathcal{O}(\epsilon)$. Now since this last quantity appears in the limits of integration necessary to evaluate the Fourier coefficients, the error incurred in the second order solution is of higher order so that the complete solution will be accurate to second order.

Proceeding in the above manner, the boundary conditions at $x = 0$ are first written as

$$P_I^{(2)} + \left(\begin{array}{l} \text{common} \\ \text{terms} \end{array} \right) = \begin{cases} F_1(\omega t) = \frac{1}{2} a^2 U_I^{(0)2} + \frac{1}{\epsilon} a U_I^{(0)} U_I^{(1)} \cos \alpha \\ \quad + \frac{1}{\epsilon^2} \frac{1}{2} U_I^{(0)2} - \frac{1}{2} u_i^{(0)2} & + \text{flow} \\ F_2(\omega t) = \frac{1}{2} \bar{c}_p a^2 U_I^{(0)2} + \frac{1}{\epsilon} \bar{c}_p a U_I^{(0)} U_I^{(1)} \cos \alpha \\ \quad + \frac{1}{\epsilon^2} \bar{c}_p \frac{1}{2} U_I^{(0)2} & - \text{flow} \end{cases}$$

The function to be expanded is then

$$Y_1(\omega t) = \begin{cases} F_1(\omega t) & 0 < \omega t < \pi \\ F_2(\omega t) & \pi < \omega t < 2\pi, \text{ etc} \end{cases}$$

after performing the expansion, the boundary conditions at $x = 0$ become:

$$\begin{aligned} \rho_1^{(2)} = & G_0 + G_1 \cos \omega t + G_2 \sin \omega t + G_3 \cos 2\omega t \\ & + G_4 \sin 2\omega t + G_5 \sum_{\substack{n=1 \\ n \text{ odd}}}^{\infty} \frac{\cos n\omega t}{4-n^2} + G_6 \sum_{\substack{n=2 \\ n \text{ even}}}^{\infty} \frac{\cos n\omega t}{1-n^2} \\ & + G_7 \sum_{\substack{n=1 \\ n \text{ odd}}}^{\infty} \frac{\sin n\omega t}{n} + G_8 \sum_{\substack{n=1 \\ n \text{ odd}}}^{\infty} \frac{n}{n^2-4} \sin n\omega t \\ & + G_9 \sum_{\substack{n=2 \\ n \text{ even}}}^{\infty} \frac{n}{n^2-1} \sin n\omega t + G_{10} \sum_{\substack{n=1 \\ n \text{ odd}}}^{\infty} \frac{1}{n(n^2-4)} \sin n\omega t \\ & + G_{11} \sum_{n=2}^{\infty} (e_{p,n} \cos n\omega t + q_{p,n} \sin n\omega t) \end{aligned} \quad (35)$$

where the coefficients are defined as

$$G_0 = \frac{1}{2} a^2 (e_u^2 + q_u^2) (1 + \bar{c}_p) + \frac{1}{\epsilon^2} \frac{1}{4} U_I^{(0)2} (1 + \bar{c}_p) + \frac{1}{\epsilon} \frac{1}{\pi} a q_u U_I^{(0)} \cos \alpha (1 - \bar{c}_p) - \frac{1}{8} \frac{1}{\gamma^2} A^2 \cos^2 \omega - \frac{\gamma-1}{4 \gamma^2}$$

$$G_1 = \frac{1}{\epsilon} \frac{1}{2} a U_I^{(0)} e_u \cos \alpha (1 + \bar{c}_p)$$

$$G_2 = \frac{1}{\epsilon} \frac{1}{2} a U_I^{(0)} q_u \cos \alpha (1 + \bar{c}_p) + \frac{1}{8} q_p$$

$$G_3 = \frac{1}{8} a^2 (e_u^2 + q_u^2) (1 + \bar{c}_p) + \frac{1}{8} \frac{1}{\gamma^2} A^2 \cos^2 \omega - \frac{\gamma-1}{4 \gamma^2}$$

$$G_4 = \frac{1}{4} a^2 e_u q_u (1 + \bar{c}_p)$$

$$G_5 = \frac{2}{\pi} a^2 e_u q_u (1 - \bar{C}_p)$$

$$G_6 = \frac{1}{\epsilon} \frac{2}{\pi} a U_I^{(0)} q_u \cos \alpha (1 - \bar{C}_p)$$

$$G_7 = \frac{1}{\pi} \left[\frac{1}{2} a^2 (e_u^2 + q_u^2) + \frac{1}{\epsilon^2} U_I^{(0)2} \right] (1 - \bar{C}_p)$$

$$G_8 = \frac{1}{2\pi} a^2 (e_u^2 + q_u^2) (1 - \bar{C}_p)$$

$$G_9 = \frac{1}{\epsilon} \frac{2}{\pi} a U_I^{(0)} e_u \cos \alpha (1 - \bar{C}_p)$$

$$G_{10} = \frac{2}{\pi} \frac{1}{8} A^2 \cos^2 \omega, \quad G_{11} = \frac{1}{8}$$

As a check, it can be verified that for $\bar{C}_p = 1$, the boundary condition reduces to almost the same thing as that for flow into the orifice - the only difference being due to the $\frac{1}{2} U_I^{(0)2}$ term.

The boundary condition at $x = 1$ is treated in a similar fashion. The function to be expanded is

$$Y_2(\omega t) = \begin{cases} 0 & 0 < \omega t < \pi \\ -\frac{\omega}{2\gamma^2} [A \cos \omega + \sin \omega]^2 \sin 2\omega t & \pi < \omega t < 2\pi, \\ & \text{etc.} \end{cases}$$

so that at $x = 1$, after the expansion is performed

$$\frac{d\rho_2^{(2)}}{dt} - \beta U_2^{(2)} = J_1 \sin 2\omega t + J_2 \sum_{\substack{n=1 \\ n \text{ odd}}}^{\infty} \frac{1}{4-n^2} \cos n\omega t \quad (36)$$

where

$$J_1 = \frac{1}{2} \frac{1}{\gamma^2} \beta [\cos \omega - A \sin \omega] [A \cos \omega + \sin \omega] - \frac{\omega}{4\gamma^2} [A \cos \omega + \sin \omega]^2$$

$$J_2 = \frac{2\omega}{\pi \gamma^2} [A \cos \omega + \sin \omega]$$

The most general harmonic solution of the homogeneous version of Equations (24) and (26) is given by Equations (29) and (30). The presence of constants and higher harmonics in the above boundary conditions indicates that for this homogeneous version, a solution with terms other than first harmonics is necessary. Thus, considering all possible solutions, it is known a priori that whatever the solution of the homogeneous equations, it can be represented by

$$\left. \begin{aligned} \mathcal{U}_H^{(2)} &= \sum_{n=2}^{\infty} \left[(M'_n \cos n\omega x - S'_n \sin n\omega x) \cos n\omega t \right. \\ &\quad \left. + (-N'_n \cos n\omega x - R'_n \sin n\omega x) \sin n\omega t \right] + E \\ \varrho_H^{(2)} &= \sum_{n=1}^{\infty} \left[(-R'_n \cos n\omega x + N'_n \sin n\omega x) \cos n\omega t \right. \\ &\quad \left. + (S'_n \cos n\omega x + M'_n \sin n\omega x) \sin n\omega t \right] + D \end{aligned} \right\} \quad (37)$$

Thus, at $x = 0$,

$$\begin{aligned} \varrho_i^{(2)} &= \varrho_{P1}^{(2)} + \varrho_{H1}^{(2)} = \sum_{n=1}^{\infty} [-R'_n \cos n\omega t + S'_n \sin n\omega t] + D \\ &\quad + \frac{1}{4\omega^2} Q + \frac{1}{4\omega} \left(\frac{1}{2\omega} Q \right) \cos 2\omega t \end{aligned}$$

Matching the above with Equation (35) gives

$$D = 0$$

$$R'_1 = -G_1 - \frac{1}{3} G_5$$

$$R'_2 = -G_3 + \frac{1}{3} G_6 + \frac{1}{8\omega^2} Q - G_{11} e_{P,2}$$

$$R'_n = \frac{1}{n^2-4} G_5 - G_{11} e_{P,n}; \quad n \geq 3, \text{ odd}$$

$$R'_n = \frac{1}{n^2-1} G_6 - G_{11} e_{P,n}; \quad n > 2, \text{ even}$$

$$S'_1 = G_2 + G_7 - \frac{1}{3} G_8 - \frac{1}{3} G_{10}$$

$$S'_2 = G_4 + \frac{2}{3} G_9 + G_{11} q_{P,2}$$

$$S'_n = \frac{1}{n} G_7 + \frac{1}{n^2-4} G_8 + \frac{1}{n(n^2-4)} G_{10} + G_{11} q_{P,n}; \quad n > 1, \text{ odd}$$

$$S'_n = \frac{n}{n^2-1} G_9 + G_{11} q_{P,n}; \quad n > 2, \text{ even}$$

Making use of Equation (36) yields

$$\begin{aligned}
 & -\frac{1}{2} \left[\left(\frac{1}{2\omega} - M \right) \sin 2\omega + \left(\frac{1}{2\omega} Q - N \right) \cos 2\omega \right] \sin 2\omega t \\
 & + \sum_{n=1}^{\infty} n\omega \left[\left(R'_n \cos n\omega - N'_n \sin n\omega \right) \sin n\omega t + \left(S'_n \cos n\omega + M'_n \sin n\omega \right) \cos n\omega t \right] \\
 & - \sum_{n=1}^{\infty} \left[\left(M'_n \cos n\omega - S'_n \sin n\omega \right) \cos n\omega t - \left(N'_n \cos n\omega + R'_n \sin n\omega \right) \sin n\omega t \right] \beta \\
 & - \beta \frac{1}{4\omega} \left[M \cos 2\omega - N \sin 2\omega \right] \sin 2\omega t - \beta E \\
 & = J_1 \sin 2\omega t + J_2 \sum_{\substack{n=1 \\ n \text{ odd}}}^{\infty} \frac{1}{4-n^2} \cos n\omega t
 \end{aligned}$$

and, after matching

$$E = 0$$

$$N'_1 = A R'_1$$

$$\begin{aligned}
 N'_2 = & \frac{1}{\beta \cos 2\omega - 2\omega \sin 2\omega} \left\{ \frac{1}{2} \frac{\beta}{\gamma^2} [\cos \omega - A \sin \omega] [A \cos \omega + \sin \omega] \right. \\
 & - \frac{\omega}{4\gamma^2} [A \cos \omega + \sin \omega]^2 - [2\omega \cos 2\omega + \beta \sin 2\omega] R'_2 \\
 & + \frac{1}{2} \left[\left(\frac{1}{2\omega} P - M \right) \sin 2\omega + \left(\frac{1}{2\omega} Q - N \right) \cos 2\omega \right] \\
 & \left. + \frac{\beta}{4\omega} [M \cos 2\omega - N \sin 2\omega] \right\}
 \end{aligned}$$

$$N'_n = \left[\frac{n\omega \cos n\omega + \beta \sin n\omega}{n\omega \sin n\omega - \beta \cos n\omega} \right] R'_n ; n > 2$$

$$M'_n = \left[\frac{\beta \sin n\omega + n\omega \cos n\omega}{\beta \cos n\omega - n\omega \sin n\omega} \right] S'_n ; n \text{ even}$$

$$\begin{aligned}
 M'_n = & \frac{1}{\beta \cos n\omega - n\omega \sin n\omega} \left[(\beta \sin n\omega + n\omega \cos n\omega) S'_n \right. \\
 & \left. + \frac{1}{n^2 - 4} J_2 \right] ; n \text{ odd}
 \end{aligned}$$

All of the constants in the homogeneous solution have been evaluated so that the second order solutions for $u^{(2)}$ and $\rho^{(2)}$ are now complete.

Cavity Pressure

The cavity pressure could now be obtained by making use of Equations (19) to (22). In the second order expressions, a Fourier expansions must be done. The function to be expanded is

$$Y_3(\omega t) = \begin{cases} 0 & 0 < \omega t < \pi \\ \frac{1}{4\gamma^2} [A \cos \omega + \sin \omega]^2 (\cos 2\omega t - 1) & \pi < \omega t < 2\pi, \text{ etc.} \end{cases}$$

The results of this expansion give

$$Y_3(\omega t) = -\frac{1}{2} Z^2 + \frac{1}{2} Z^2 \cos 2\omega t + \frac{\beta Z^2}{\pi} \sum_{\substack{n=1 \\ n \text{ odd}}}^{\infty} \frac{1}{n(4-n^2)} \sin n\omega t$$

where

$$Z^2 = \frac{1}{4\gamma^2} [A \cos \omega + \sin \omega]^2$$

Therefore

$$P_{II}^{(1)} = \left[-\frac{\omega \cos \omega + \beta \sin \omega}{\omega \sin \omega - \beta \cos \omega} \sin \omega + \cos \omega \right] \cos \omega t$$

$$P_{II}^{(2)} = \frac{1}{2} \frac{\gamma-1}{\gamma} P_{II}^{(1)2} - \gamma Y_3(\omega t) + \gamma \rho_2^{(2)}$$

Resonance Solution

The details of the near-resonance solution will not be given here, merely the highlights of this solution will be presented. The characteristic difference of this solution from the above (from which all other differences follow) is that the orifice velocity and density

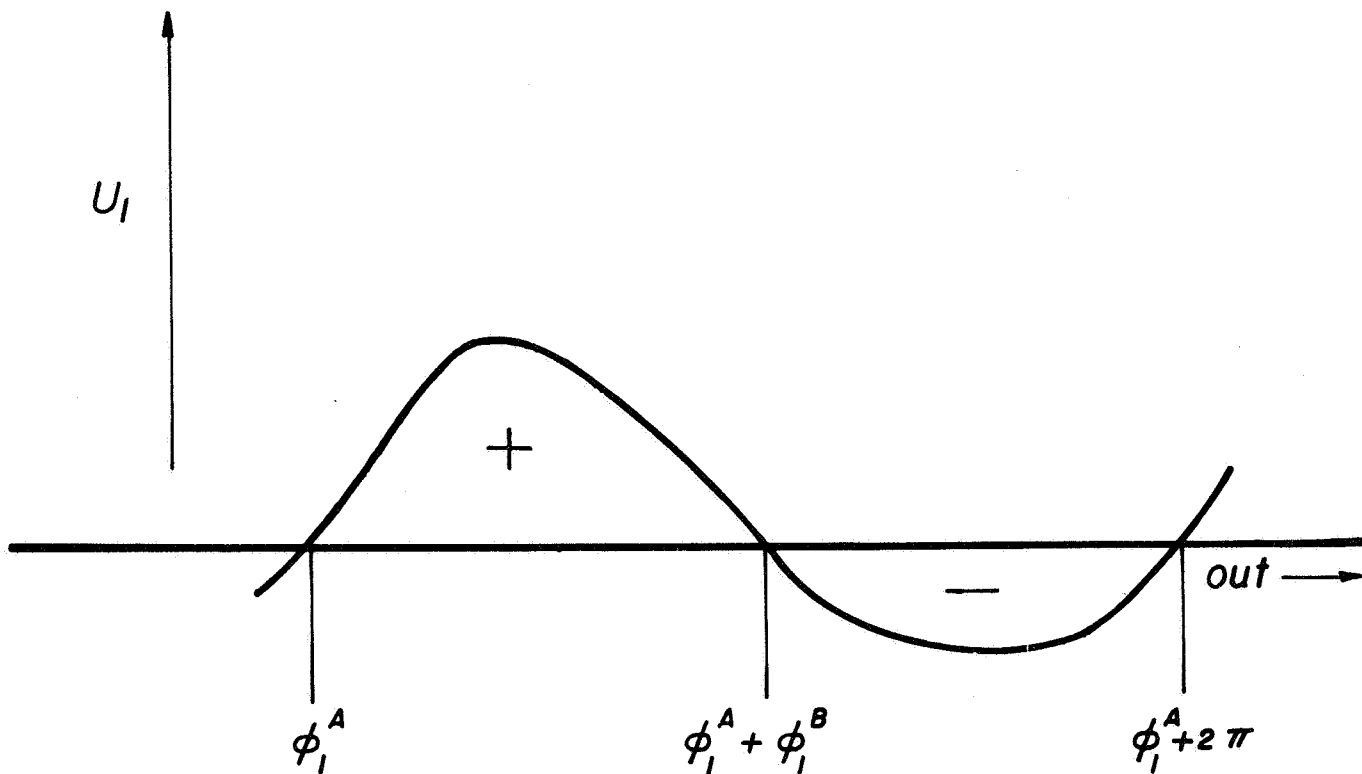
fluctuations are ordered so that they vary as the square root of the chamber pressure fluctuations. With this ordering then, the pressure work done on the system will be balanced by the kinetic energy dispersed by the jet.

The algebraic manipulations become exceedingly more involved - the difficulty being the fact that an $(n+1)$ order study must be made in order to obtain a complete (n) order result. Because of this difficulty, it is not permissible to expand the boundary conditions based on the values in time in which the first order velocity goes through zero; namely because second order equations must be used in order to determine the first order velocity, and if the second order equations are inaccurate, this will reflect upon the first order terms. A correct method of attack was alluded to previously; i.e., the points of flow reversal are treated as unknowns in the problem, and once the final expressions have been found, these unknowns can be evaluated from their very definition.

A more detailed explanation is as follows. It is assumed that at the ends of the orifice, the period of velocity oscillations is divided into two regions: 1) a jet exists on the cavity side (+ flow) and 2) a jet exists on the chamber side (- flow) - see Fig. 1. Let φ_1^a be the value of ωt for which the velocity at $x = 0$ goes through zero and in which positive flow exists immediately after this point. Let $\varphi_1^a + \varphi_1^b$ be the next value of ωt for which the velocity passes through zero. Negative velocity will then occur immediately after this second point, and the next point of flow reversal will be $\omega t = \varphi_1^a + 2\pi$ - the start of periodicity. At $x = 1$, the corresponding values of φ_2^a and φ_2^b are similarly defined (which will in general differ from corresponding values of φ_1^a and φ_1^b). The solution of the problem is then formally with the φ 's, and an expression for the velocity accurate to second order can be obtained such as

$$u = u(x, \omega t, \varphi_1^a, \varphi_1^b, \varphi_2^a, \varphi_2^b)$$

Definition of ϕ_1 's used in near-resonance solution



JP 21 R 4329 - 68

Figure 1

The φ 's can then be found from the following four algebraic equations:

$$\begin{aligned} u(0, \varphi_1^A, \varphi_1^B, \varphi_2^A, \varphi_2^B) &= 0 \\ u(0, \varphi_1^A + \varphi_1^B, \varphi_2^A, \varphi_2^B) &= 0 \\ u(1, \varphi_2^A, \varphi_2^B, \varphi_1^A, \varphi_1^B) &= 0 \\ u(1, \varphi_2^A + \varphi_2^B, \varphi_1^A, \varphi_1^B) &= 0 \end{aligned}$$

The solution in which positive velocity occurs after φ_1^A and φ_2^A is desired. Note that any solution of the form $\varphi_i^{j'} = \varphi_i^j + n2\pi$ is acceptable since the φ 's appear only in the limits of the integrals necessary for evaluating Fourier coefficients. The justification for using the value of ωt in which the approximate velocity (accuracy of $\mathcal{O}(\epsilon^2)$) passes through zero follows the same reasoning justifying the procedure used in the off-resonance solution.

It should be noted that the above four equations cannot be solved as a unit. Four more equations exist for the determination of the arbitrary constants of the various homogeneous solutions - two constants for first order (from second order equations), and two constants for second order (from third order equations). Thus, for calculation purposes, it will be necessary to numerically solve a system of 8 algebraic transcendental equations.

The region of validity of this near resonance solution is dictated by the expression

$$\frac{1}{\epsilon} [\omega \tan \omega - \varrho] = \mathcal{O}(1) \quad (38)$$

In applications, ϱ is much smaller than unity so that this rules out ω becoming very large, and thus $\tan \omega$ will be greater than zero. It is interesting to note that from this criterion, the solution can be valid also for cases in which the chamber frequency of oscillations is far away (although smaller than) the Helmholtz frequency. It is also interesting to note that this is the criterion which predicts when the off-resonance solution becomes invalid (see Equation (33)). Thus, the two solutions are complementary.

The details of this solution have been performed and a solution accurate to order ϵ^2 has been obtained.

Future Work

Having obtained the analytical results, the point is reached where significant feedback can be made between theory and experiment. One direction of investigation will be to determine what geometrical configurations of the liner system lead to optimum dissipation. Certain trends should be predictable from these analytical results, and the facilities here at Princeton will allow both cold flow and hot flow experimental verification (the experimental programs are discussed in other sections of this report).

NOMENCLATURE

a	proportionality constant relating chamber pressure fluctuations to chamber velocity fluctuations
A	orifice cross sectional area
c	average speed of sound
C_p	specific heat at constant pressure
\bar{C}_p	average pressure coefficient for jet on chamber side
$e_{p,n}$	coefficient of the n^{th} harmonic (cosine) in the second order chamber pressure
e_u	coefficient of the cosine component in the first order chamber velocity
f	frequency of chamber oscillations
$q_{p,n}$	coefficient of the n^{th} harmonic (sine) in the second order chamber pressure
q_u	coefficient of the sine component in the first order chamber velocity
l	orifice length
P	pressure nondimensionalized with respect to the mean chamber static pressure
t	nondimensional time = (actual time) (c/l)
U_x	chamber velocity nondimensionalized with respect to c
u	orifice velocity nondimensionalized with respect to c
x	distance along orifice measured from chamber side divided by l

NOMENCLATURE - continued

V	cavity volume
α	angle between chamber mean flow and chamber perturbed flow
γ	ratio of specific heats
ϵ	nondimensional pressure amplitude parameter
ω	nondimensional frequency of chamber oscillations = $2\pi f l / c$

Subscripts:

0	stagnation conditions in chamber
1	conditions at chamber end of orifice
2	conditions at cavity end of orifice
I	static conditions in chamber
II	conditions in cavity

Superscripts:

0, 1, 2, . . . indicates order of term

positive flow direction is from chamber to cavity.

nondimensionalization indicated above does not apply if noted.

above subscripts do not apply to constants and incidental functions within solution details.

B. LINER ACOUSTIC ADMITTANCE

The admittance of an acoustic cavity is defined as the ratio of the velocity to the perturbation pressure in the chamber of the rocket. If both these quantities are sinusoidal, then the admittance will be a complex number, carrying magnitude and phase information. If the velocity in the orifice and the chamber pressure are non-sinusoidal, then there is a separate admittance for each Fourier component of these quantities. The investigation attempts to find out what the admittances are for a wide range of conditions, and use the information gathered to try to define a single, useful admittance coefficient.

The computer program written by Stinger, and described in the last yearly report, was used to solve for the flow conditions. The assump-

tions made to arrive at this formulation were that the velocity in the orifice is constant at any time, and the orifice flow is isentropic, with different mean temperatures in the chamber and the cavity. A complete derivation of the program can be found in the last yearly report.

The input variables are: The chamber pressure, in its Fourier components; $\beta = A_l/V$, which is an inverted measure of the cavity volume; α , which is a measure of the cavity temperature; A_1 , which is the perturbation chamber pressure magnitude divided by the mean chamber pressure; and $FREQ$, which is the frequency of the oscillations divided by the Helmholtz natural frequency.

Two different wave shapes were used as input for the chamber pressure, one of them sinusoidal and the other a typical wave found experimentally. For each of these wave shapes, the amplitude was varied from .1 to .4 times the mean chamber pressure, α was varied from .05 to 1.0 in six steps, and $FREQ$ was varied from .6 to 2.2. β was kept constant at the value of .142 corresponding to the test rocket at Princeton. This was done mainly to keep the volume of data down, and partially because the effect of small changes did not seem to be significant. If further investigation into this problem is deemed desirable, one of the possible directions is to vary β .

Four sets of graphs have been obtained in this study. The first two sets present the ratio of the second frequency velocity component divided by the first frequency velocity component for each of the two wave shapes. This velocity ratio will indicate when it is necessary to consider the second frequency component of the admittance ratio. The other two sets of graphs present the admittance ratio versus the frequency ratio for each of the two wave shapes. For the sinusoidal case, both the real imaginary components are plotted with the magnitude of the admittance ratio. For the actual wave shape, just the magnitude is plotted for each of the two frequency components of the admittance ratio. If the real and imaginary components are also desired, they are available. Typical examples of these various plots are presented in Figures 2 to 7 of this report.

In general, the velocity ratio for the sinusoidal case has the

same overall shape for all the graphs, with an increase in the frequency, or a decrease in either Alpha or the amplitude causing an increase in this ratio. The velocity ratio also generally hovers around 0.2 for the Alpha's under 0.75, which is a normal running condition. Figs. 2 and 3 illustrate these trends. This is a good indication of the nonlinearity of the problem, since for this case there is no second frequency component of chamber pressure, giving an infinite admittance.

For the case of the actual pressure wave shape, the average value of the velocity ratio is generally higher, as would be expected with the inclusion of a driving pressure at the second frequency. Again, the shapes of the velocity ratio curves are quite similar over the range of Alpha and A_1 . However, this shape is quite different from the shape found in the perfect sinusoidal case, even though the second frequency component of the chamber pressure is only .18 times the first frequency component. The principal change in shape is a significant dip around the resonant frequency (see Fig. 4). Since at this point the velocity ratio goes to about .1, it would be a good approximation to just use the first frequency component of the admittance around resonance. For large values of Alpha, the velocity ratio is almost constantly under .1, and the inclusion of only the first component of the admittance ratio could safely become a general rule. For these cases, however, Alpha is .75 or higher, which is abnormally hot for the cavity.

The admittance for the first frequency component seems to be a fairly "nice" function for the perfect sinusoid case, especially for high amplitude. When the amplitude of the pressure is .4, the admittance is fairly constant. It should be noted, however, that for the cases with low values of Alpha, the flow became choked with the pressure amplitude of .4. For the case of the amplitude equal to .25, the admittance is also quite flat, centering around 2, for all values of Alpha tested (see Fig. 5). For the case of the amplitude equal to .1, the admittance varies from around 2 to 3.5.

Although the first reaction to these results may be favorable, it can soon be seen that they are not so pleasant. The major change in admittance can be seen to come from changes in amplitude of the pressure

waves (compare Fig. 5 and Fig. 6). Since in the process of damping out a disturbance the amplitude changes continually, this sensitivity makes it more difficult to define a single admittance.

A comparison of the actual wave admittances with the perfect sinusoidal described above show that the first component of the admittance for the actual wave behaves the same way that the perfect sinusoid does. However, the second component of the admittance has a different shape. The main difference is a dip around resonant frequency, that is a result of the decrease in the second component of velocity (see Fig. 7). As for the sinusoidal case, the curves are more constant for higher amplitude. For these cases, it appears that a reasonable approximation is to say that the second frequency component is zero around resonance ($FREQ = 1.0 \pm .2$), and equal to the first component of the admittance at other frequencies. For the low amplitude case, the second frequency component of the admittance is also more erratic.

The accuracy desired will, of course, have to determine how far it is deemed reasonable to go with these approximations. There is some question as to the validity of the underlying assumptions of this analysis, so experimental verification will definitely be necessary. If the predictions of this analysis are borne out, then the admittance can be obtained from a graph, or a general value such as 2 can be used. The ability to neglect the second component around resonance and treat it as equal to the first component away from resonance is a good simplification, but it ignores the main complication which is the great sensitivity of the admittance to changes in amplitude. This is especially critical when the chamber pressure will be going through a series of amplitudes. In the case where the amplitude is constant, the admittance can be fairly well defined. In the case where there are reasonable changes in the amplitude of the chamber pressure perturbation, then an average will have to be taken over a large range (from typical results as shown in Figs. 5, 6 and 7) or the idea of a single admittance will have to be discarded.

Velocity ratio
 $\alpha = .10$

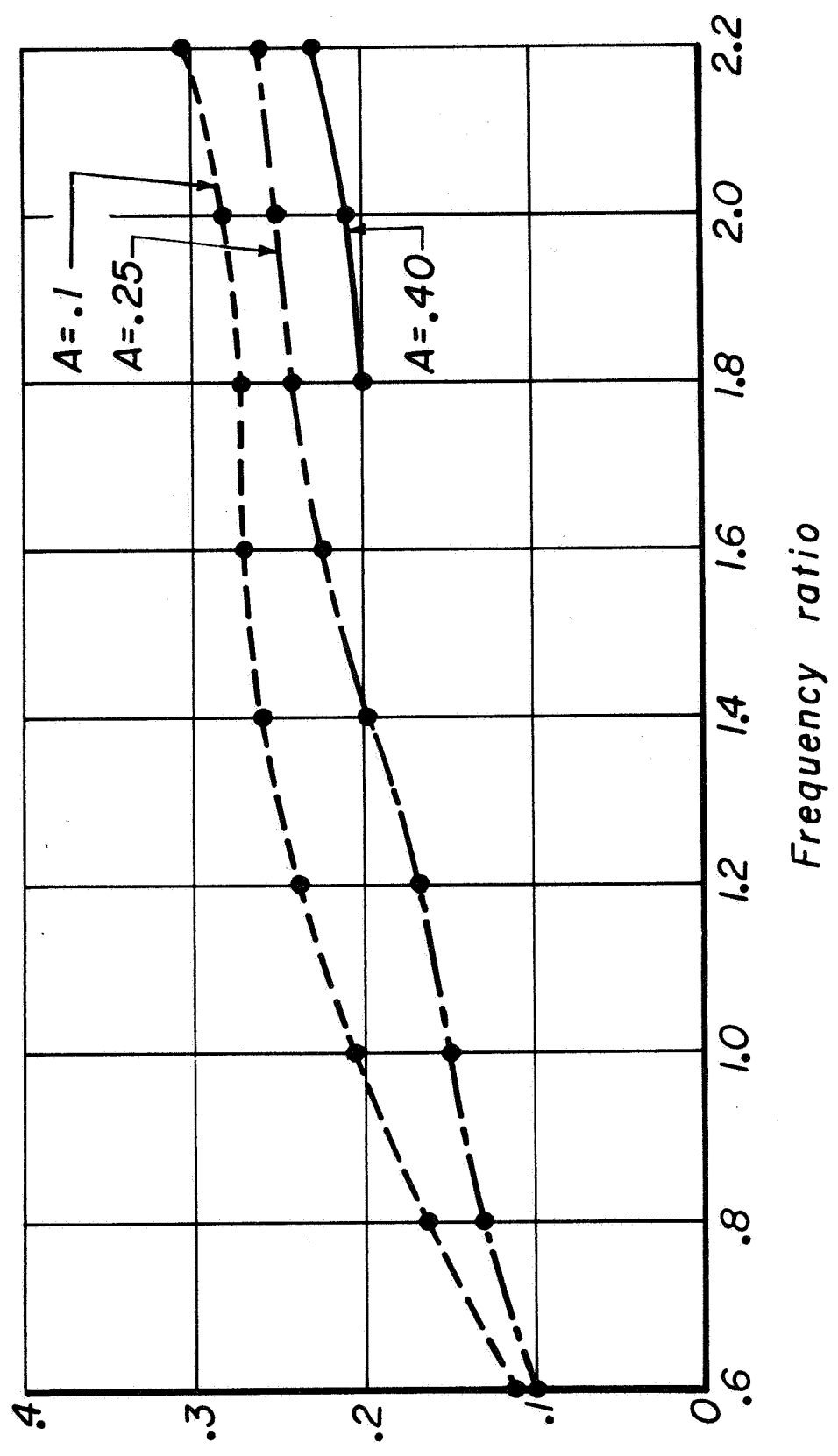


Figure 2

Velocity ratio
 $\alpha = 1.0$

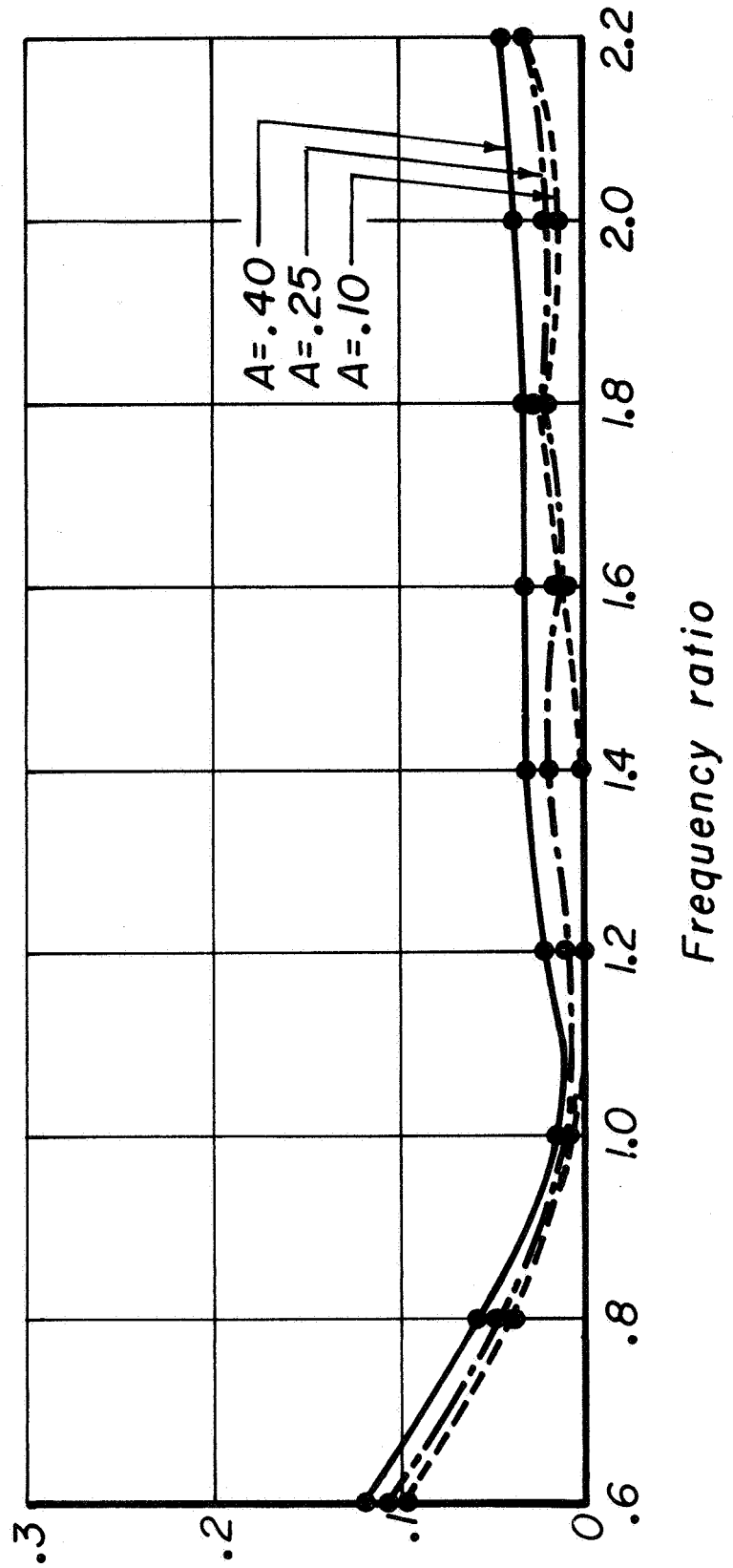


Figure 3

JP 21 R 4334 - 68

Velocity ratio
Actual wave

$\alpha = .05$

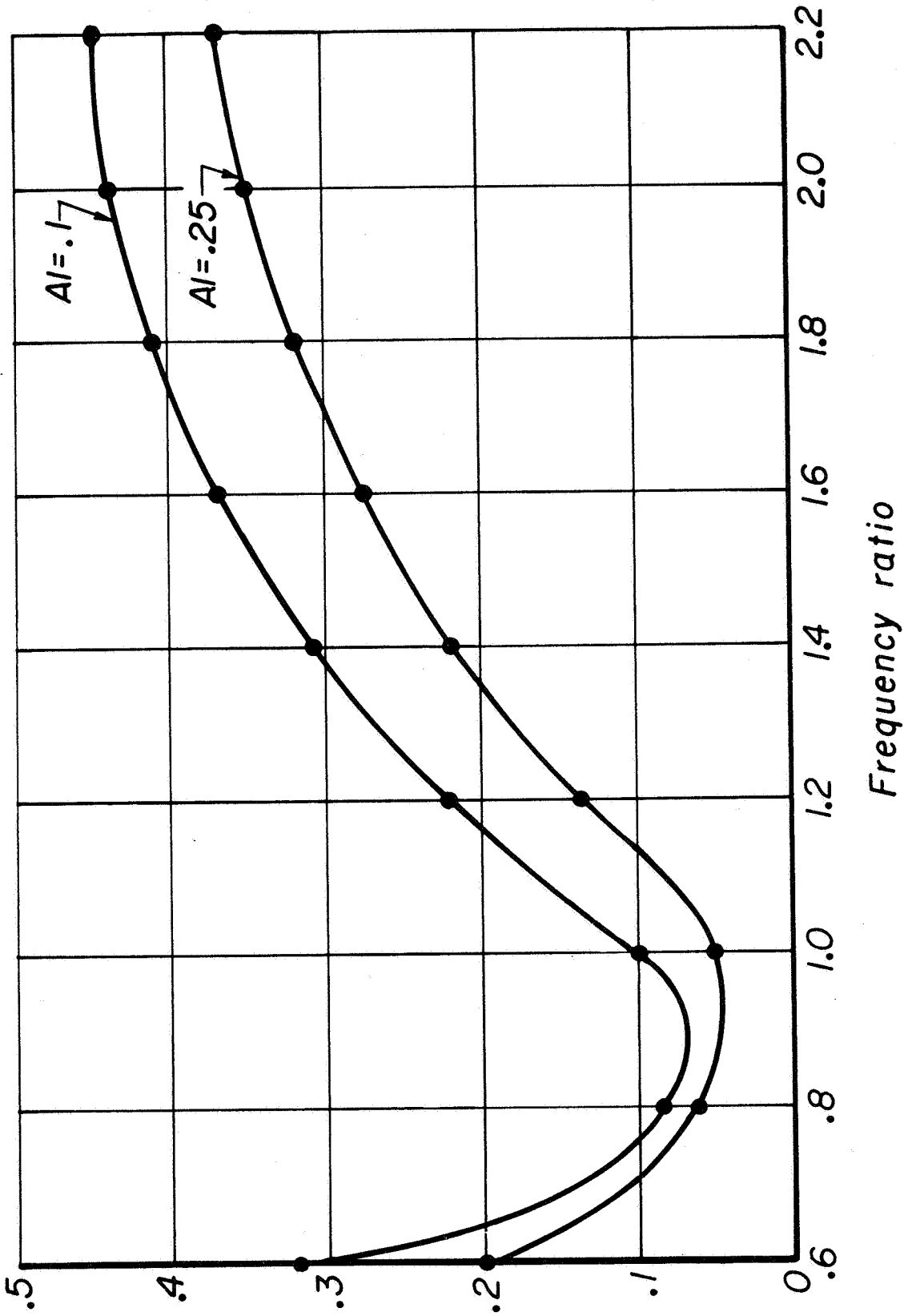


Figure 4

JP 21 R 4335 - 68

Admittance ratio
 $\alpha = .195 \quad A1 = .25$

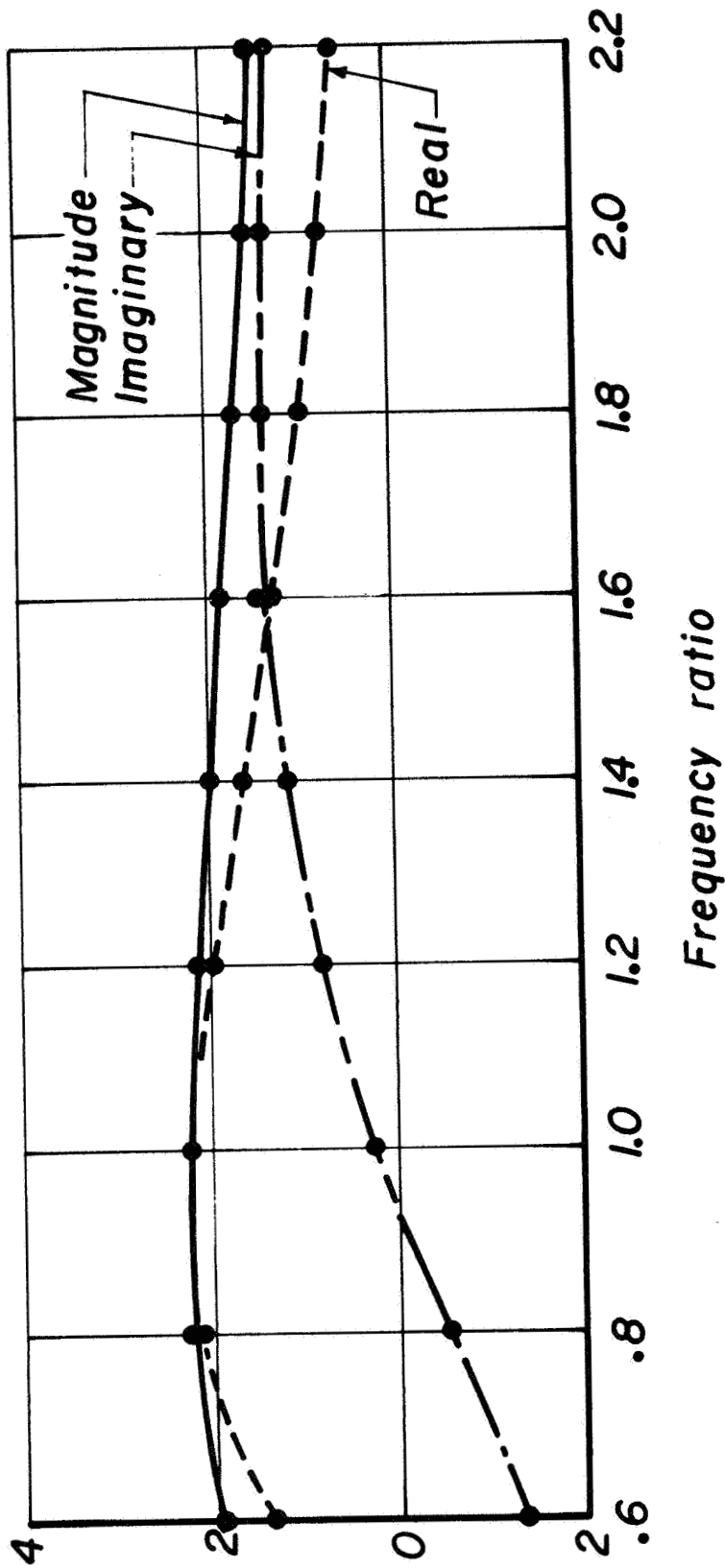


Figure 5

JP 21 'R 4340-68

Admittance ratio

$Q = .10 \quad AI = .10$

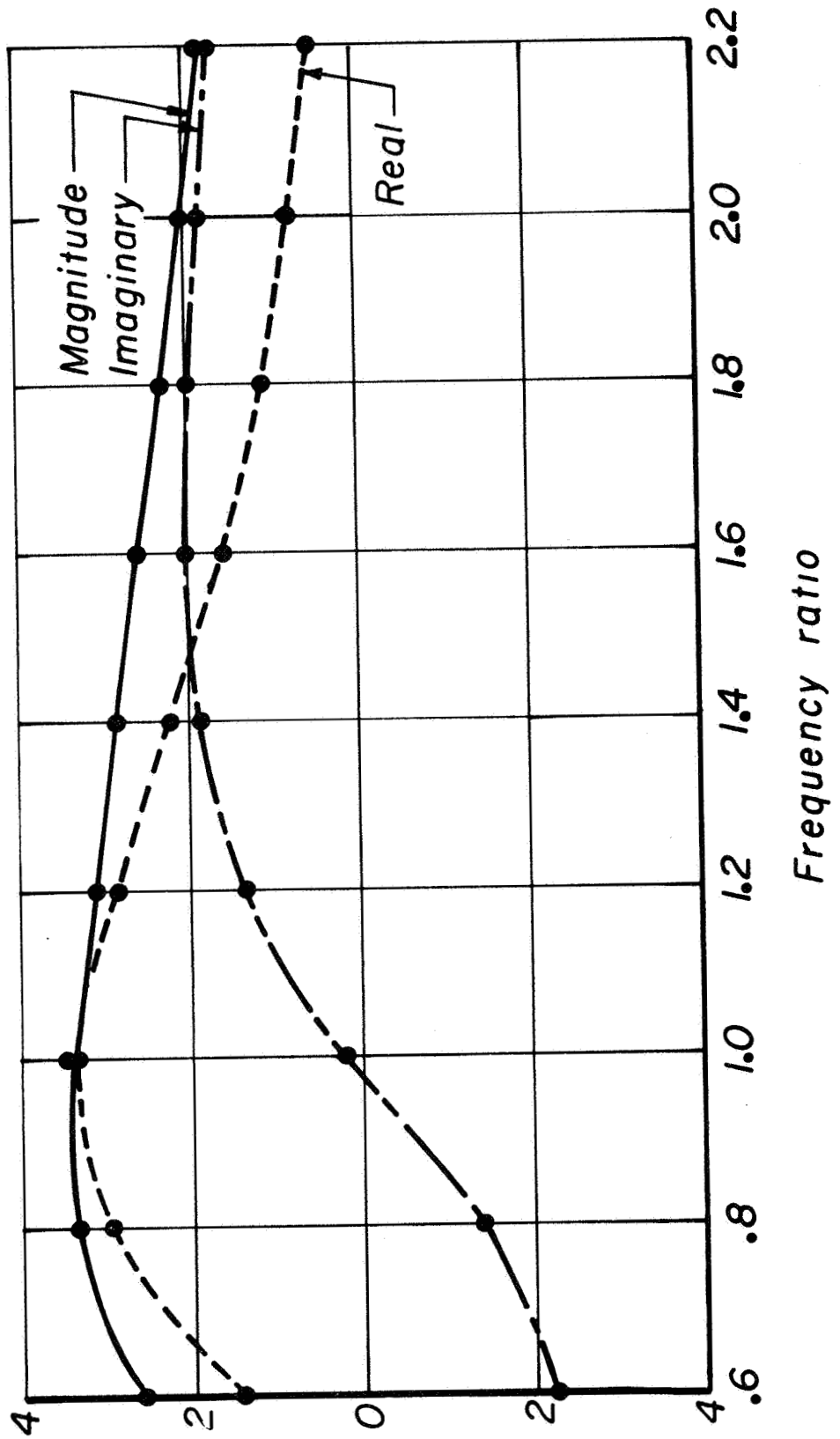


Figure 6

Admittance magnitudes
Actual wave
 $Q = .195 \quad A1 = .25$

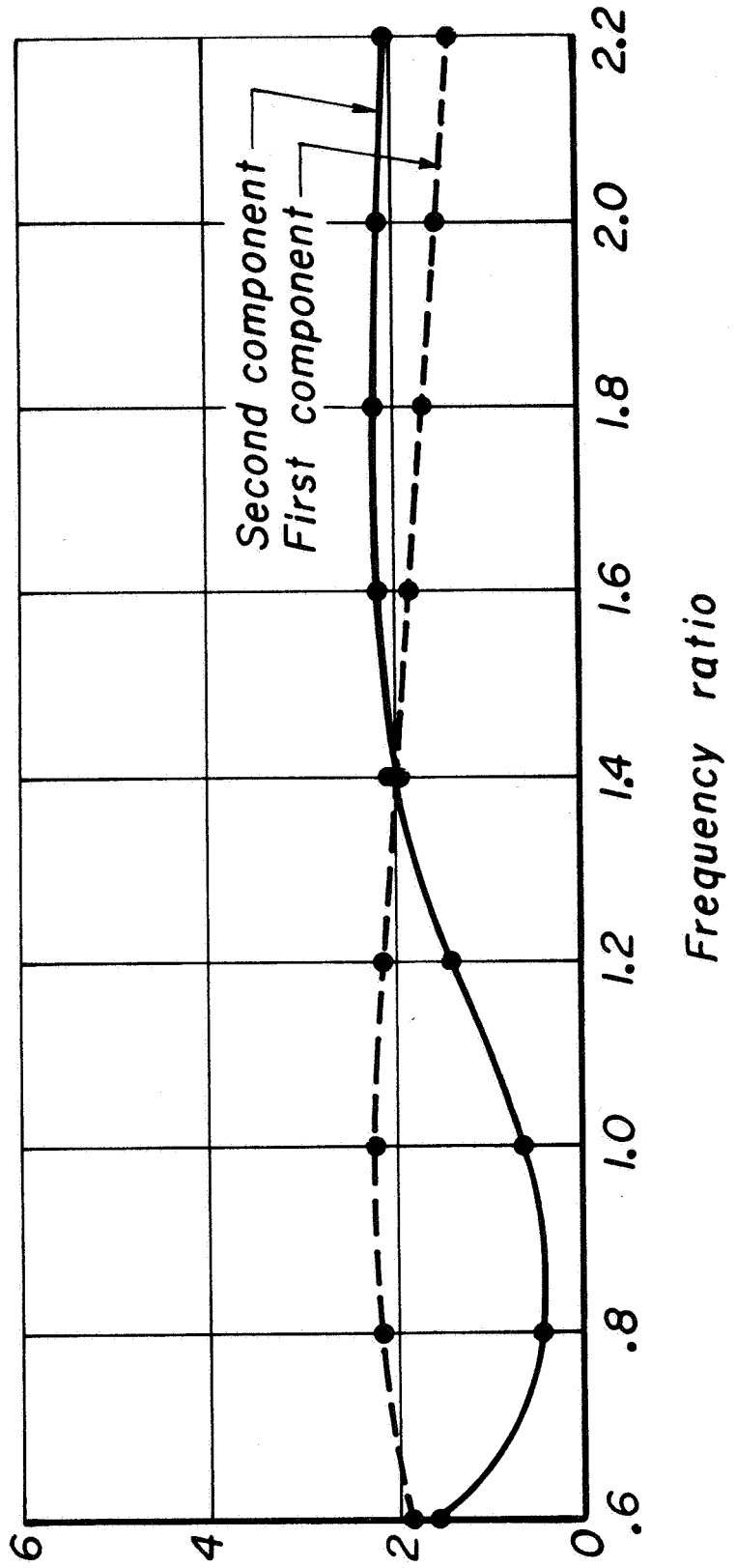


Figure 7

C. PLACEMENT OF DAMPING DEVICES

Often in the cases of practical rocket motor design there are only limited locations where damping devices can be placed. More specifically, for liner-type damping approaches, it would prove quite useful to know the most effective axial and circumferential locations for the placement of acoustic dampers. For the axial locations, tests at P and W, Lewis Lab - NASA, RPL and Princeton have all shown the location closest to the injector face to be far more effective than locations downstream. With regard to circumferential locations, far less is known. However, placement in limited circumferential locations, e.g., at 120° intervals, has been previously reported by Princeton.^{1,2} The purpose of the current effort is to study the case of the liner used in conjunction with a minimum baffle. The baffle fixes the mode (e.g., a three-bladed baffle would still allow a third tangential standing mode to exist between the blades) thus allowing the acoustic resonators to be tuned for a specific frequency. Since the effective damping range of these devices covers a very narrow frequency band, instability mode restrictions are highly desirable. Therefore, a prime consideration in this study was to determine which circumferential locations for the acoustic dampers were the most effective.

Tests were made on the 1 x 16 injector (sixteen spuds of like-on-like design), which experienced first tangential mode instability of 250 psi pk-pk amplitude following a tangential pulse. These LOX/ethanol tests were made to check the concept of using a limited number of acoustic dampers to bring dynamic stability to an otherwise nonlinearly unstable system (characterized at 150 psia chamber pressure). Damping was accomplished with as few as three resonating cavities spaced at 120° intervals around the circumference of the liner. The acoustic damper had six, $\frac{1}{2}$ inch long, .100 inch diameter, orifices entering an acoustically tuned cavity.^{1,2} It was found that the time to damp was short, being of the order of 25 milliseconds for nine active cavities and 17 milliseconds for 27 active dampers. A cavity volume of approximately three times the design volume was reached before marginal damping was experienced. Design frequency of 60% of that desired could still provide stable operation.

In summary, for this chamber-injector configuration, only a limited number of acoustic resonators were necessary and these provided damping over a sufficient band to eliminate the finite amplitude disturbances encountered.

Certain injector arrangements, where the propellant flow was made circumferentially non-uniform, caused standing modes which often avoided the locations where optimum damping was provided via the resonating cavities. Hence, baffles were used to control the modes and maximize the damping. It was found that with such a three-bladed baffle the instability was damped in less than 10 cycles and hence, it was difficult to maintain instability for testing damper effectiveness. The mixture ratio variations (and hence temperature striations) were apparent from the marking on the aluminum oxide chamber wall coatings. Cavity measurements indicated an out of resonance condition immediately following the passage of the initial high amplitude wave. Actual conditions were sometimes far from those assumed in the design. For example, in one case the cavity frequency was initially depressed more than 10% and required 10 cycles to reach nominal frequency (2780 Hz). Beyond that point there was a phase lag of 138° across the orifice. If the phase map constructed from the nonlinear flow behavior model discussed in the Seventh Yearly Report¹ (NASA CR 72270, Figure 25) was used, the implications were that the cavity temperature was only of the order of 600°R , even after a regime phase reading had been reached. Another cavity in the same test had a phase lag of only 78° which would be representative of about 2000°R temperature. Tungsten-rhenium thermocouples placed around the perimeter showed there was a relatively cool region from the center of the spud, through the fuel portion and approximately 60% of the distance to the adjacent spud. In the cool region the temperature stabilized in the 500 to 1000°R while in the hot zone it remained in the $2000\text{-}3000^{\circ}\text{R}$ range. (These temperatures were in agreement with the phase measurements.) Along the zone interfaces there were severe temperature fluctuations.

The spuds were reoriented in an attempt to equalize the wall surface temperatures by putting the fuel rich zone toward the wall. It was also hoped that the new configuration would lead to greater instability

because damping was occurring in about 50 milliseconds with only a few cavities active. Stability was still easily obtained thus presenting an unsuitable test condition. Therefore, an unlike-doublet injector was used since it was known to be inherently unstable. A limited-length cruciform baffle design to select the second tangential mode was used in conjunction with the liner. With the liner adjusted to the second tangential mode, a first tangential mode oscillation of low amplitude was observed in the chamber. When the cavities were tuned for the first tangential mode, the second tangential mode appeared in the chamber. A three-bladed baffle was used instead of the four-bladed design, and groups of cavities (using all the available liner) were tuned to eliminate the first and second tangential modes. This reduced the amplitude of both, but the first radial and several combined modes appeared. In summary, for this unlike injector the instability could not be damped with any combination of cavity tuning.

A combination of spuds from the like-on-like, which was stable under all conditions, and from the unlike impingement, which was extremely unstable, was tried in an effort to reach a marginal instability range which was necessary to determine the optimum placement of the resonating cavities at pressure or velocity nodes. However, the combined injector scheme was still unstable and more closely resembled the unlike tests.

Rather than continue in the quest for a proper rocket test bed for determining optimum circumferential locations for the acoustic dampers, attention was turned toward cold flow simulation. Perhaps one of the principal sources of difficulty in the hot firings was that the level of uniformity reached in higher thrust multi-element injector designs cannot be achieved in 12 or even 16 spud motors. This would appear to be particularly true for the wall conditions where barrier coolant improves uniformity for the full scale combustors.

The cold flow testing is being conducted in an apparatus formerly designed for oscillating heat transfer research.¹⁴ A new test section was fabricated which included a variable volume cavity and a connecting orifice equipped with hot-wire anemometer ports so that local flow can be measured. Pressure in the cavity and in the main duct (at the damper

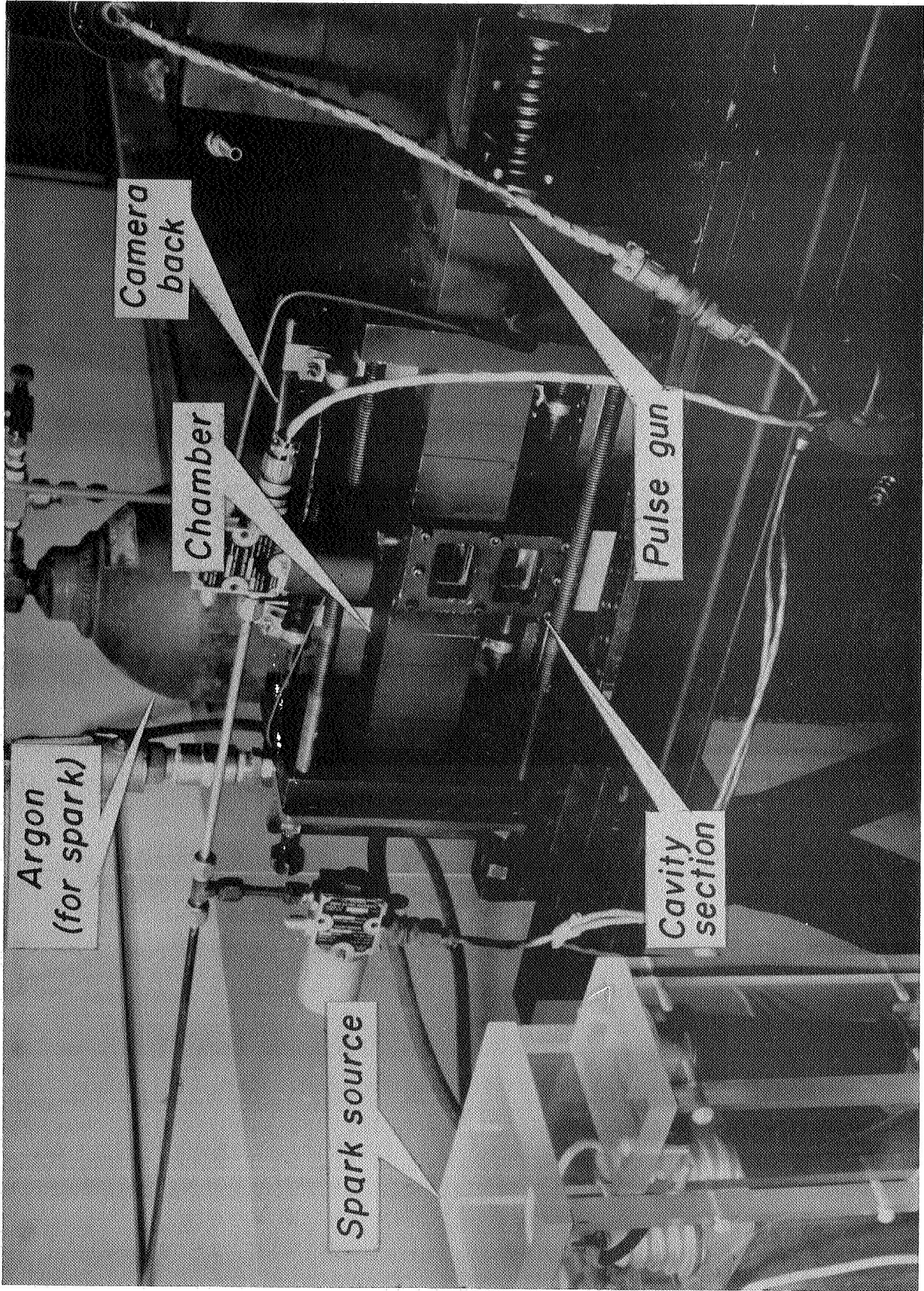
location) are measured by flush-mounted Kistler 601A transducers. Hot-wire probe ports are also included in the duct. The test section is mounted on an axially traversing section of the duct so that both node and anti-node locations can be checked for duct longitudinal mode frequencies of 270 cps or higher. Because such longitudinal velocity and amplitude characteristics are very similar to the baffle cavity modes, this survey should provide information on optimum circumferential placement of the damping cavities. In addition, and possibly more important, will be acquisition of pressure and velocity data with regard to both phase and amplitude. These data together with the nonlinear studies discussed next should provide an improved basis for optimum damper design.

Preliminary results have indicated improved damper efficiencies with the volume in excess of the design volume. This is in agreement with the hot firing data previously mentioned, where lower frequency (higher volume) designs proved highly effective. The results of these studies will be reported at the 5th ICRPG Conference this fall.

D. DAMPING OF SHOCK-TYPE WAVES

One aspect of the problem of acoustic liner design is the effectiveness of damping shock-type waves. Since this type wave in the tangential mode is characteristic of some of the large diameter chambers as well as in some of the smaller diameter chambers with reactive propellants (JPL experience in the 11-inch chamber¹⁵), and is representative of the longitudinal mode, this study was initiated to determine how a liner behaves under such an environment.

The apparatus used in this experimental study (as shown in Fig. 8) consists of a shock wave generation device, a variable-length shock tube (with a windowed resonator cavity segment), pressure transducers and photographic equipment. The high amplitude shock wave is generated at one end of the tube (referred to as the "chamber") and rapidly steepens into a planar shock which subsequently interacts with a properly tuned Helmholtz resonator (referred to as the "cavity"). The following describes the preliminary, qualitative findings from a study of that



Experimental apparatus for shock wave damping study

Figure 8

JP21 P-74 - 68

interaction.

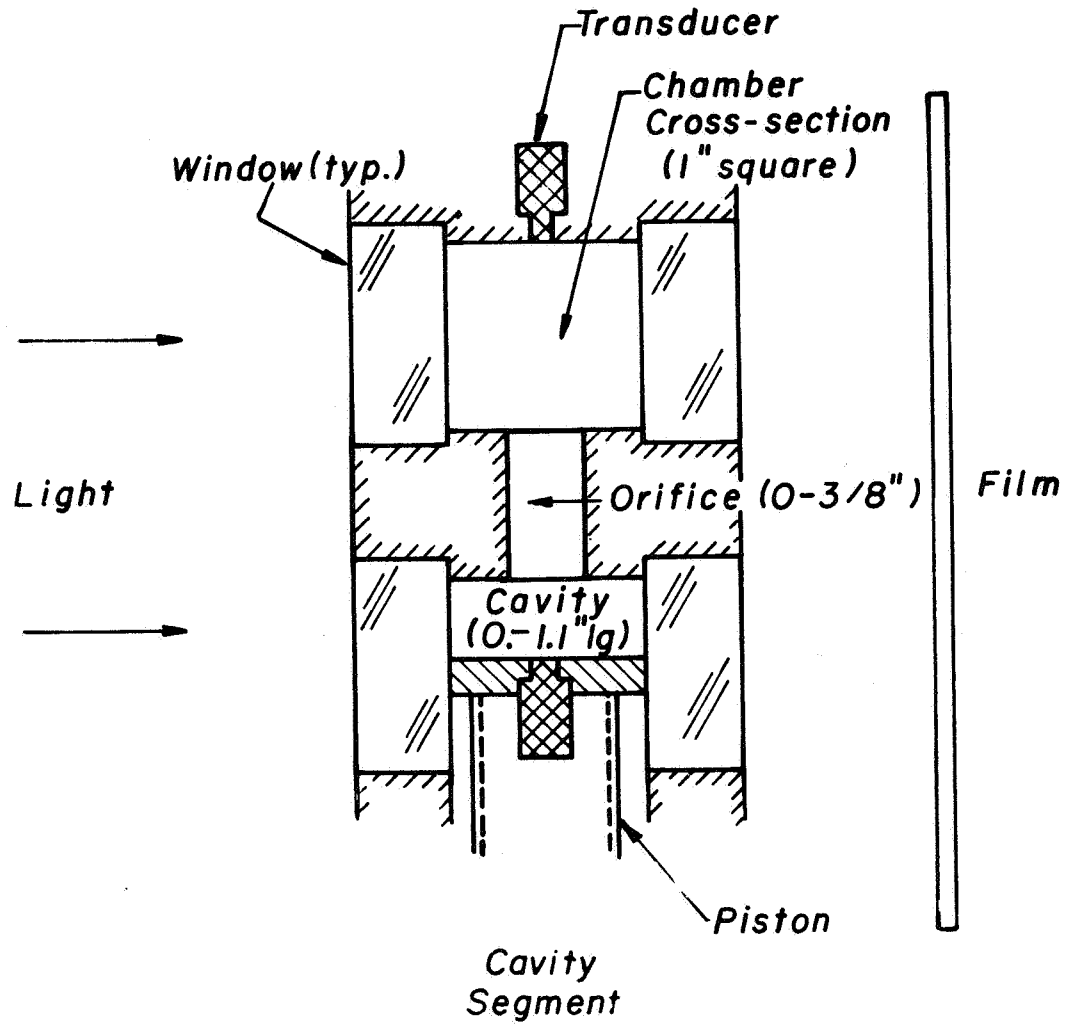
Data taken were of two forms, pressure vs. time plots and shadowgraph pictures. The pressure plots yielded information on damping rates and relationships between cavity/chamber wave amplitudes. The photographs portray a single cycle in detail, illustrating jets, vortices, and shock wave deformation.

First, a more detailed description of the experimental apparatus is necessary. The chamber is 12 inches long and has a one inch square cross section. It is segmented, allowing the cavity segment (Fig. 9) to be placed almost anywhere along the chamber length. The cavity section has windows which allow observation of the entire cavity and that part of the chamber immediately adjacent to the orifice. The acoustical volume of the cavity can be continuously varied (via a square piston) and the orifice diameter can be changed from zero to three-eighths inches (via a removable orifice section).

The pulse gun consists of a spring-powered, cigar-shaped, ram which slides through the "hole" of a doughnut-shaped, high-pressure plenum chamber. The ram is hollow. A half-inch long port on the ram allows a burst of high pressure gas (N_2) to enter the ram's interior (and thus, the chamber) as the ram slides quickly by the plenum. The pulse generated by the pulse gun is actually two shock waves - a low amplitude wave immediately followed by a much stronger wave. This pulse gun was used as a matter of convenience and was considered adequate for this preliminary study.

The pressure sensors used are Kistler 601 transducers. They are installed as shown in Fig. 9 . These signals are amplified, recorded on a Honeywell 7600 recorder, and played back onto a Honeywell 1108 Visicorder plot. See Fig. 10 for a typical Visicorder plot.

The last piece of apparatus is the photographic equipment. The shadowgraph system is simply a point light source from a one microsecond duration spark and a camera back (no lens or shutter) placed immediately behind the cavity section (see Fig. 9). Two types of film were employed, polaroid (3000 ASA) and 70mm (1600 ASA Kodak Recording 2475, on a motor-driven film transport). The spark is triggered by an accurate (\pm .01 millisecc),

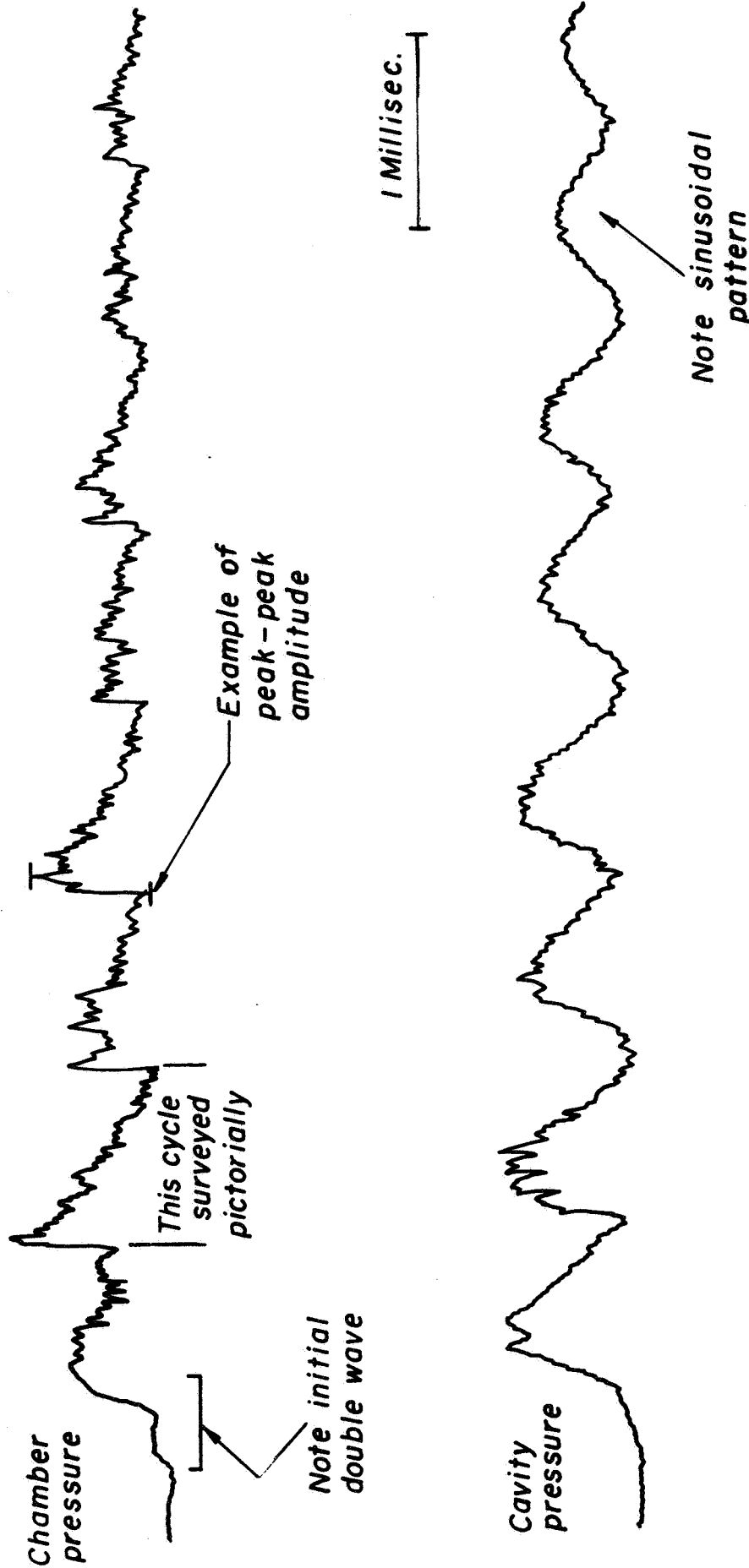


Experimental arrangement for shock wave damping study

JP 21 R 4341 - 68

Figure 9

Typical Visicorder pressure plot



Cavity at middle of foot - long chamber

$$\frac{\text{Average apparent shock frequency}}{\text{Natural cavity frequency}} = 1.01$$

$$\frac{\text{Initial PK - PK pressure}}{\text{Average chamber pressure}} = .69$$

Figure 10

adjustable delay circuit. The delay circuit is activated by the initial pressure pulse from the chamber transducer. Because the flow under study was shown to be reproducible, it was reconstructed by pictures of different test runs taken at progressively longer delays. This method was judged superior to a high-speed camera (6000 frames per second) because more pictures per cycle and better clarity could be obtained.

With this apparatus, it is possible to vary many parameters. The versatile design of the chamber and cavity make it possible to vary apparent shock frequency (defined as the frequency based on the observed wave passage time), cavity frequency, orifice diameter, and apparent shock strength (pk-pk amplitude at cavity section which can be varied by placing the cavity at a pressure node or anti-node). Actual shock strength may be varied continuously by adjusting pulse gun or chamber pressure. Also, more than one gas may be used in the system.

In this preliminary study, only a certain few parameters were varied. The cavity located was in three positions:

1. at middle of foot-long chamber (i.e., pressure node)
with ~ 1100 Hz observed
2. at end of foot-long chamber (pressure anti-node)
with ~ 550 Hz observed
3. at end of six-inch-long chamber (pressure anti-node)
with ~ 1100 Hz observed.

Shock strengths investigated covered a range of ϵ values (ratio of pk-pk first wave amplitude to steady-state chamber pressure) from .25-1.5, where average chamber pressure was held at ~ 68 psia. Initial chamber pressure was 65 psia for all test runs. The average apparent shock frequency (based on the first eight waves) was kept within 10% of the observed natural frequency of the cavity. The orifice diameter was not varied. Only the nitrogen tests are reported here.

As has been stated, the data were taken in two forms, pressure plots and shadowgraph pictures. The data will be discussed in that order. The damping of high amplitude waves by a resonator was studied through pressure plots. The effects of two parameters, shock strength and apparent shock frequency, were studied. Various shock strengths ($\epsilon = .25, .44, .70, 1.0, 1.5$) were observed. The results of this study with the cavity

at the end of the foot-long tube is presented in Fig. 11. Note that there is always a sizable difference between the damped and the undamped cases. There is not, however, a clear indication that higher amplitude waves are damped more effectively than lower amplitude waves or vice versa. Thus, from this series of tests the effect of shock strength on resonator damping efficiency does not seem to be dominating.

To isolate the effect of apparent shock frequency on damping, two series of tests were run. In the first series, the cavity (tuned for 550 Hz) was at the end of a foot-long chamber with the orifice blocked and open. This configuration provided an apparent shock frequency of ~ 550 Hz. In the second series, the cavity (tuned for 1100 Hz) was at the end of a six-inch-long chamber, with the orifice blocked and open. In this case the apparent shock frequency was ~ 1100 Hz. Note that in both series the cavity was at a pressure anti-node and velocity node. Equal strength shocks were observed in both series ($\epsilon = .70$). The higher frequency series (second series) produced very little difference between the damped and the undamped cases. Thus, there would appear to be a frequency effect influencing the damping efficiency - a point that must be checked with a refined shock pulse generator.

Fig. 12 illustrates a result found early in the study, namely that the resonator is more effective at the end of the foot-long chamber than at the middle. The "end" represents a pressure anti-node, velocity node, and an apparent shock frequency of ~ 550 Hz. At the middle, is the opposite situation, pressure node, velocity anti-node, and an apparent shock frequency of ~ 1100 Hz. The two preceding paragraphs show that a resonator cavity at the end position is more efficient because it operates at a lower frequency. Further tests (with the refined shock pulse generator) are needed to determine the effect of the velocity in the chamber on damping efficiency.

Aside from pressure data, many pictures were taken of the shock wave's interaction with the cavity. To date the most important pictorial data provide a detailed survey of a single cycle. The cycle under scrutiny is described in Figs. 10 and 13. Fig. 14 (note orifice outline) shows the shock wave entering the field of view. As it proceeds down the chamber

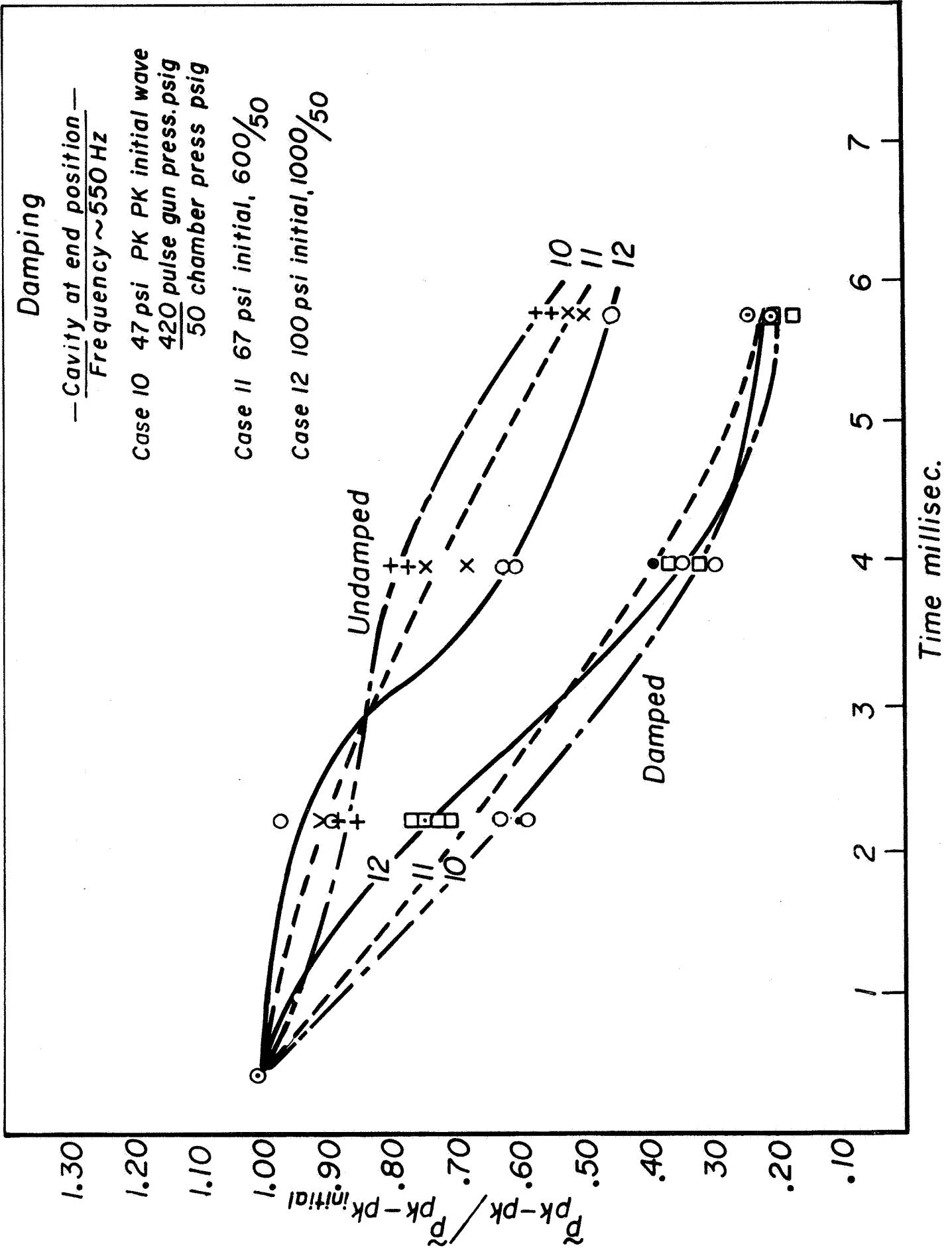


Figure 11

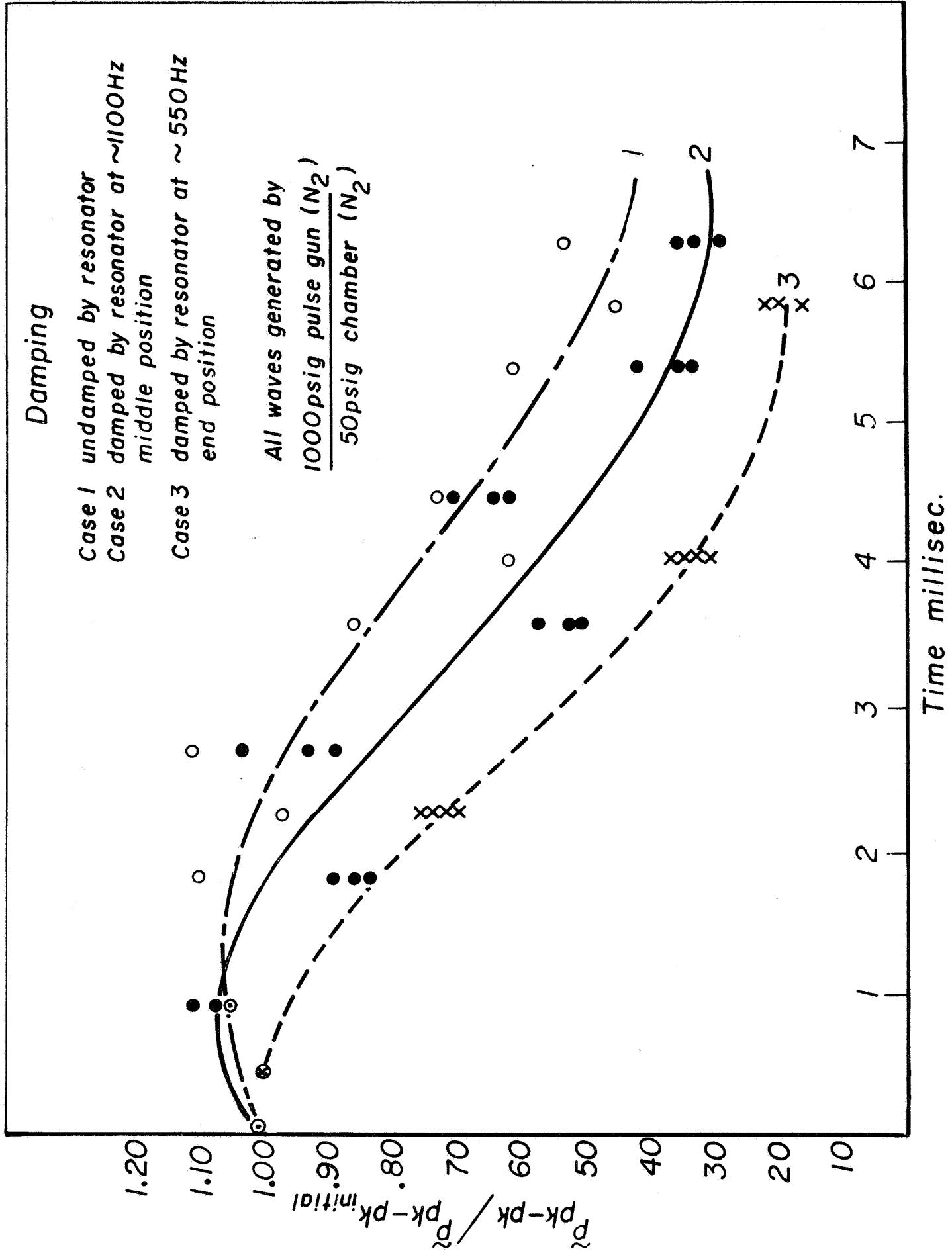


Figure 12

to the left, passing over the orifice it develops a "leg" (Fig.15).

When the shock is just out of the field of view, a vortex ring is visible just beneath the orifice in the cavity. These vortex rings are evidence that a jet is streaming into the cavity¹⁶. Also seen in the cavity at this time is what looks like a weak, curved shock wave propagating upward from the bottom of the cavity. Perhaps the weak cavity shock resulted from the formation of the main (chamber) shock's "leg". Figs. 16 and 17 show vortex rings and cavity shock wave. As the shock continues down the chamber, the cavity jet increases in intensity and the vortex rings become very pronounced (Fig.18).

Just after the shock reflects off the wall near the pulse-gun, i.e., a little more than half-cycle, the cavity jet dies down. Turbulent activity is noted at the orifice in the chamber. Figures 19-21 shows this transition region of the cycle.

As the shock continues toward the middle, the chamber jet intensifies (Fig. 22). Precisely when the chamber jet disappears is not clear, but it is not visible when the shock wave is again within view.

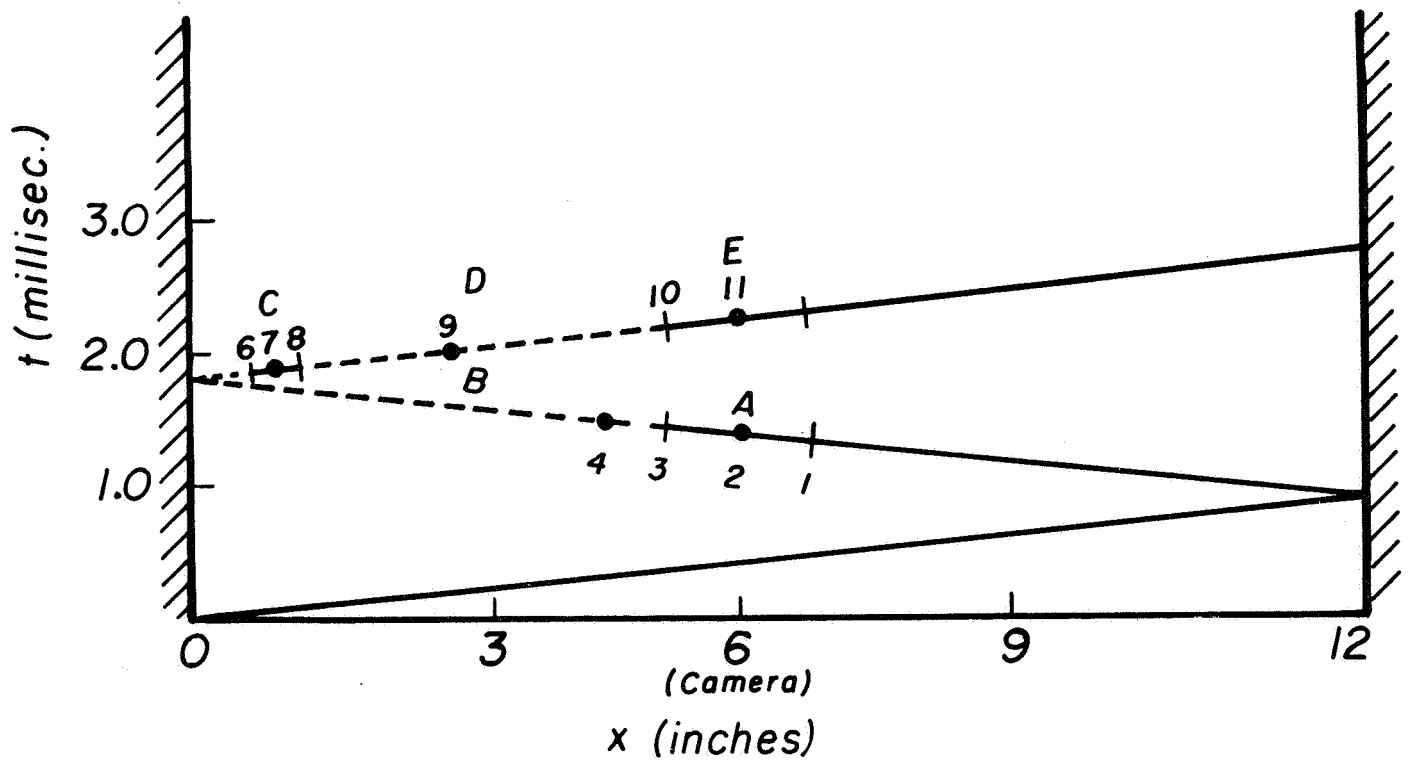
It is noteworthy that the cavity jet seems to last longer than the chamber jet.

Fig. 23 shows the shock (traveling to the right) entering field of view. There is what may be the last vestiges of chamber jet activity around the orifice. Figure 24 shows the shock a bit later, over the orifice. Compare the picture with Fig. 25 which was taken at the same corresponding time, with the orifice closed. This comparison leaves little doubt that the orifice is responsible for the formation of the "leg" on the shock wave.

This has been a report on the preliminary study of the interaction of high amplitude (shock) waves with a properly tuned Helmholtz resonator. Further study will utilize a more sophisticated shock wave generator to eliminate this double-wave complexities inherent in the present system. This will make possible a quantitative study of the interaction. Future work will study the effects of all variable parameters, including the use of two gases to more closely duplicate the conditions in a hot-flow combustion chamber.

Cycle of pictorial survey

x-t Plot of shock wave



Key

Regions (A-E)

A - Shock visible, moving to left

B - Cavity jet seen

C - Transition to chamber jet

D - Chamber jet seen

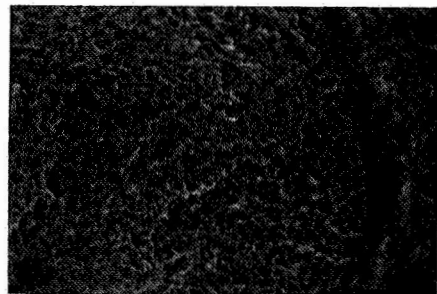
E - Chamber jet ends, shock visible, moving to right

Points (1-11)

denote where pictures were taken

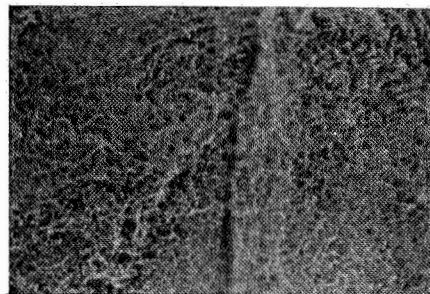
JP 21 R 4338 - 68

Figure 13



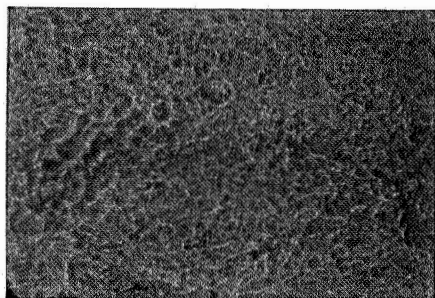
(1)

Figure 14



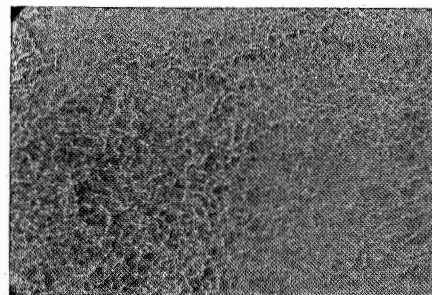
(2)

Figure 15



(3)

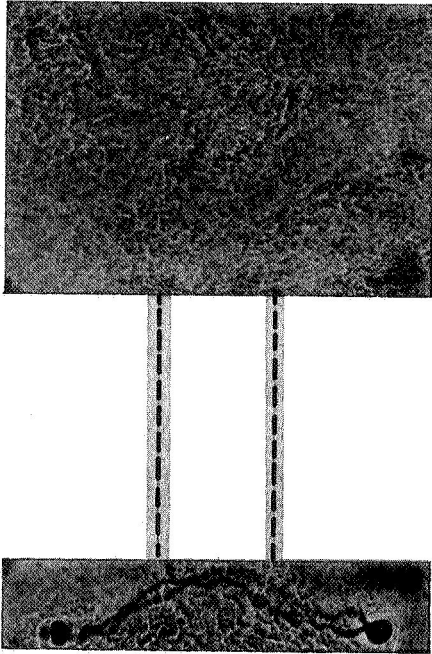
Figure 16



(4)

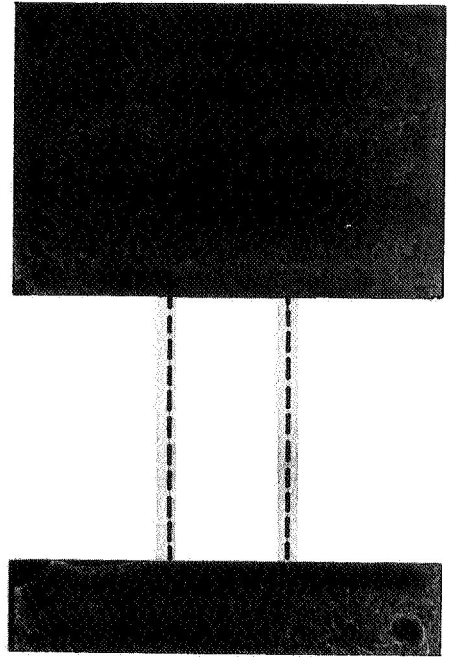
Figure 17

JP21 P71 - 68



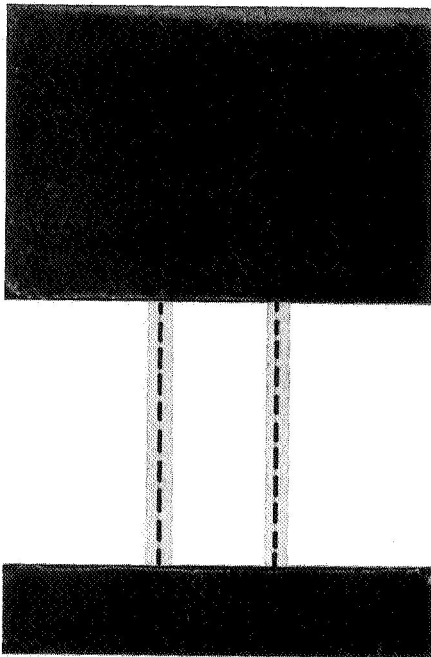
(5)

Figure 18



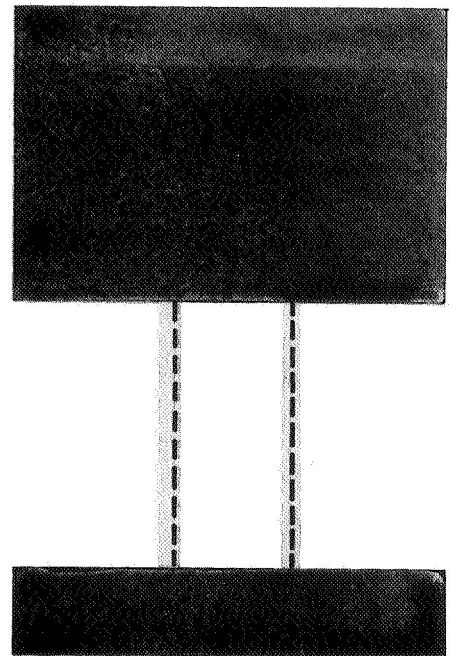
(6)

Figure 19



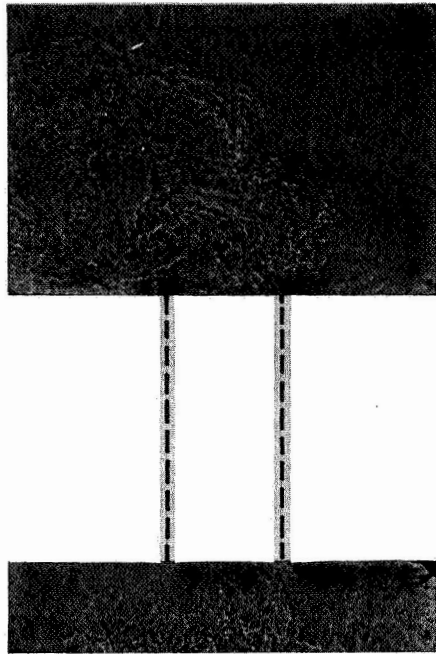
(7)

Figure 20



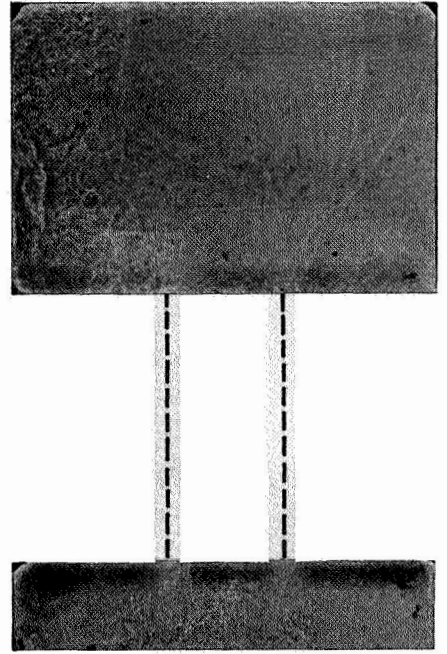
(8)

Figure 21



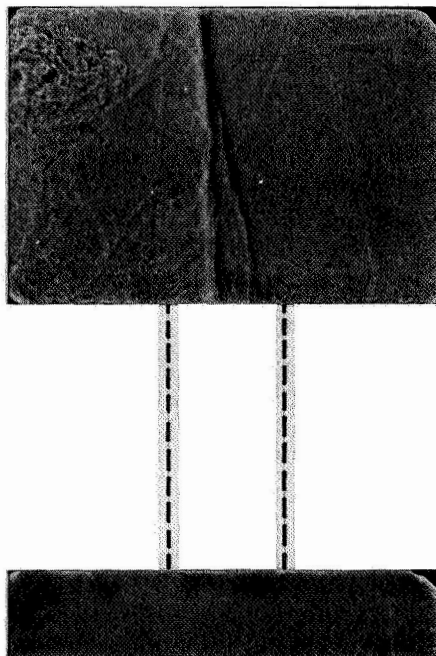
(9)

Figure 22



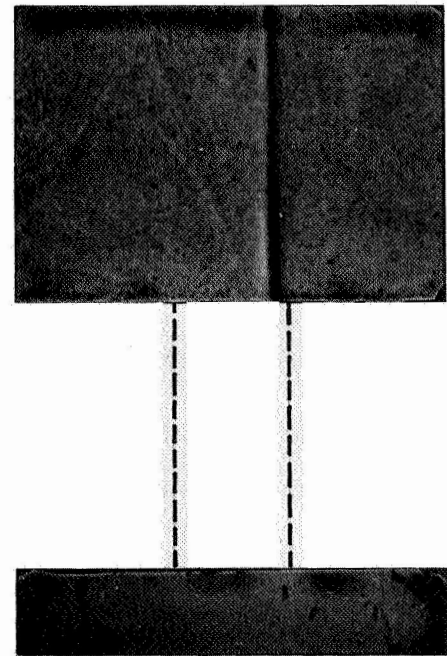
(10)

Figure 23



(II)

Figure 24



(II)

Figure 25

IV. ENERGY SOURCES

A. USE OF SHOCK WAVES TO STUDY COMBUSTION PARAMETERS

The purpose of this research, which was described in NASA CR 72270¹ and in NASA CR 72371, is to investigate the functional forms of the mass, momentum and energy sources in a combustion chamber. Thus the components in the liquid phase are visualized as sources (or sinks) for the components in the gaseous phase.

The usual way of performing such an investigation would be to solve a set of equations and then to compare the solution with experimental results. To follow this approach it is necessary to have as many equations as unknowns. Since the number of basic equations are always less than the number of unknowns, extra equations would be needed. These added equations would reflect assumed models for the sources to be investigated. Furthermore, a large number of equations would finally result and additional simplifying assumptions would generally be needed if they are to be solved. The final comparison between analytical and experimental results would not be too conclusive, particularly so if discrepancies between analytical and experimental results are found.

Another way of performing this investigation is to use directly the experimental results to determine some of the unknowns instead of adding extra equations. Thus one ends up with a smaller number of equations which satisfy "exactly" the experimental results. Moreover, having a smaller number of equations one can usually solve them more accurately. Solutions for the functional forms of the sources are found in this approach, instead of assumed and then verified. Thus in the direct use of measured parameters, one exchanges known information about these parameters for unknown information about the sources. This direct approach therefore requires a smaller number of assumptions, leads to fewer and simpler equations, and is more accurate.

We chose to follow this second, direct approach but unfortunately there are three sources (of mass, momentum and energy) and it is difficult to measure directly and completely three parameters. Thus it was necessary

to settle for a compromised approach. It may be noted that, in the direct approach, the accuracy and reliability of the measurements are very important, but, in principle, they are no more important than in the indirect approach.

Actually instead of directly measuring some combustion parameters, a shock can be induced in the combustion chamber and some of the shock parameters can be measured. Information on the combustion parameters can be gained by studying the propagation into the combustion chamber of this externally generated shock. Consider a long combustion chamber where one-dimensional steady-state, distributed combustion is assumed to occur. The parameters of a shock, started, say, at the nozzle end, will depend on the steady-state condition of the undisturbed gas ahead of the shock as well as on the changes of the combustion process which occur after the shock front. These changes are primarily due to the particle velocity induced by the shock if the shock is of moderate strength and droplet shattering is excluded.

More specifically, through the shock front the Rankine-Hugoniot equations hold regardless of whatever mass, momentum and energy additions (or subtractions) occur after the shock front. Thus the use of the Rankine-Hugoniot equations through the shock front together with the steady-state conservation equations for the undisturbed gas between the injector end and the shock front, can be applied to yield information on the steady-state combustion parameters. This part of the problem is here referred to, as the study of the "steady-state" combustion. On the other hand, suppose now that the steady-state parameters of the gas ahead of the shock front are known, together with the parameters of the shock front, and of the shocked gas at some initial time, then the values of these parameters could be calculated at any later time, if the functional forms of the mass, momentum and energy sources were known. Conversely, if three of these parameters were measured in their time and space domains, we could deduce the functional forms of the mass, momentum and energy sources. This part of the problem is here referred to, as the study of the "unsteady-state" combustion. We will measure only pressure and shock velocities, thus some extra assumptions will have to be

made. However, the goal is still that of deducing the functional forms of the sources based upon some directly measured parameters. Notice that before attempting solutions to the "unsteady" part of the problem it is necessary to solve for the "steady" part first.

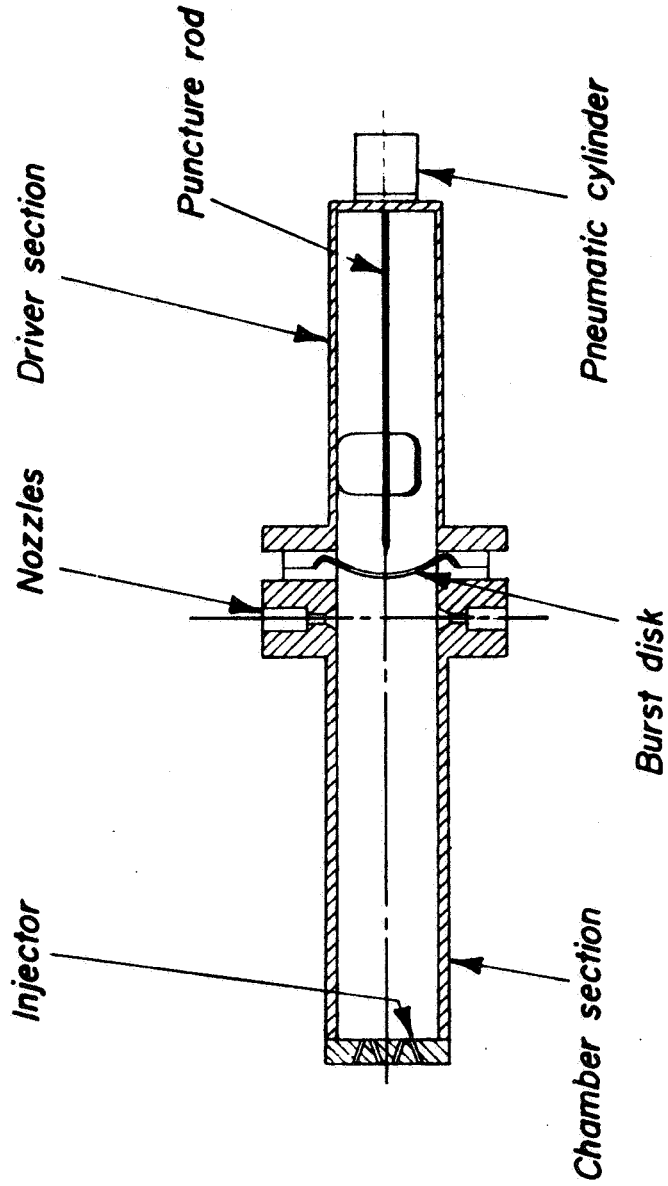
The results of the steady-state calculations will presently be discussed together with some considerations on the equations for the unsteady part. But first a brief description of the experimental set up.

The Experimental Apparatus

A liquid propellant rocket motor with square cross section (area equivalent to a circular section of 3-inch diameter) is the principal piece of test apparatus in this research. The motor is made up of sections which can be added so as to form a chamber up to more than 20 diameters in length. Transducers are then inserted at appropriate intervals with as many as six Kistler piezoelectric crystal transducers used simultaneously to record local pressures. Rocket tests are expected to be reproducible and they are checked for this property via repeated testing.

Further details of the design are as follows: the injector utilizes a 16-doublet, like-on-like design to produce axially-distributed combustion which is an important aspect of the investigation. The shock itself is produced by a shock tube^{*} mounted at the nozzle end of the chamber, facing the injector, with the nozzle consisting of 12 individual radially oriented nozzles (see Fig.26). The diameter of the shock tube is equal to the diameter of the motor so as to facilitate the generation of a simple planer shock front. Nitrogen is normally used as the pressurant in the shock tube. If the combustion chamber were filled with inert gases the shock generated by the shock tube would be an almost perfect step function moving at constant speed, however, with the combustion present the shape and velocity of the shock is altered. Through the study of these alterations we are attempting to infer the functional form of the sources due to the presence of the liquid propellants and of the combustion. Undoubtedly, the production and recording of the data which is required, with the accuracy which is necessary, is a difficult

* Pressures to 1500 psig have been used and together with thin stainless steel burst disks (.008 to .015 inches) the desired shocks are generated.



Shock tube combustion chamber for studies of combustion response

experimental task. Up to now the success has been limited, but encouraging.

The measurement and recording techniques, which have been necessary to obtain suitable data, are representative of the current state of the art. Pressure measurements require flush-mounted pickups with high frequency response since the waves to be measured are steep-fronted. The most successful approach has been the use of ablative coatings to protect the diaphragms of Kistler 603A transducers which possess a natural frequency in excess of 400 kHz.

Protection of Kistler-type piezoelectric transducers was first demonstrated by Rogero at JPL^{15,17}. The tests described here use similar arrangements with the addition of a water cooled-housing to prevent heat soak and to limit the thermal drift during short duration rocket firings and during any prerun temperature variations. The water passage simply surrounds the transducer to eliminate heat transfer paths other than through the ablative itself.

Side-mounting of the transducer in the square-motor allowed typical shock transient times greater than ten microseconds, which was a less stringent condition than the transient times of five microseconds or less on the wall of an actual rocket chamber. On -the-other-hand, the shock wave presented a waveform that was steeper than many of the wave shapes encountered in an unstable rocket. Although not a necessary condition for these tests, end-mounting presented the limiting situation of zero transient time (all portions of transducer face received the pressure signal simultaneously) and the wave was a steep-fronted shock of high strength. Based on these differences it was found in the tests that side-mounting of the transducers was far less critical than end-mounting from the standpoint of initial overshoot and cavity resonance. By cavity resonance, reference is to the cavity separating the transducer diaphragm from the chamber wall which has an associated frequency spectrum. The cavity resonance was evident in only the tests without ablative and using the .125 inch recess (this ablative thickness is routinely used on the transverse mode tests where the wave shape is often less critical from a measurement standpoint and the heat transfer environment is more

severe. The side-mounted, thick ablative coating still exhibited an initial overshoot of 20%, however, while the thin ablative and flush-mounted configurations experienced no overshoot when similarly mounted.

The ringing frequency of the transducer following the shock arrival was used as a measure of the natural frequency of each unit. The flush-mounted transducers provided the 400 kHz basis for comparison. The thin ablative coating indicated frequencies of 300 kHz while for the case of the thick ablative the transducer natural frequency was reduced to 90 kHz. These data are summarized in Table I.

The point to be made here is that even the thick ablative approach will be found to often possess better frequency characteristics than many typical transducer types and mountings. A 90 kHz natural frequency is still quite high when compared to many strain gage and capacitance-type transducers which are flush-mounted but require water-cooled diaphragms. Therefore in limited duration firings (less than five seconds) the use of suitable ablative coatings may prove to be highly beneficial - especially when analyzing higher modes, and nonlinear or shock-type waves.

One other transducer approach that has proven successful to researchers at the University of Michigan¹⁸ has involved the use of a ferroelectric element. Specifically, the use of lead metaniobate (with a tin backing rod designed for removal of the reflected wave within the sensor) is the basis for the transducer design. This approach is being carried along as an alternate. Testing has revealed the design to be less rugged than the Kistler transducers although the initial wave shape recording is quite good. Later testing may still require this approach.

Returning to the other principal factor in successful data collection, the recording system, the approach utilizes a Honeywell 7600 tape recorder. This equipment limits dynamic time displacement error between channels to less than ± 1 microsecond. Through the use of the optimum transient response filters in the 1 7/8 inch/sec playback, overshoot is reduced to a minimum level (order of 5%). The function of the double extended response mode allows an 80 kHz band width at a tape speed

of 120 inches/sec. and a small sacrifice in the signal-to-noise ratio (order of 3 db). Signal conditioning equipment of the charge amplifier type was specifically designed for these tests. The equipment is capable of conditioning the signals from a wider range of transducers than standard charge amplifiers (e.g., both the piezoelectric and ferroelectric transducer types can be accommodated). The history of the overall recording arrangement has been one of small improvements at a number of points in the system resulting in the final desired data.

Fig. 27 shows the pressure traces associated with the helium-filled chamber tests previously mentioned. Both time of arrival data and step amplitude are recorded to the desired accuracy. For comparison the same chamber with combustion taking place presents a somewhat different situation as shown in Fig. 28. The downstream pressure traces are very similar to the inert gas tests. However, as the shock wave moves into the region of greatest interest, that zone in which the major portion of the combustion is taking place, the step-like shape is considerably altered. Pressure is seen to rise following the passage of the wave and there are considerable pressure variations present. These variations are not because of transducer ringing or other instrumentation effects but are a function of location, and hence a function of the combustion conditions present.

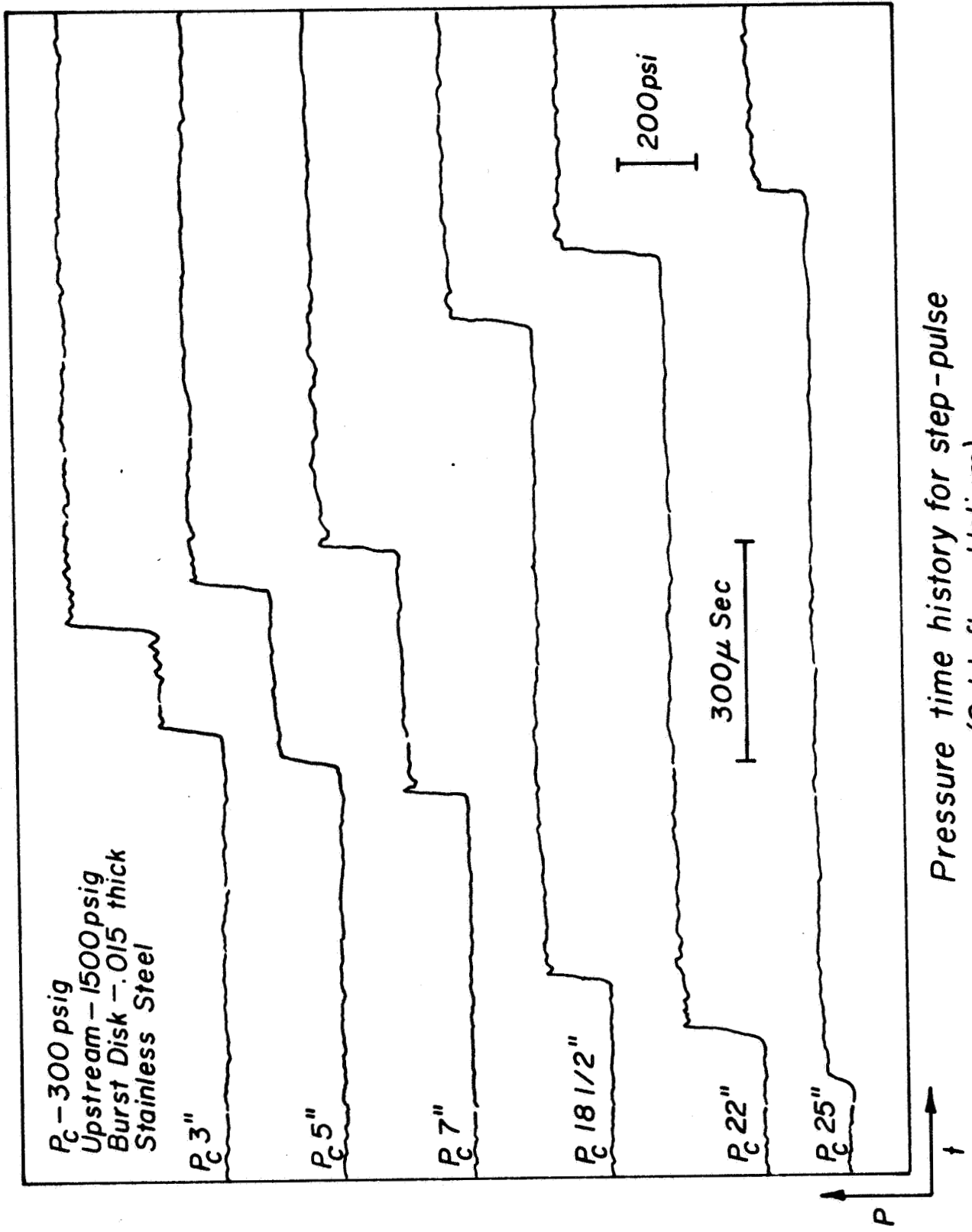
It is from records such as these, together with the theory presented, that the alterations from the ideal case will be analyzed and interpreted to explain the steady-state and finally the unsteady combustion phenomena.

Calculation of the Steady-State Combustion Parameters

In last year's progress report¹ (NASA CR 72270), equations were given which allow the calculation of the steady-state combustion parameters after having measured the static pressure in the combustion chamber and the velocity and overpressure of an externally induced shock wave. For the derivation of those equations it was assumed:

- 1) steady state between the injector end and the station of interest
- 2) one-dimensional flow

JP 21 R 4343-68



Pressure time history for step-pulse
(Cold flow - Helium)

Figure 27

JP 21 R. 4342-68

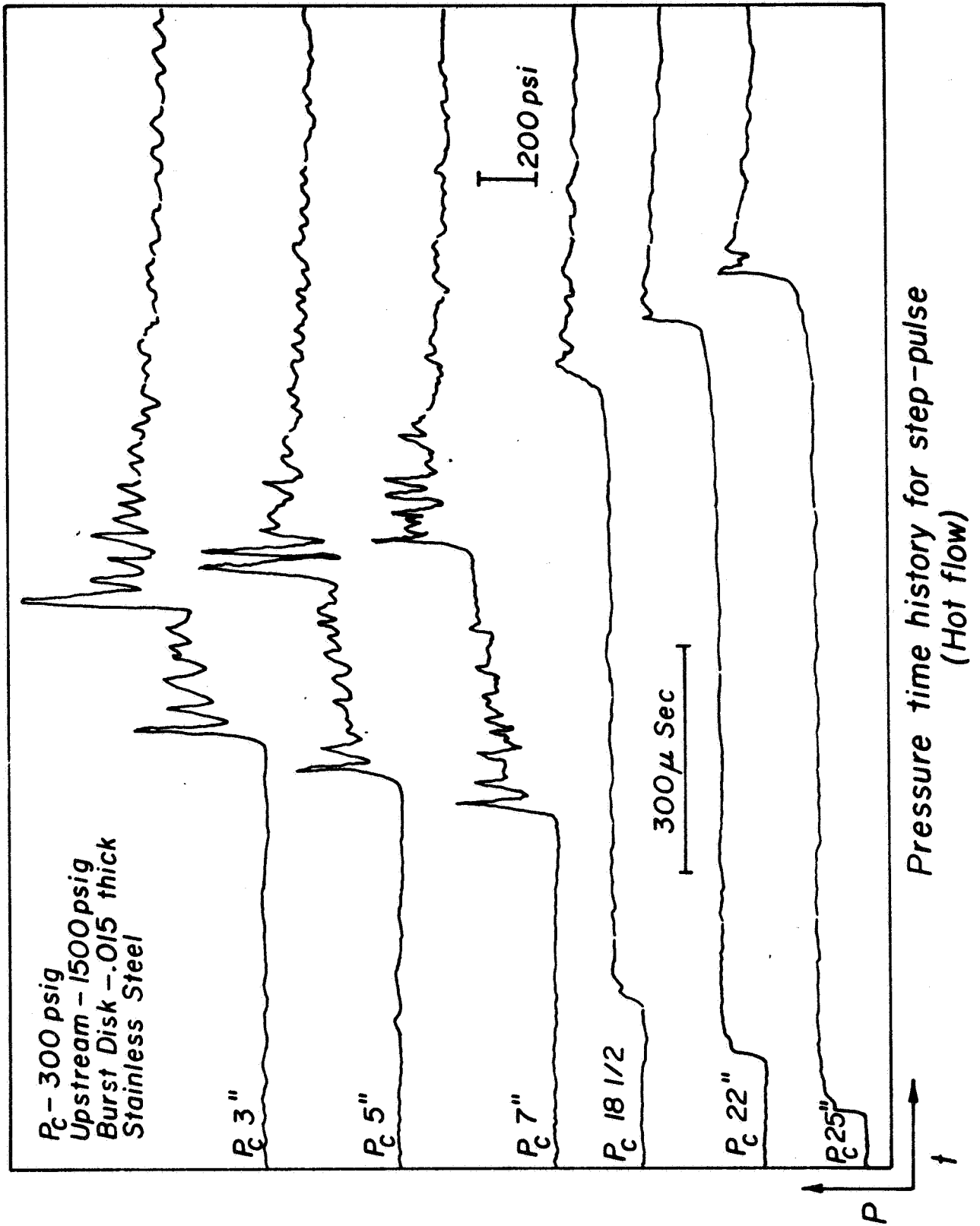


Figure 28

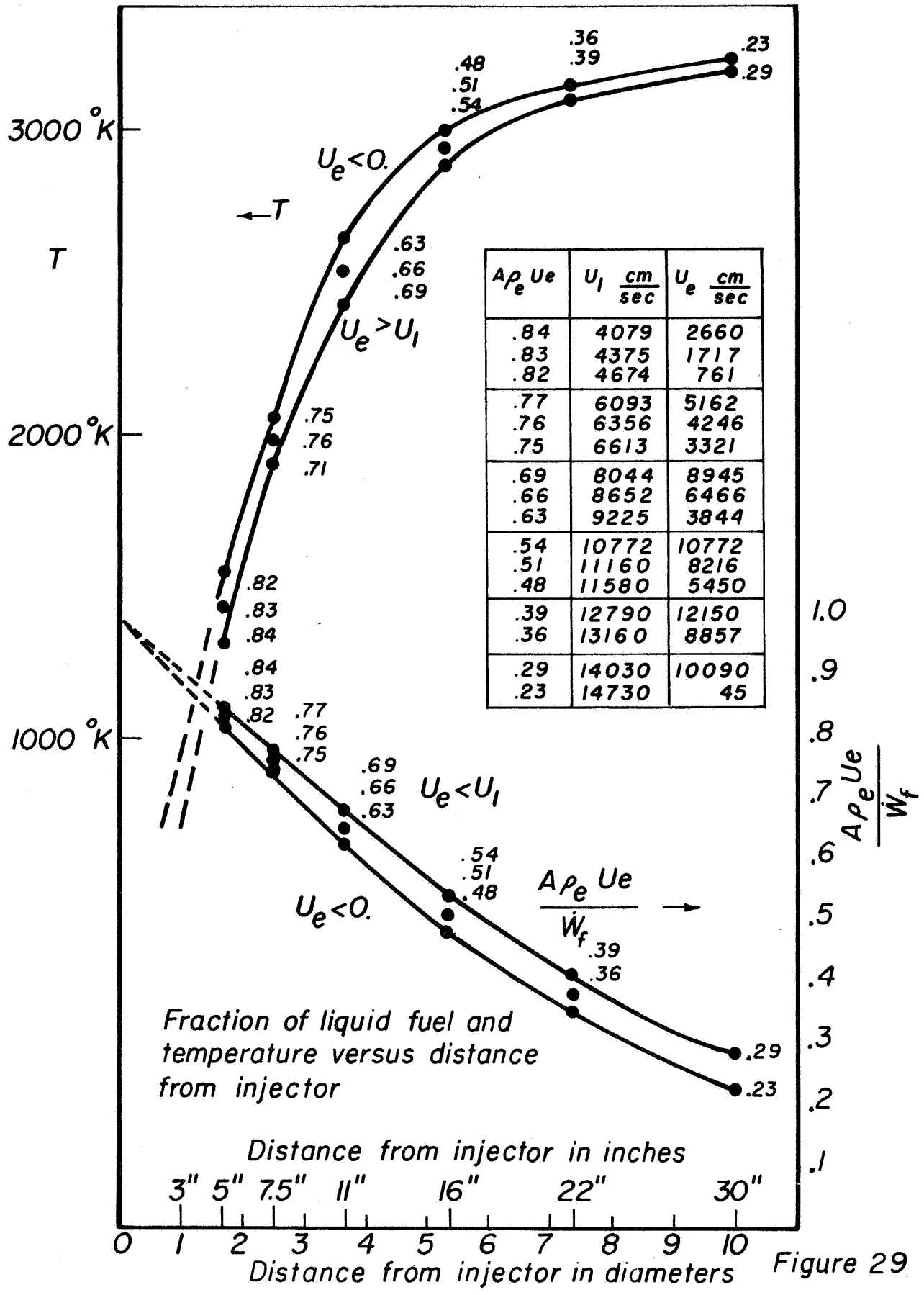
- 3) instantaneous vaporization of the oxidizer and distributed vaporization of the fuel
- 4) no change in the mass, momentum and energy of the drops through the shock front itself
- 5) plane shock front
- 6) boiling temperature of the fuel drops
- 7) instantaneous reaction of gaseous fuel and oxidizer to give equilibrium reaction products.

Notice that no droplet drag and evaporation model was assumed. The measured shock velocity and shock overpressure complete the system of equations, otherwise, two more relationships would have been needed.

Those equations are for a fuel-oxidizer system made up of C, H, O and the products are allowed to contain the following eight compounds: OH, CO, CO₂, O, O₂, H₂, H₂O, H. Since the eight combustion products are assumed to be in equilibrium before and after the shock front we have 16 chemical equilibrium equations, which added to the three conservation equations from the injector to the shock front, and to the three Rankine-Hugoniot relations through the shock front, give a total of 22 nonlinear algebraic equations to be solved simultaneously. The solution of the system presented some difficulty but finally it was achieved, however, not by the method indicated in last year's progress report.¹ The actual solution was accomplished by using, as a parameter, the factor $\rho_l u_l A$ which gives the mass flow per unit time of the liquid drops at any given station (ρ_l = mass of liquid per unit volume of the combustion chamber, u_l = average liquid velocity, A = cross section area of the combustion chamber). In this approach the shock velocity (U) is among the calculated parameters. We can then plot $\rho_l u_l A$ versus U for any given pressure ratio through the shock front. The measured U will then supply information as to the actual value of $\rho_l u_l A$ thus determining the entire solution. Actually the solution of the system is very sensitive to the value of $\rho_l u_l A$. Only within a narrow range of $\rho_l u_l A$ is the velocity of liquid less than the velocity of the gas and greater than zero. Hence the solution of the system is determined within an acceptable range even without the measurement of U . The measured U should then fall within the calculated range. The

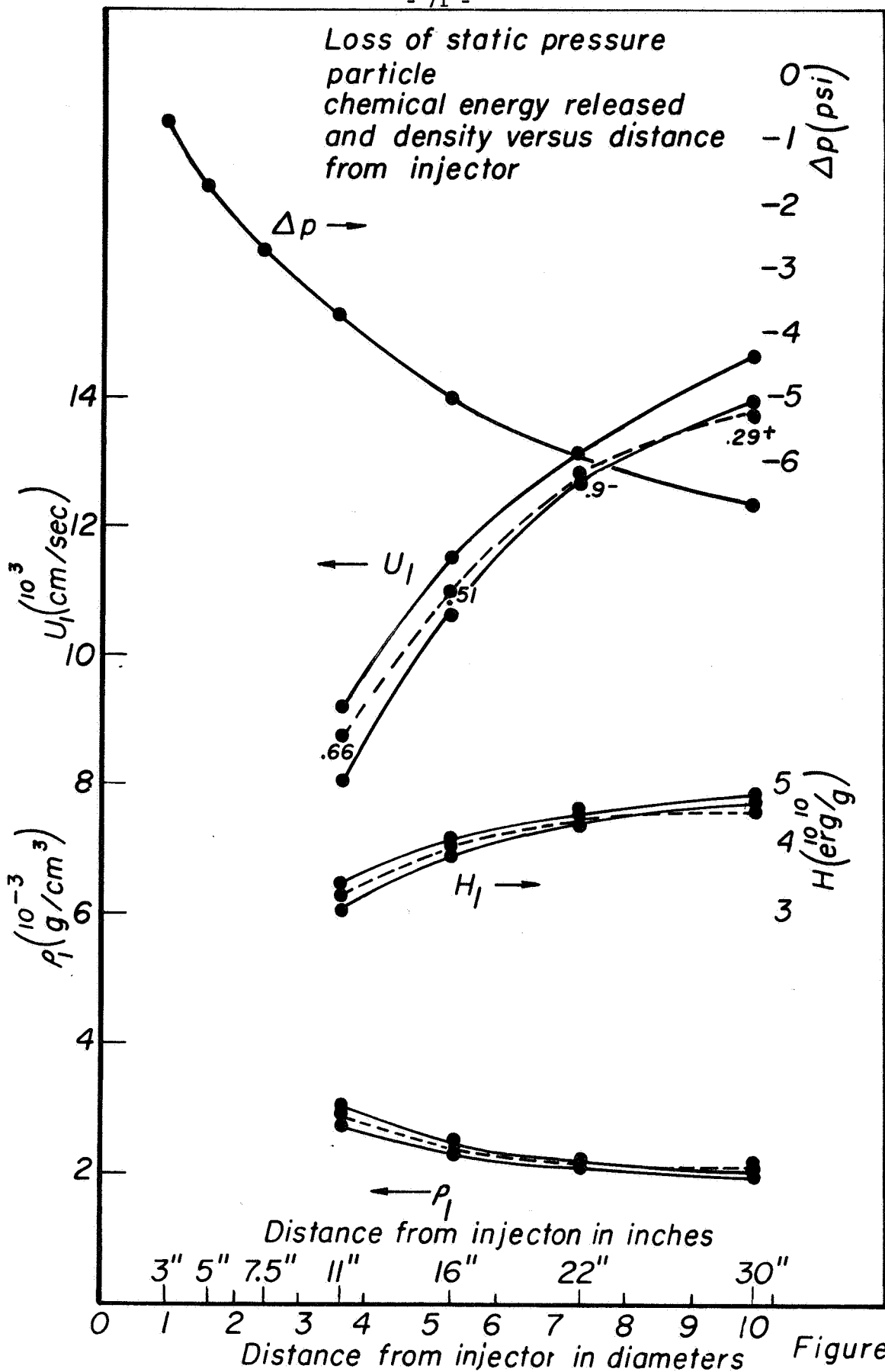
measured static pressure along the combustion chamber was also used directly to obtain the above solution. The reason for the leading role played by $\rho_e u_e A$ is its controlling effect in the energy equation. The amount of fuel in the liquid phase does not greatly influence the momentum equation. It influences the mass equation. But, most of all, it influences the energy equation since it controls the amount of chemical energy released and this, in turn, is what makes the entire engine work.

The results may be discussed with the help of Figs. 29 and 30. These data were calculated for ethyl alcohol and liquid oxygen; fuel mass flow = 428. g/sec ; oxidizer mass flow = 986 g/sec , and static pressure in the engine at the injector = 296. psi. In Fig. 29 the fraction of fuel still in liquid form ($A \rho_e u_e / \dot{w}_F$) is plotted versus the distance from the injector. In the table the values of the gas velocity (u_1) and liquid velocity (u_l) for each value of the above fraction are noted. For instance, at 30" from the injector the acceptable value of $A \rho_e u_e / \dot{w}_F$ ranges roughly between .29 and .23 . For .29, $u = 10,090$ cm/sec and $u_l = 14,030$ cm/sec ; for .23, $u = 45$ cm/sec and $u_l = 14,730$ cm/sec . It can be concluded, then, that $A \rho_e u_e / \dot{w}_F$ cannot be much less than .23, otherwise the liquid would be moving toward the injector. This term cannot be much more than .29, otherwise the liquid would be moving faster than the gas at a distance of 10 chamber diameters. Similarly, the other acceptable values of the combustion parameters vary in narrow ranges. We have already seen that u_1 must be roughly between 14,030 and 14,730 cm/sec . From Fig. 29 we see that the temperature (T) must be between 3199°K and 3236°K . The selection of the exact value of $A \rho_e u_e / \dot{w}_F$ is to be made by the measured shock velocity for a given shock front over-pressure. From a practical viewpoint, the values of the acceptable shock velocity also varies in a narrow range (within the limit of the experimental error) and therefore it is then only necessary to verify that the measured velocity is compatible with the calculated one. In Fig. 30 we have the measured static pressure loss which was used directly in the calculations, and the approximate acceptable ranges for the values of the gas velocity (u_1) , the gas density (ρ_1) and the chemical energy



JP21 R 4330 - 68

Figure 29



JP 21 R 4331 - 68

Figure 30

released per unit weight of the combustion products (H_1). The dashed lines within the ranges are the likely values under the assumption that the velocity of the liquid drops approach the gas velocity as the distance from the injector increases.

The most important of the findings is that one (or more) of the stated assumptions is not valid for the region between the injector and about 3 or 4 diameters from it. It was assumed that the oxidizer vaporizes immediately and completely (Assumption 3) and that instantaneous reaction of the gaseous fuel to equilibrium combustion products occurs (Assumption 7). Thus, very close to the injector, a very low calculated temperature was expected, since there the fuel to oxidizer ratio is very unfavorable. We expected this region to extend out to, perhaps, one diameter from the injector and we were ready to accept the failure of the model in this region. In other words, we expected the temperature curve of Fig. to be shifted to the left by approximately two diameters. The actual findings are in contradiction with expected ones for a distance from the injector too long to be acceptable. A critical review of the 7 assumptions made, in the light of the theoretical and experimental results indicates that Assumption 1 is verified, Assumptions 4, 5 and 6 are not very influential so that one or more of Assumptions 2, 3 and 7 should be responsible for the calculated results. It is felt that the assumption of immediate vaporization of the oxidizer (Assumption 3) is the weaker one. Since some fuel is calculated to exist in liquid form even at 10 diameters from the injector, it is not unreasonable to expect some oxidizer to exist in liquid form out to 3 or 4 diameters from the injector.

Accordingly, we have modified our equations to account for the presence of liquid oxidizer in the vicinity of the injector. We have assumed that the average velocity of the liquid oxidizer is equal to that of the liquid fuel and we have added a new variable, expressing the mass of liquid oxidizer per unit volume of the combustion chamber. Then one more quantity needs to be measured. We are now using two shocks, one from the nozzle and one from the injector. Measurements of these shock velocities and overpressures are sufficient to obtain solutions to this

case involving liquid oxygen near the injector. However, it turns out that it is not convenient to solve the new set of equations for the expected values of the experimental results and then to select the actual solution later (as it was done for the no-liquid-oxidizer case). We must wait for sufficient experimental results before performing this second calculation. The solutions given in Figs. 29 and 30 are still expected to hold for distances from the injector greater than 3 or 4 diameters.

Other interesting steady-state results are:

- 1) If the static pressure drop from the injector to any station is taken to be of order 1, then the change of momentum of the gas between the injector and that station is of order 1 and the change of momentum of the liquid is of order 10^{-1} (combined effect of drag and vaporization). In other words, for the calculation of the steady state the influence of the liquid in the momentum equation of the gas is negligible: changes of momentum of the gas are balanced almost exclusively by changes in static pressure.
- 2) The factor $A \rho_e u_e$ is determinable due to its strong influence on the energy equation while ρ_e and u_e cannot be determined due to their weak influence on the momentum equation.
- 3) The energy source is a function of the mass source of the local fuel to oxidizer ratio and of the local temperature. Local fuel to oxidizer ratio and local temperature are then related to each other through the hypothesis of chemical equilibrium.
- 4) γ (ratio of specific heats) varies along the chamber approximately from 1.27 (near injector) to 1.22 (far from injector).
- 5) If the local speed of sound is calculated with $\sqrt{\gamma p/\rho}$, even using the local γ , the error might be as high as 10% due to having neglected the chemical processes.

6) The chemical energy released (H_1) is approximately redistributed as follows:

65% internal energy (warming up of the combustion products from the liquid temperature to the combustion chamber temperature)

20% mechanical work (p/ρ)

7% vaporization of fuel

7% vaporization of oxidizer
kinetic energies of the gas and of the liquid
are negligible

Summary

In conclusion, two sets of equations were developed for the computation of the steady-state combustion parameters using directly measured values of overpressure and velocity of an externally induced shock wave. One set of equations is valid for regions where only liquid fuel is expected to be present. This set of equations can actually be solved without experimental data and such data can then be used a posteriori. A specific set of solutions are presented in Figs. 29 and 30. Although complete experimental data have not yet been collected, preliminary experimental data fall in the expected calculated range. The second set of equations is valid for regions where both liquid fuel and liquid oxidizer are expected to be present. For the use of this second set, experimental data must be available a priori. We are presently gathering these experimental data. However, this second set of equations has already been solved using assumed values for the variable to be measured. To complete the steady-state solution it will be necessary to gather sufficient experimental results, and these tests are presently in progress.

The study of the unsteady-state has also been initiated. Great effort has been concentrated in the selection of the proper set of assumptions and of equations in the light of the preliminary results of the steady-state portion and of experimental data. It should be evident that final solutions are meaningful only if consistent assumptions and proper equations are used. We are presently nearing the end of this

selection process. The next step will be the solution of the selected set (or sets) of equations. Simultaneously, experimental data for the unsteady part of the problem will continue to be gathered. Perhaps the most severe experimental problem encountered in recent weeks has been the occurrence of spontaneous instability because of the reduced damping associated with the radial nozzle, shock tube design. The limited use of acoustic dampers at the nozzle section has already been shown to be highly successful in eliminating this problem.

B. CHEMICAL KINETICS AS A DRIVING MECHANISM FOR LIQUID PROPELLANT ROCKET COMBUSTION INSTABILITY

The Combustion Process and Combustion Instability

It is widely accepted that high-frequency combustion instability consists of organized oscillations of the properties within the chamber, which are maintained and amplified by the combustion process itself. The combustion chamber gases are put into a forced oscillation driven by the combustion process interacting with the resonance effects of the chamber geometry. The resulting oscillation patterns are very similar to those of the acoustic modes of the chamber.¹¹ Thus, there seem to be coupling mechanisms between the combustion process and the acoustic properties of the chamber which can organize and amplify random perturbations into periodic oscillations and then maintain these organized oscillations at a significant amplitude. Questions arise as to the nature of these coupling mechanisms involving the combustion process: how they organize and drive the oscillations, and which phase of the complex combustion process they are associated with.

The "combustion process" in a liquid propellant rocket engine involves everything that happens to the propellants between the instant they are injected into the chamber and the moment conversion to gaseous products is completed. Involved are atomization, vaporization, mixing, burning, recirculation, and many other steps. Since it is the chemical reaction of burning (fast oxidation) that supplies all of the energy generated within the chamber, it seems logical that this process also

supplies the energy for the organized oscillations of instability. The problem is how this energy release is related to the organized acoustic-mode oscillations.

The rate of energy release depends on the rate of chemical reaction. For example, if the rate of the reaction - the kinetics - varied periodically, so would the rate of energy release. Such effects, involving when and where energy is released in the chamber, could have direct bearing on the nature of the oscillations produced. It was felt that further study of the nature of a kinetic coupling mechanism should be conducted to provide a fuller understanding of combustion instability and of the combustion process itself.

Joint Study

During the past year, a program has been implemented at Princeton to investigate such an assumed coupling. This program attempts to determine what relationship, if any, chemical kinetics has with combustion instability associated with liquid propellants, and the nature of that relationship with regard to factors such as phasing and amplitude.

Because this investigation would study both the combustion process and combustion instability, it was implemented by both the Combustion Group, under Professor Glassman, and the Liquid Rocket Group, under Professor Crocco and Mr. Harrje, as a joint project. The essence of the investigation, then, is to combine both avenues of research, combustion processes and liquid rocket instability, to glean a broader knowledge in areas of common interest.

The Combustion Group has had much experience in pure kinetic studies. One important piece of equipment developed by that group is the flow reactor which is being used in fundamental studies of oxidation (combustion) reactions. The reactor spreads out the oxidation reaction in both time and space, thus allowing precise measurements of kinetic data. Hydrazine and nitrogen tetroxide oxidations have been studied extensively, and hydrocarbon studies are just beginning. Also the Group is studying combustion instability in a gas rocket, where all liquid

effects and changes of state are nonexistent. Thus the combustion process is much simpler, and the kinetics are exposed for study without the added complexities of atomization, vaporization, etc. The Liquid Propellant Rocket Group provides rocket test facilities and long experience in the study of combustion instability in liquid propellant engines. It was felt that a combination of these three methods of investigation in order of increasing complexity - reaction kinetics, gas rocket instability, and liquid rocket instability - would carry the study step-by-step to a useful conclusion. What would be learned from each step could be applied to the next one to advance knowledge in a systematic manner. A unified treatment could be achieved because the same chemical systems could be studied from each point of view, and data from one approach would be directly applicable to the others.

Methane-Oxygen Propellant System

The investigation has begun with the simplest hydrocarbon propellant system: methane (CH_4) and oxygen (O_2). In addition to the propellant simplicity, this propellant combination is related to the hydrocarbon fuels previously tested in the instability research, and possesses performance characteristics that make it an attractive choice for future propulsion applications.

Concerning the interrelated studies, the flow reactor has just undergone extensive modifications; its first investigation will be the kinetics of methane oxidation. (The modifications were necessary because of the unusually long induction time - * of methane compared with other hydrocarbons and other compounds, such as alcohols.) Some experimental work has been done with gas rocket instability of methane-oxygen propellants ¹⁹ and more is planned. Thus the kinetics and gaseous combustion of methane should be further clarified within the near future. The liquid propellant rocket facilities have been modified so that methane may be used as a propellant. The methane-oxygen system in the liquid program becomes, of course, liquid methane-liquid oxygen. We shall abbreviate this propellant combination as LOX/LCH₄. Both substances in their liquid forms are cryogenics. The normal boiling point of LCH₄ is

* the delay between injection and reaction initiation

- 259°F (201°R). Its freezing point is - 298°F (162°R), so its liquid range is small. This causes a number of difficulties in its use.

From the particular point of view of the liquid rocket test program, the LOX/LCH₄ propellant system offers an additional check of present theoretical models, and a further tool for unraveling experimental mysteries. The double-cryogenic propellant combination offers a new system to study from an n - ζ standpoint, and further investigation of the velocity effects model of transverse instability.^{11,20} Also, this system provides a firm base on which to begin kinetics studies in the rocket motor and to investigate the puzzle of the direction of spin of transverse modes of instability.

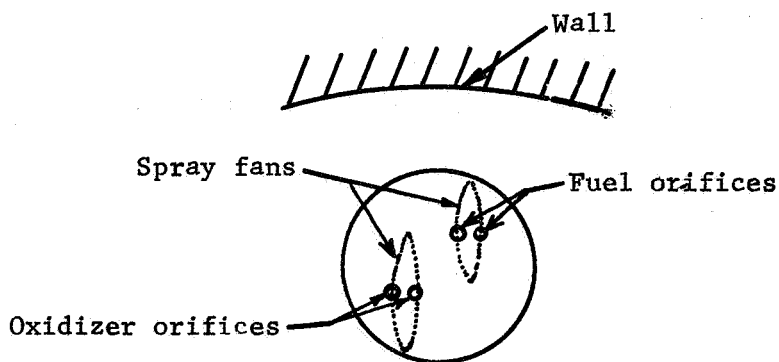
Spin Direction Dependency Upon Fuel

It was decided that the point of departure of the experimental program would be an interesting series of previous tests concerned with the spinning first tangential (1T) mode of instability: it had been found that for two different propellant combinations, liquid oxygen and RP-1, and liquid oxygen and ethyl alcohol, the directions of spin of the 1T mode were different. The spin directions were in opposite directions for the two propellant systems; that is, with the same injector-chamber configuration, one system had instability spinning clockwise, while the other system had instability spinning counterclockwise³. These results were repeatable, and evidently they represented characteristics of the propellant systems. Here, then, was an effect that clearly might be related to the combustion kinetics. Therefore, the investigation was begun at this point in an effort to discover the reason for such an effect due to propellants.

Nomenclature

It will be helpful to introduce some nomenclature at this point. Liquid oxygen is abbreviated LOX, and ethyl alcohol is abbreviated ALC. F stands for fuel; O stands for oxidizer. The injector used the "spud" design with each spud containing injection orifices. The spuds could be like-on-like impinging (L-L) or unlike impinging (U). An L-L spud has

two pairs of holes, one pair for fuel, one pair for oxidizer. The spray fans formed by the impinging liquid streams overlap. The line of centers of the orifices may be oriented tangentially (T), or radially (R), with respect to the chamber geometry. The fuel orifices are placed nearer the wall because of heat transfer considerations. The pairs of orifices must be displaced because of manifolding requirements. A typical L-L, T spud is shown below



SPUD ORIENTATION

A bar is placed over the F to indicate that the fuel orifices were nearer the wall: \bar{F} . The direction of spin of the instability is noted by the order in which the pressure wave crosses the respective orifices: $O \rightarrow F$ (clockwise) or $F \rightarrow O$ (counterclockwise).

Previous Testing and Planned Program

The results of the previous tests on spin direction had been the following: LOX/ALC spun $O \rightarrow F$; LOX/RP-1 spun $F \rightarrow O$.³ It was reasonable to presume that kinetics could have something to do with the spin direction because ethanol and RP-1 are fundamentally different types of molecule. Ethanol is an alcohol, with the specific functional group hydroxyl; RP-1 is a mixture of hydrocarbons with no functional groups. But not only simple chemical differences exist between these two substances. There is a considerable difference in molecular structural complexity, and therefore presumably, other than chemical differences exist between them. These differences could be minimized by using a hydrocarbon

and its corresponding alcohol, methane and methanol, ethane and ethanol, for example, as fuels. Thus, a better assessment of the importance of the functional group could be made. Additional tests could then be made with other fuels, with chemical properties changed step-by-step by chain lengthening and side chain addition. Hopefully, this series of tests would isolate the chemical effects and their influence on instability by correlating changes in instability pattern with changes in fuel system. Clarification of the coupling mechanism would be further enhanced if variations in physical properties associated with the combustion process; e.g., surface tension, heat capacity, boiling point, and heat of vaporization, were minimized.

Liquid Methane Facility Modification

Since the first series of liquid rocket tests were made using the LOX/LCH₄ propellant system, the first requirement was the modification of the liquid propellant rocket test facilities for use of liquid methane fuel. Liquid methane is cryogenic, and while the facility had for many years used cryogenic liquid oxygen, a cryogenic fuel presented additional problems. The boiloff gases are combustible with the ambient air, and their low density allows them to collect in pockets near ceilings if care is not taken in the same manner as with liquid hydrogen.

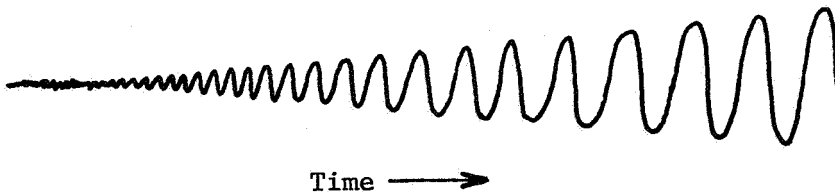
The liquefaction of the methane and its storage in liquid form presented problems also. To buy liquid methane would not only be expensive but also inconvenient from a delivery and storage standpoint. It was decided to buy gaseous methane and then liquefy it at the facility. This decision required the design and construction of a methane condenser with adequate capacity for the projected use rate of methane. A simple coiled tube, through which gaseous methane is flowed, is immersed in a bath of liquid nitrogen. This arrangement provides ample liquid methane, and at a factor of four savings over commercial purchase. Even so, the liquid methane costs about \$2.50 per pound, so it cannot be wasted. A vacuum-jacketed pressure tank is used for runs, and it is able to store liquid methane for sufficient periods of time. The tank temperature is controlled by flowing liquid nitrogen into the vacuum jacket and then

draining when the tank is cold enough. Because the liquid methane is so expensive, liquid nitrogen is used for all other cooldown operations as well. Since liquid nitrogen is cold enough to have the capability of freezing liquid methane, care must be taken during the condensation process that the methane flow rate does not become too low. It appears that all problems with the liquefaction process, cooldown, and storage have now been solved. Routine procedures have been developed for every phase of the operation.

Results of First LOX/LCH₄ Tests

So far, thirteen runs have been made with the LOX/LCH₄ propellant system. Four injector configurations have been used, and a three-blade baffle was added to three of them. Mixture ratios varied between about 1.9 and 4.0; this range corresponds to a range of equivalence ratios ($r/r_{\text{stoichiometric}}$) between 0.5 and 1.0. Chamber pressure was nominally 150 psia.

All tests showed spontaneous instability growing out of the combustion noise. The oscillations began randomly, with essentially zero magnitude and organized into periodic oscillations while the amplitude increased to significant values. The growth of a typical oscillation can be schematically pictured as



The oscillations always began smoothly; there never appeared any pulse or spike which might have triggered them.

The mode was mostly the first tangential (1T) spinning mode, although four runs showed basically 2T modes. These four runs employed a three-bladed baffle. The spin direction was always $\vec{F} \rightarrow 0$. This spin direction characteristic of LOX/LCH₄ is the same as the direction pre-

ferred by LOX/RP-1, and opposite to that of LOX/ALC. Note that both RP-1 and methane are hydrocarbons. Thus their similar behavior, as contrasted with that of alcohol, is not surprising.

Four runs showed mixed modes, with basically 2T mode, and frequencies higher than the 2T superimposed over it. The instability damped out of its own accord in four other runs in which the three-blade baffle was used. In one run, the motor was pulsed in the $0 \rightarrow F$ direction; however, after the pulse decayed, the instability returned to its original direction, $F \rightarrow 0$, with about the same amplitude as before.

Peak-to-peak amplitudes ranged between 20 psi and 420 psi, the magnitude depending on the injector system and the presence of the baffle. There appears to be no correlation between either amplitude or frequency and mixture ratio; rather, both appear to correlate with the injector-baffle system.

The first four runs, 2227-2230 were made with a 1 x 16 like-on-like impinging doublet injector in the tangential orientation. In the past, this injector has exhibited stable operation with the ability to produce nonlinear instability with other propellant systems. All instability in these tests was spontaneous, in the 1T spinning mode in the $\bar{F} \rightarrow 0$ direction. The instability did not damp out. The corresponding amplitudes and frequencies are detailed in the table to follow. These amplitudes and frequencies are given for well-developed instability: as the instability grows out of the noise, its amplitude and frequency normally increase together until they reach roughly fixed values.

The next four runs, 2238-2241, were made with a 6 x 2 mixed spud injector, alternating groups of two spuds with like-on-like impinging doublets with groups of two spuds with unlike impinging doublets. A three-bladed baffle was also used. Again, instability was spontaneous, and it did not damp out. It was of the spinning type, $\bar{F} \rightarrow 0$, but the mode was mixed. The mode was mostly second tangential, but higher frequency modes were superimposed over that, often obscuring it. A pattern of development of these higher frequencies was noticed. When the mode

was primarily 2T, at the beginning of the run, it was usually of higher frequency, and when the higher overtones became prominent, the 2T frequency decreased. Amplitudes varied with the frequency, as shown below.

The following three runs, 2242-2244, were made, again with the three-bladed baffle, but with a 1 x 12 like-on like impinging doublet injector. This injector has shown more stable operation than the 1 x 16 injector in the past. Instability was still spontaneous, but in these runs, it damped out by itself before the end of the run, and the remainder of the run was stable. The mode was 1T, spinning, $\bar{F} \rightarrow 0$. The frequencies were all around 2500 cps, and the maximum amplitudes were all around 40 psi. Damping took 0.34 to 0.53 second after reaching maximum amplitude. The damping times were about ten times as long as the times taken for the instability to develop fully.

The last two runs, 2245 and 2246, were made with the 1 x 12 like-on-like injector from the annular motor. This injector uses recessed doublets with a smaller impingement angle¹ and is extremely stable, with associated lower performance. The three-bladed baffle was again used. The instability was spontaneous in the 1T, spinning $\bar{F} \rightarrow 0$ mode, but it attained an amplitude of only about 25 psi and a frequency of around 2000 cps. Run 2245 damped out very quickly, in about 70 millisecc. after reaching full development. Run 2246 was pulsed with the gun in the $0 \rightarrow F$ direction. Before the pulse, it had been spontaneously unstable in the $F \rightarrow 0$ direction. After the pulse, it resumed its $F \rightarrow 0$ direction at about the same amplitude. It seemed to begin damping toward the end of the run.

The results of these tests are conveniently summarized in the following table. Question marks in the \bar{F} column indicate that the mixture ratio was unknown due to a malfunction of the metering system, which could not be repaired once a series of tests was in progress. The value entered is the desired quantity. The true value was probably fairly close. Question marks in the Frequency column indicate that analysis was difficult because of the mixed modes.

Run No.	F	Injector	Baffle	Instability Mode	Frequency cycles/sec	Amplitude psi	Direction		
							Direction	Pulse	Damping
2227	3.1?	LX16 L-L, 1.4, 0.2", T	NONE	SPONTANEOUS 1 T	2600	330	F → 0	NONE	NONE
2228	2.0?	LX16 L-L, 1.4 0.2", T	NONE	SPONTANEOUS 1 T	3100	140- 170	F → 0	NONE	NONE
2229	3.24	LX16 L-L, 1.4 0.2", T	NONE	SPONTANEOUS 1 T	3200	250	F → 0	NONE	NONE
2230	3.55	LX16 L-L, 1.4 0.2", T	NONE	SPONTANEOUS 1 T	2600- 3000	425	F → 0	NONE	NONE
2238	3.1?	6X2 Mixed, 1.4 0.2", T	3-Blade	SPONTANEOUS 2 T	3300	40	-	NONE	NONE
2239	3.1?	6X2 Mixed, 1.4 0.2", T	3-Blade	SPONTANEOUS Mixed 1 T	2400	60	-	NONE	NONE
2240	2.0?	6X2 Mixed, 1.4 0.2", T	3-Blade	SPONTANEOUS 2 T	3900	60	-	NONE	NONE
2241	4.0?	6X2 Mixed, 1.4 0.2", T	3-Blade	SPONTANEOUS Mixed 1T, Mixed	4800 ? 3350-3500 3700 3000 2550	100-150 20 40 75 60	-	NONE	NONE
2242	2.0?	LX12 L-L, 1.4 0.2", T	3-Blade	SPONTANEOUS 1 T	2600	40	F → 0	NONE	Complete, but slow
2243	3.1?	LX12 L-L, 1.4 0.2", T	3-Blade	SPONTANEOUS 1 T	2500	35	F → 0	NONE	Complete but slow
2244	4.0?	LX12 L-L, 1.4 0.2", T	3-Blade	SPONTANEOUS 1 T	2600	40	F → 0	NONE	Complete, but slow
2245	2.09	LX12 Annular L-L, T	3-Blade	SPONTANEOUS 1 T	2200	23	F → 0	NONE	Complete, and fast
2246	3.09	LX12 Annular L-L, T	3-Blade	SPONTANEOUS 1 T	1800	25	F → 0	0 → F	NONE ?

LOX/LCH₄ PROPELLANT SYSTEM, 9-inch MOTOR, RUN DURATION ≈ 1 second

Analysis and Conclusions

The liquid oxygen-liquid methane propellant system obviously has a high tendency toward instability. Every test so far has shown linear instability spontaneously growing from combustion noise into organized oscillations. In all tests, the transverse instability appeared in the spinning form, and the direction of spin was always $F \rightarrow O$. This spin direction is evidently characteristic of LOX/LCH₄, and strongly preferred by it, as shown by the inability of a pulse from the opposite direction to reverse the spin. The $F \rightarrow O$ tendency overcame the applied pulse direction to return to its original direction. The mode, frequency, amplitude, and damping observed seemed to be dependent upon the injector used and the presence of the baffle. Thus the characteristics of the propellant system alone are taken to be the spontaneity of instability, its appearance in spinning form, and the direction of this spin. These are the factors which may be compared with those of other propellant systems to determine which part the combustion process plays in driving instability.

A comparison may be made between these results and previous results obtained in the same motor with two other propellant systems, LOX/RP-1, and LOX/ALC. All three series of tests used the tangential spud orientation. Hence, all the systems were sensitive to the mixing effects of the tangential velocity associated with the spinning wave.¹¹ The tangential velocity effects are always present in spinning modes. The velocity effects referred to here involve movement of one propellant relative to the other, thus setting up regions of unequal mixture ratio which therefore have different energy release rates. That propellant which vaporizes more easily is more likely to be moved relative to the other, for the gaseous component of the propellants will respond most readily to pressure and velocity perturbations. This effect is intensified if the vaporization rate of the second propellant is so slow that its droplets are still very large and thus are not carried along with the gases. It is possible that this effect helps to determine the spin direction. Accordingly, vaporization data for LOX, RP-1, ethanol, and liquid methane are presented on the next page.

PROPERTY	LOX	ETHANOL	RP-1	LCH ₄
Normal Boiling Point, °K	90	351	490	111
Thermal Conductivity $\frac{\text{Btu}}{\text{hr ft } ^\circ\text{F}}$	0.08	0.094	0.077	0.11
Heat Capacity Btu/lbm °R	0.41	0.60	0.5	0.85
Heat of Vaporization, $\frac{\text{Btu}}{\text{lbm}}$	92	362	125	219
Spin Direction	-	O → F	F → O	F → O

Notice the low boiling point of liquid oxygen, and its small heat capacity. Therefore, it will reach its boiling point very quickly, and its low heat of vaporization assures that it also will vaporize quickly. For these reasons, one can confidently predict that in any propellant system involving LOX and one of the listed fuels, the LOX will vaporize first, and leave the fuel in droplet form in the oxidizing atmosphere.

Grouping the fuels on the basis of heat of vaporization seems about the only way to handle them. The other properties are too widely divergent. Both of the hydrocarbons, RP-1 and LCH₄ can be placed in some sort of intermediate category based on heat of vaporization. The heat of vaporization of ethanol is very much larger than those of the hydrocarbons. Therefore, if the heat of vaporization is controlling the direction of spin instability, then the two hydrocarbons, having roughly similar heats of vaporization, would be expected to behave in a similar manner, which has been shown. Ethanol, having a very different heat of vaporization, behaves differently, as expected. These differences in

heat of vaporization might affect the sign of the velocity index, which determines the direction of spin of the wave. (The wave spins in the positive direction.)

A further attempt at analysis may be made by considering some of the chemical properties of the fuels, specifically, their combustion traits. Not much data are available at the present time, but more should be forthcoming as soon as the kinetic flow reactor studies get underway.

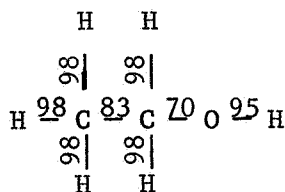
Again it is found that the hydrocarbons may be classed together, apart from alcohol, in oxidation characteristics. The more fundamental data of bond strengths is first considered. All values of bond strength are approximate.

SUBSTANCE	MOLECULE	BOND	STRENGTH, $\frac{\text{k cal}}{\text{mole}}$
ethanol	$\begin{array}{c} \text{H} \quad \text{H} \\ \quad \\ \text{H} - \text{C} - \text{C} - \text{O} - \text{H} \\ \quad \\ \text{H} \quad \text{H} \end{array}$	C - O H	70
		O - H	95
methanol	$\begin{array}{c} \text{H} \\ \\ \text{H} - \text{C} - \text{O} - \text{H} \\ \\ \text{H} \end{array}$	O - H	100
methane	$\begin{array}{c} \text{H} \\ \\ \text{H} - \text{C} - \text{H} \\ \\ \text{H} \end{array}$	C - H	101
ethane	$\begin{array}{c} \text{H} \quad \text{H} \\ \quad \\ \text{H} - \text{C} - \text{C} - \text{H} \\ \quad \\ \text{H} \quad \text{H} \end{array}$	C - H	98
		C - C	83

Data taken from Handbook of Chemistry and Physics, and Pauling The Nature of the Chemical Bond.

The table on the preceding page of bond strengths will at least give a relative idea of how the molecule will begin to react in a high-temperature environment. The weaker bonds will be broken first, and the molecule will probably react by that route rather than by another one requiring the breaking of a stronger bond. Also, an idea of the relative ease of reaction (oxidation in this case) of different molecules may be obtained by comparing the strengths of their bonds, and in particular, their weakest bonds.

Consider ethanol. The strength of its bonds are shown below for easy comparison:



Ethanol will react most readily by a route which involves breaking the C - O bond and detaching the hydroxyl group. Before it loses one of its hydrogens, it will cleave the C - C bond and break the molecule up further, forming additional radicals.

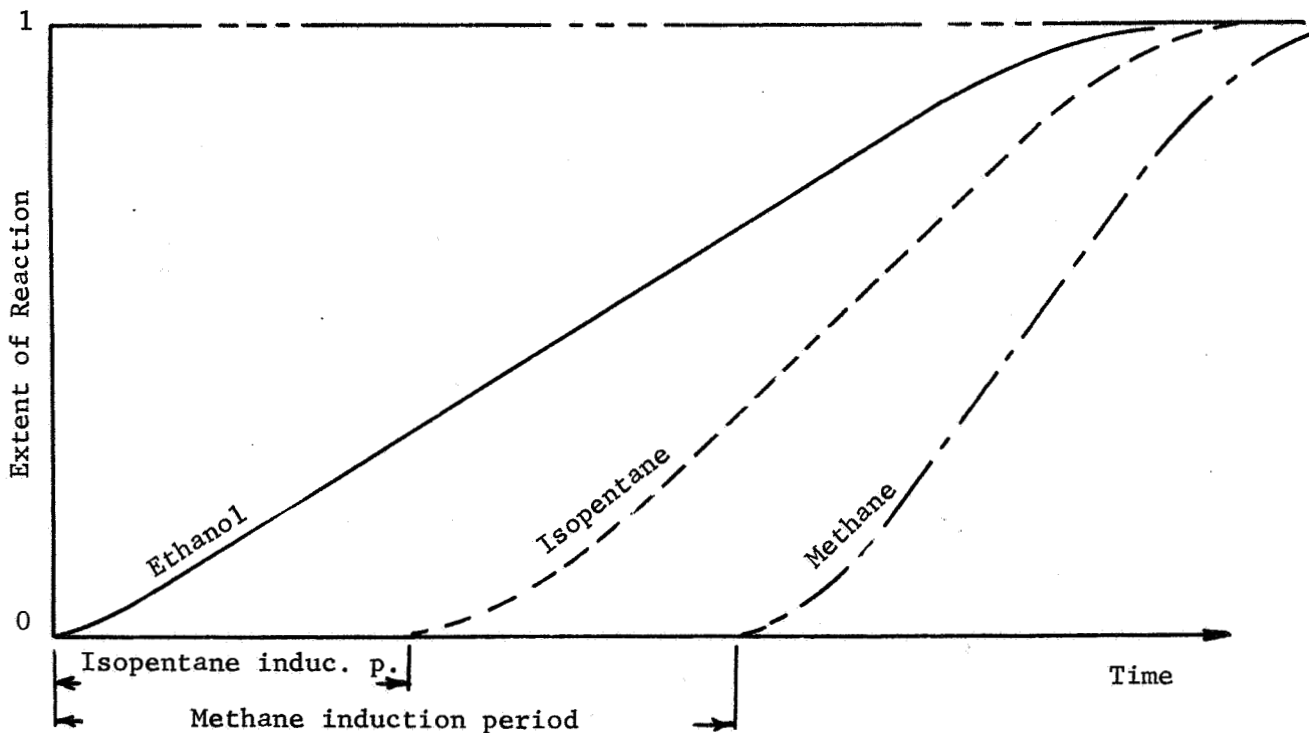
Now consider ethane. In the absence of more data for more complex hydrocarbons, ethane can at least give an idea of the relative strengths of bonds in higher hydrocarbons like RP-1. (Note that RP-1 has no aromatic components, so it is proper to use only aliphatic hydrocarbons as models.) Before ethane loses a hydrogen, it will cleave the C - C bond. So we can expect higher hydrocarbons to react through methyl radicals and other small units, rather than through larger radicals.

Methane has only one type of bond to break, the C - H bond and must react by some route involving methyl radicals.

Now consider the relative rates of reaction of these three molecules. Clearly, the ethanol will react more quickly than the hydrocarbons because the OH group detaches very easily. Much more energy is required in the case of a hydrocarbon to cleave the C - C bond. And methane requires very much more than that to react. Thus it would be

expected that ethanol would begin to react much sooner than would hydrocarbons, and that methane would wait a long time before beginning reaction while it absorbed the energy necessary to dissociate.

Preliminary studies in the flow reactor confirm these suspicions²¹. Tests with ethanol and isopentane established that ethanol began reaction much sooner and continued at a fairly steady rate. After a significant delay, called the induction period, the isopentane then began to react. Its reaction occurred at a much faster rate than that of the alcohol once it began, though. Methane has been found to have even a longer induction period than isopentane. The reaction may be schematically pictured as:



OXIDATION OF THREE FUELS

- Reaction of $C_2H_5OH - O_2$
- - - - Reaction of $CH_3CH_2CH(CH_3)CH_3 - O_2$
- · - · Reaction of $CH_4 - O_2$

From these reaction rate data, together with the information on vaporization rate, some tentative, and probably very tenuous, conclusions can be drawn about the combustion behavior of hydrocarbon and alcohol fuels in a rocket motor.

It seems probable that ignition of alcohol occurs immediately upon injection, very close to the injector face, with a slow combustion rate because of the slow rate of vaporization and the slow kinetics. Hydrocarbon fuels, like RP-1 and methane, however, probably must travel some distance into the chamber before they can ignite. And then, because of their rapid kinetics, once the induction period has been passed, and their easy vaporization, they probably burn very rapidly in a very short distance. As a contrast, the alcohol combustion, because of its slowness, is probably distributed over a longer distance. So the combustion of hydrocarbons is probably much more concentrated than that of alcohol, the alcohol combustion being much more evenly distributed, but the ignition of the alcohol probably occurs first.

These tentative thoughts on the location of ignition and combustion of the two types of fuels, together with another bit of experimental data, provide a vague indication of the relationship of the combustion process to the spin direction.

It has been found²⁰ that the spinning form of instability in the LOX/ALC propellant system is prevented by the presence of a baffle attached to the injector face. A destructable baffle was used. Stable operation existed until the baffle burned out, and then unstable operation began spontaneously in the spinning form. Thus, with the baffle present, LOX/ALC could not generate spinning instability; without the baffle, it did. Contrast this behavior with that observed in the LOX/LCH₄ tests quoted above. Here, a baffle could not prevent the spontaneous formation of the spinning instability. Even in those tests with a baffle present, the spinning mode occurred. Amplitudes were significantly less, and some damping occurred with the baffle, but the spin was still there, whereas it had not been present at all for the LOX/ALC system. Now it is known that a baffle must have a certain minimum length in order to be effective, indicating that whatever it affects exists primarily in the

early combustion zone. But how early is "early"? The early combustion zone for alcohol might, as shown above, lie closer to the injector face than that of a hydrocarbon fuel, particularly methane. If the coupling which produces the spinning instability, and which determines the direction, operates near the point of ignition, it would be overcome by a baffle in the case of alcohol, but not in the case of methane, for then the baffle would not be long enough (2-inch baffles were used). Clearly here is an easy point to check with a longer baffle. If this analysis is correct, it shows that the induction time for the reactions - a kinetic effect - does have a significant bearing on combustion instability.

Of course, these conclusions are based on very meager data, and so they should not be given too much weight unless they are corroborated by further tests. But the direction they point is promising. More testing is underway to carry the study further.

V. EXTENSIONS TO THE THEORY

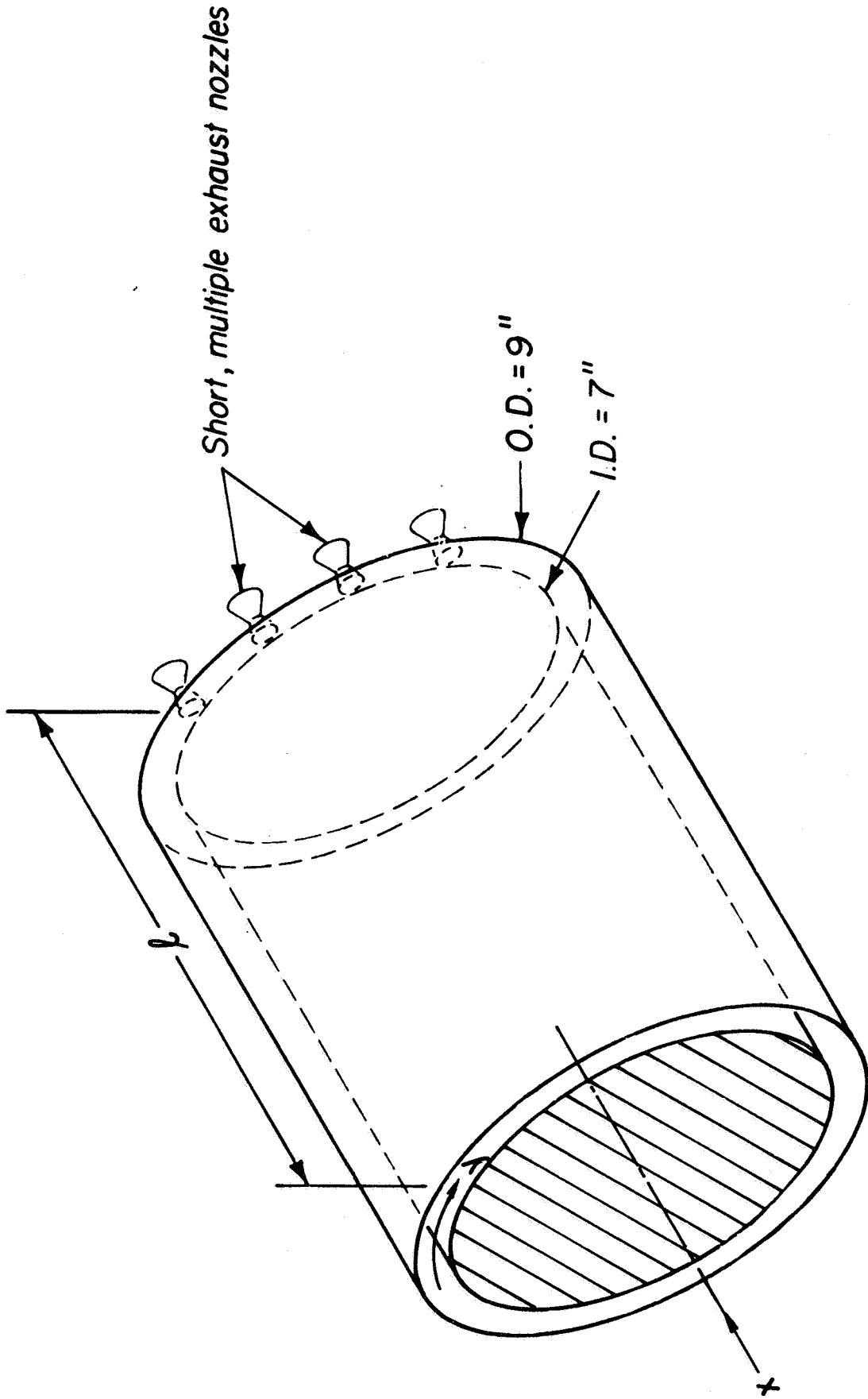
A. THEORY OF NONLINEAR TRANSVERSE INSTABILITY

1. Gas Dynamic Equations

Theoretical research work in the area of nonlinear transverse instability using a droplet evaporation model is continuing. The analysis is applicable to a thin annular chamber in which the oscillations can be assumed to be purely transversal - the dependence on the radial coordinate can be disregarded and the relevant independent variables are t , x and y (the circumferential coordinate) Fig. 31. For the assumed geometry the combustion chamber conservation equations can be derived. The following fundamental assumptions are made:

- 1) The gaseous material contained in the chamber is in the form of gases of perfect combustion. The liquid, its vapors and intermediate products of combustion occupy negligible volume. This assumption is justified by the fact that observed oscillation frequencies are quite close to theoretically predicted values which implies that throughout the chamber the actual sonic velocity is nearly the same as that of the combustion gases at their adiabatic flame temperature. This would not be true if considerable volumes of gas were at lower temperatures.
- 2) The combustion gases are assumed to be thermally and calorically perfect, and homo-compositional. Viscous and heat conduction effects are neglected, except for the possibility of existence of shock waves and the necessary heat exchange between liquid propellents and the hot combustion gases.
- 3) The liquid phase is well dispersed in the gaseous phase and can be characterised by the density ρ_l = mass of liquid per unit volume of gas.
- 4) The drag of the droplets is considered negligible. Therefore the droplet velocity is constant in space and time.
- 5) The transformation into burned gases immediately follows the evaporation of the propellants, so that the rate of combustion coincides with the rate of evaporation.

JP 21 R 4334-68



Annular motor geometry

Figure 31

Then the non-dimensional conservation equations for the chamber gases are:

$$\rho_t + \nabla \cdot (\rho \underline{q}) = Q \quad (1.1)$$

$$\rho \left[\underline{q}_t + (\underline{q} \cdot \nabla) \underline{q} \right] + \frac{\nabla p}{\gamma} = -Q(\underline{q} - \underline{q}_i) \quad (1.2)$$

$$\frac{p_t}{\gamma} + \nabla \cdot (p \underline{q}) + \frac{\gamma-1}{2} \left[(\rho q^2)_t + \nabla \cdot (\rho q^2 \underline{q}) \right] = Q \quad (1.3)$$

All quantities are normalized according to a scheme wherein the reference state of the gas is its state at the injector end under steady-state conditions. The reference velocity is the sonic velocity in the reference state. The reference length is the circumferential development of the annulus. The reference time is the ratio of the reference length and the reference velocity.

The RHS of the three conservation equations represent the mass, momentum and energy sources corresponding to the combustion rate of the liquid propellants. The energy source term Q coincides with the mass source term only because in the non-dimensionalization the energy content of any mass generated is taken to be unity.

Using the ideal gas relation $\rho = p e^{-\frac{1}{\gamma} \sigma}$ the equations for the annular geometry become:

$$\frac{p_t}{\gamma} + u \frac{p_x}{\gamma} + v \frac{p_y}{\gamma} + p(u_x + v_y) = Q \left[1 - \frac{\gamma-1}{2} (2u_x u - u^2 - v^2) \right] \quad (1.4)$$

$$u_t + uu_x + vv_y + p^{-\frac{1}{\gamma} \sigma} \frac{p_x}{\gamma} = -p^{-\frac{1}{\gamma} \sigma} Q(u - u_i) \quad (1.5)$$

$$v_t + uv_x + vv_y + p^{-\frac{1}{\gamma} \sigma} \frac{p_y}{\gamma} = -p^{-\frac{1}{\gamma} \sigma} Qv \quad (1.6)$$

$$\sigma_t + u\sigma_x + v\sigma_y = Q \left[\frac{1}{p} - p^{-\frac{1}{\gamma} \sigma} - \frac{\gamma-1}{2p} (2u_x u - u^2 - v^2) \right] \quad (1.7)$$

The boundary condition on the chamber walls is $q_n = 0$ under the inviscid assumption. Also at the injector $x = 0$, $u = 0$. To complete the boundary conditions the condition at the choked nozzle throat should be also added. Under the assumption that the combustion is completed at the nozzle entrance, i.e. $Q = 0$ within the nozzle, the nozzle behavior can be treated as a pure gasdynamical problem and the boundary condition expressed at the nozzle entrance. The difficulty of solving the nonlinear nozzle problem can be circumvented by considering a rather unconventional nozzle geometry consisting of a large number of short orifices. A quasi-steady nozzle condition, uniformly distributed at the nozzle end, may be obtained by this technique. Then the boundary conditions on the problem can be written as:

$$\text{at } x = 0 \quad u = 0 \quad (1.8)$$

$$x = L \quad M = u/a = \text{const.} \left\{ 1 + \frac{\gamma-1}{2} \left(\frac{q^2}{a^2} \right) \right\}^{\frac{\gamma+1}{2(\gamma-1)}} \quad (1.9)$$

where $a = \left(\frac{p}{\rho} \right)^{1/2} = p^{\gamma-1/2\gamma} e^{\sigma/2}$ is the local sonic velocity.

We assume a spinning type of instability, travelling in the positive y direction. Then all the quantities must be functions of $\alpha = ft - y$, where f is the frequency of the oscillations (still unknown at the moment) and must be periodic in x with a period of unity.

The equations can now be written in terms of α and x . We get:

$$(f-v) \frac{p_\alpha}{\gamma} + u \frac{p_x}{\gamma} + p(u_x - v_\alpha) = Q \left[1 - \frac{\gamma-1}{2} (2u_x u - u^2 - v^2) \right] \quad (1.10)$$

$$(f-v) u_\alpha + u u_x + p^{-1/8} e^{\sigma} \frac{p_x}{\gamma} = -p^{-1/8} e^{\sigma} Q (u - u_x) \quad (1.11)$$

$$(f-v) v_\alpha + u v_x - p^{-1/8} e^{\sigma} \frac{p_\alpha}{\gamma} = -p^{-1/8} e^{\sigma} Q v \quad (1.12)$$

$$(f-v) \sigma_\alpha + u \sigma_x = Q \left[\frac{1}{p} - p^{-1/8} e^{\sigma} - \frac{\gamma-1}{2p} (2u_x u - u^2 - v^2) \right] \quad (1.13)$$

Besides the x boundary conditions (1.8, 1.9) we have to add the condition of periodicity in α . In the case where the spinning wave includes a shock, the conservation conditions through the shock have also to be satisfied.

The steady-state equations may also be obtained directly from the conservation equations. These are found to be:

$$\bar{\rho} \bar{u} = \int_0^x \bar{Q} dx \quad (1.14)$$

$$\frac{\bar{p} - 1}{\gamma} = \bar{\rho} \bar{u} (u_2 - \bar{u}) \quad (1.15)$$

$$\frac{\bar{p}}{\bar{\rho}} = 1 - \frac{\gamma - 1}{2} \bar{u}^2 \quad (1.16)$$

where the bar indicates the steady-state quantities.

Rather than seeking the general solution of the above equations we restrict ourselves to the specific objective of looking for periodic solutions to the equations. The method followed is that of expansion in powers of a small parameter ϵ suitably related to the perturbation amplitude of the variables.

2. The Droplet Evaporation Model

The source strength Q is evaluated by assuming a model of droplet evaporation and combustion. An earlier analysis of nonlinear transverse instability by Crocco²² was based on the $n - \tau$ model (or sensitive time lag model) and gave promising results. However, as Crocco himself points out the $n - \tau$ model is unsatisfactory because it fails to fulfill the ultimate aim of a combustion model, i.e., the establishment of a link between the combustion rate and the physico-chemical processes involved in the combustion of the injected propellants. The droplet evaporation model is more satisfactory from this viewpoint.

Using the Priem-Heidmann model of quasi-steady droplet evaporation²³, the evaporation rate is determined by the relation

$$\frac{D_d r^*}{D t^*} = - \frac{K}{r^*} \left(1 + 0.3 Re^{1/2} Pr^{1/3} \right)$$

where * = dimensional quantities

K = constant related to properties of gases and of the droplets

$$\text{Re} = \text{Reynold's number} = \frac{2r^* \rho^* q_{rel}^*}{\mu^*}$$

Pr = Prandtl number

For simplicity, at large Reynold number values the conduction term can be neglected in comparison to the convection term.

Defining the relative droplet volume $V = r^3/r_i^3$, r_i = droplet radius at injection, and non-dimensionalising the other quantities in the usual fashion we get

$$\frac{D_x V}{Dt} = f V_x + u_x V_x = -C (V \rho q_{rel})^{1/2} \quad (2.1)$$

Further the non-dimensional evaporation rate can be shown to be

$$Q = -\beta_i \frac{D_x V}{Dt} \quad \text{where } \beta_i u_x = \mu \quad \text{the} \quad (2.2)$$

non-dimensional injection flux.

Now in steady state we will assume the combustion to be properly distributed along the chamber even for vanishingly small values of the expansion parameter. As $\bar{v} = 0$ this implies that $\bar{v}_x = 0$ also. Also $\bar{p} = O(1)$, $\bar{p} = O(1)$ and $q_{rel} = O(u_x)$. Then from (2.1), for steady-state, $u_x = C (u_x)^{1/2}$ or $C = O(u_x)^{1/2}$.

We further try to determine the proper ordering of the terms.

Consider \bar{u} , u_x and $\bar{Q} = O(\mu)$. Now v' , ρ' , p' , must be of the same order, since we want the lowest order perturbations to satisfy the wave equations. Let v' , ρ' , and $p' = O(\epsilon)$. We have to determine a relation between ϵ and μ .

Crocco²² has considered the case when the transverse velocity perturbation is much smaller than u_x and \bar{u} . The present analysis considers the case where the transverse velocity perturbation is larger than $u_x - \bar{u} = O(\mu)$. The other case, which is not covered by this report, and on which work is now in progress, is when v and $u_x - \bar{u}$ are of the same order.

Ordering of the Terms for the Case $v' \gg u_L - \bar{u}$

$$q_{rel}^2 = (u_L - u)^2 + v^2$$

For $v \gg u_L - u$

$$q_{rel} \approx v$$

Also $\bar{q}_{rel} = u_L - \bar{u}$.

Now

$$Q = \beta_{Li} C (V \rho q_{rel})^{1/2}$$

$$\approx \beta_{Li} C (V \rho v)^{1/2}$$

$$\bar{Q} = \beta_{Li} C (\bar{V} \bar{\rho} |u_L - \bar{u}|)^{1/2}$$

$$\therefore \frac{Q}{\bar{Q}} \approx \left(\frac{V}{\bar{V}}\right)^{1/2} \left(\frac{\rho}{\bar{\rho}}\right)^{1/2} \left|\frac{v}{u_L - \bar{u}}\right|^{1/2} \quad \text{or}$$

$$1 + \frac{Q'}{\bar{Q}} \approx \left(\frac{V}{\bar{V}}\right)^{1/2} \left(\frac{\rho}{\bar{\rho}}\right)^{1/2} \left|\frac{v}{u_L - \bar{u}}\right|^{1/2}$$

Now $\bar{V}, \bar{\rho} = O(1)$, $v', \rho' = O(\epsilon)$

$$1 + \frac{Q'}{\bar{Q}} \approx (1 + O(\epsilon)) \left|\frac{v}{u_L - \bar{u}}\right|^{1/2}$$

For $\frac{v}{u_L - \bar{u}} \gg 1$, this becomes

$$\frac{Q'}{\bar{Q}} = \left|\frac{v}{u_L - \bar{u}}\right|^{1/2}$$

Now Q' must be of a higher order than v' so that the lowest order equation is a wave equation. We take $Q' = O(v')^2 = O(\epsilon^2)$ as the simplest assumption. Then

$$\frac{O(\epsilon^2)}{O(\mu)} = \left(\frac{\epsilon}{\mu}\right)^{1/2}$$

$$\text{or} \quad \epsilon^3 = \mu \quad (2.3)$$

Now $\beta_{Li} u_L = \mu$ As $u_L = O(\mu)$, $\beta_{Li} = O(1)$

$$\frac{D_x V}{Dt} = - \frac{Q}{\beta_{Li}} = f V_x + u_L V_x$$

$$\therefore V' = O(Q') = O(\epsilon^2)$$

Therefore we have the following expansions:

$$\begin{aligned}
 C &= D\epsilon^{3/2} \quad \text{where } D = O(1) \\
 u_x &= \epsilon^3 u_{x3} \\
 \bar{u} &= \epsilon^3 \bar{u}_3 + \epsilon^4 \bar{u}_4 + \dots \\
 u' &= \epsilon^3 u_{3'} + \epsilon^4 u_{4'} + \dots \\
 u &= \epsilon^3 u_3 + \epsilon^4 u_4 + \dots \\
 \beta &= 1 + \epsilon\beta_1 + \epsilon^2\beta_2 + \epsilon^3\beta_3 + \dots \\
 \rho &= 1 + \epsilon\rho_1 + \epsilon^2\rho_2 + \epsilon^3\rho_3 + \dots \\
 v &= \epsilon v_1 + \epsilon^2 v_2 + \epsilon^3 v_3 + \dots \\
 \sigma &= \epsilon\sigma_1 + \epsilon^2\sigma_2 + \epsilon^3\sigma_3 + \dots \\
 f &= 1 + \epsilon f_1 + \epsilon^2 f_2 + \epsilon^3 f_3 + \dots \\
 V &= V_0 + \epsilon V_1 + \epsilon^2 V_2 + \epsilon^3 V_3 + \dots \\
 V' &= \epsilon^2 V_2' + \epsilon^3 V_3' + \dots \\
 \bar{V} &= \bar{V}_0 + \epsilon\bar{V}_1 + \epsilon^2\bar{V}_2 + \epsilon^3\bar{V}_3 + \dots \\
 \bar{Q} &= \epsilon^3 \bar{Q}_3 + \epsilon^4 \bar{Q}_4 + \dots \\
 Q' &= \epsilon^2 Q_2' + \epsilon^3 Q_3' + \epsilon^4 Q_4' + \dots \\
 Q &= \epsilon^2 Q_2 + \epsilon^3 Q_3 + \epsilon^4 Q_4 + \dots
 \end{aligned} \tag{2.4}$$

In order to avoid non-uniformly valid solutions in the perturbation approach for nonlinear problems the technique of coordinate stretching has been found to be very useful. We introduce here the stretching of both the variables α and x in order to show the general method for problems of this type. (Later we find that for the case $v \gg u_x - \bar{u}$ it is not necessary to stretch the x variable to obtain the solution for the waveform.)

The stretching expansions are:

$$\begin{aligned}\theta &= \alpha + \epsilon \theta_1(\theta, \xi) + \epsilon^2 \theta_2(\theta, \xi) + \dots \\ \xi &= x + \epsilon \xi_1(\theta, \xi) + \epsilon^2 \xi_2(\theta, \xi) + \dots\end{aligned}\quad (2.5)$$

where the functions $\theta_1, \theta_2, \xi_1, \xi_2$ etc are to be determined. All dependent variables are now functions of θ, ξ and they must be periodic in θ with period 1. If we have a travelling transverse shock, the stretching of x enables us to have the shock correspond to $\theta = 0$, and because of periodicity the shock again appears at $\theta = 1$ and further at all integral values of θ .

The derivatives of a general quantity $F = F_0 + \epsilon F_1 + \epsilon^2 F_2 + \dots$ can be calculated to be

$$\begin{aligned}F_x &= F_{0\theta} + \epsilon \left[F_{1\theta} + F_{0\xi} \xi_{1\theta} + F_{0\theta} \theta_{1\theta} \right] \\ &+ \epsilon^2 \left[F_{2\theta} - F_{1\theta} \xi_{1\xi} - F_{0\theta} \xi_{2\xi} + F_{1\xi} \xi_{1\theta} + F_{0\xi} \xi_{2\theta} \right. \\ &\quad + (F_{1\theta} + F_{0\xi} \xi_{1\theta} - F_{0\theta} \xi_{1\xi}) (\xi_{1\xi} + \theta_{1\theta}) \\ &\quad \left. + F_{0\theta} (\xi_{2\xi} - \xi_{1\xi} \theta_{1\theta} + \theta_{2\theta} + \xi_{1\theta} \theta_{1\xi}) \right] \\ &\quad + O(\epsilon^3).\end{aligned}\quad (2.6)$$

$$\begin{aligned}F_x &= F_{0\xi} + \epsilon \left[F_{1\xi} + F_{0\theta} \theta_{1\xi} + F_{0\xi} \xi_{1\xi} \right] \\ &+ \epsilon^2 \left[F_{2\xi} - F_{1\xi} \theta_{1\theta} - F_{0\xi} \theta_{2\theta} + F_{0\theta} \theta_{2\xi} + F_{1\theta} \theta_{1\xi} \right. \\ &\quad + (F_{1\xi} - F_{0\xi} \theta_{1\theta} + F_{0\theta} \theta_{1\xi}) (\xi_{1\xi} + \theta_{1\theta}) \\ &\quad \left. + F_{0\xi} (\xi_{2\xi} - \xi_{1\xi} \theta_{1\theta} + \theta_{2\theta} + \xi_{1\theta} \theta_{1\xi}) \right] \\ &\quad + O(\epsilon^3).\end{aligned}$$

Introducing the expansions 2.4, 2.5 and 2.6 in the equations 1.10 - 1.13 and separating terms of various orders of ϵ we get the following set of equations. The equations of $O(\epsilon)$ are

$$\begin{aligned} p_{10}/\gamma - v_{10} &= 0 \\ p_{1\xi}/\gamma &= 0 \\ v_{10} - p_{10}/\gamma &= 0 \\ \sigma_{10} &= 0 \end{aligned} \tag{2.7}$$

The equations of $O(\epsilon^2)$ are:

$$\begin{aligned} p_{20}/\gamma + p_{10}\theta_{10}/\gamma + p_{1\xi}\xi_{10}/\gamma + (f_1 - v_1)p_{10}/\gamma - p_1 v_{10} - v_{20} \\ - v_{10}\theta_{10} - v_{1\xi}\xi_{10} &= Q_2 \\ p_{2\xi}/\gamma + p_{10}\theta_{1\xi}/\gamma + p_{1\xi}\xi_{1\xi}/\gamma - p_1 p_{1\xi}/\gamma + \sigma_1 p_{1\xi} &= 0 \\ (f_1 - v_1)v_{10} + v_{20} + v_{10}\theta_{10} + v_{1\xi}\xi_{10} - (\sigma_1 - \frac{p_1}{\gamma})p_{10}/\gamma \\ - (p_{20} + p_{10}\theta_{10} + p_{1\xi}\xi_{10})/\gamma &= 0 \\ (f_1 - v_1)\sigma_{10} + \sigma_{20} + \sigma_{10}\theta_{10} + \sigma_{1\xi}\xi_{10} &= 0 \end{aligned} \tag{2.8}$$

Consider the ϵ order equations. The unsteady equation becomes

$$\frac{p'_{10}}{\gamma} = v_{10} \quad \text{Let } v_1 = \phi(\theta)$$

Then

$$\frac{p'_1}{\gamma} = \phi(\theta) + c(\xi).$$

as $p_{1\xi} = 0$, C must be a constant

$$p_1'/\gamma = \phi(\theta) + C$$

Also

$$\sigma_1' = b$$

Therefore the ϵ order equations have the solution

$$v_1 = \phi(\theta), \quad \frac{p_1'}{\gamma} = \phi(\theta) + C, \quad \sigma_1' = b \quad (2.9)$$

Using the ϵ order equations to simplify the higher order equations we get,

$$p_{2\theta}/\gamma + (f_1 - v_1 - p_1)\phi_\theta - v_{2\theta} = Q_2$$

$$p_{2\xi}/\gamma + p_{1\theta}\theta_{1\xi}/\gamma = 0$$

$$(f_1 - v_1)v_{1\theta} + v_{2\theta} + v_{1\theta}\theta_{1\theta} - \left(\sigma_1 - \frac{p_1}{\gamma}\right)\frac{p_{1\theta}}{\gamma} - (p_{2\theta} + p_{1\theta}\theta_{1\theta})/\gamma = 0 \quad (2.10)$$

$$\sigma_{2\theta} + \sigma_{1\xi}\xi_{1\theta} = 0$$

Using the steady-state results, the equations for the unsteady components becomes,

$$\frac{p'_{2\theta}}{\gamma} - v'_{2\theta} = Q_2' + \left[(\gamma+1)\phi + \gamma C - f_1 \right] \phi_\theta$$

$$\frac{p'_{2\xi}}{\gamma} = -\phi_\theta \theta_{1\xi}$$

(2.11)

$$v'_{2\theta} - \frac{p'_{2\theta}}{\gamma} = -\left[f_1 + C - b \right] \phi_\theta$$

$$\sigma'_{2\theta} + \sigma_{1\xi}\xi'_{1\theta} = 0$$

Our objective is to determine an equation for the wave shape $\phi(\theta)$. To complete the solution we need to determine an expression for Q_2' , the source term.

$$Q = \rho_{li} C (V p q_{rd})^{1/2}$$

$$\therefore \epsilon^2 Q_2 + \epsilon^3 Q_3 + \dots = \frac{1}{u_{l3}} D \epsilon^{3/2} |v_1|^{1/2} \epsilon^{1/2} V_0^{1/2} [1 + o(\epsilon)]$$

$$\therefore Q_2 = \frac{D}{u_{l3}} |v_1|^{1/2} V_0^{1/2}$$

$$\bar{Q}_2 = 0 \quad \text{as } \bar{v}_1 = 0$$

$$Q_2' = \frac{D}{u_{l3}} |v_1|^{1/2} V_0^{1/2}$$

Also

$$\bar{Q} = \epsilon^3 \bar{Q}_3 + \epsilon^4 \bar{Q}_4 + \dots = \frac{D \epsilon^{3/2}}{u_{l3}} [\bar{\rho} \bar{v} q_{rd}]^{1/2}$$

$$= \frac{D \epsilon^{3/2}}{u_{l3}} \left[(1 + \epsilon \bar{\rho}_1 + \dots)^{1/2} (\bar{V}_0 + \epsilon \bar{V}_1 + \dots)^{1/2} \epsilon^{3/2} |u_{l3} - \bar{u}_3|^{1/2} \right]$$

$$\therefore \bar{Q}_3 = \frac{D}{u_{l3}} |u_{l3} - \bar{u}_3|^{1/2} \bar{V}_0^{1/2}$$

Also $\epsilon^3 \bar{Q}_3 + \dots = -\rho_{li} \epsilon^3 u_{l3} \bar{V}_x$

$$= -\rho_{li} \epsilon^3 u_{l3} [V_{0f} + o(\epsilon)]$$

as $\rho_{li} \epsilon^3 u_{l3} = o(\epsilon^3)$ we get

$$\bar{Q}_3 = -V_{0f}$$

$$\therefore V_{0f} = -\frac{D V_0^{1/2}}{u_{l3}} |u_{l3} - \bar{u}_3|^{1/2}$$

From the steady-state equation 1.14

$$\bar{u}_3 = \int_0^x \bar{Q}_3 dx$$

$$\bar{u}_{3x} \cong \bar{u}_{3\xi} \cong \bar{Q}_3 = \frac{DV_0}{u_{\lambda_3}} |u_{\lambda_3} - \bar{u}_3|^{1/2}$$

$$\therefore Q_2' = |v_1|^{1/2} \bar{u}_{3\xi} / |u_{\lambda_3} - \bar{u}_3|^{1/2}$$

$$\text{or } Q_2' = |\phi|^{1/2} \frac{\bar{u}_{3\xi}}{|u_{\lambda_3} - \bar{u}_3|^{1/2}} \quad (2.12)$$

Using this expression in 2.11, we have

$$p'_{20}/\gamma - v'_{20} = |\phi|^{1/2} \frac{\bar{u}_{3\xi}}{|u_{\lambda_3} - \bar{u}_3|^{1/2}} + [(\gamma+1)\phi + \gamma c - f_1] \phi_\theta$$

$$= [f_1 + c - b] \phi_\theta$$

$$\therefore \phi_\theta [(\gamma+1)\phi + \gamma c - f_1 - f_1 - c + b] + |\phi|^{1/2} \frac{\bar{u}_{3\xi}}{|u_{\lambda_3} - \bar{u}_3|^{1/2}} = 0$$

f_1 , by definition, is the mean value of $v_1' + a_1'$ across the shock and

$$f_1 = v_{1m} + \frac{\gamma-1}{2\gamma} p'_{1m} + \frac{\sigma_1'}{2}$$

$$= \phi_m + \frac{\gamma-1}{2} \phi_m + \frac{\gamma-1}{2} c + \frac{b}{2}$$

Therefore, the governing equation is

$$\phi_\theta [(\gamma+1)(\phi - \phi_m)] + |\phi|^{1/2} \frac{\bar{u}_{3\xi}}{|u_{\lambda_3} - \bar{u}_3|^{1/2}} = 0$$

Integrate the equation from $\xi = 0$ to λ to find the average over the length of the combustion chamber

$$\phi_\theta (\gamma+1) \lambda (\phi - \phi_m) + |\phi|^{1/2} \int_0^\lambda \frac{\bar{u}_{3\xi} d\xi}{|u_{\lambda 3} - \bar{u}_3|^{1/2}} = 0 \quad (2.13)$$

which is the equation for the wave shape. The integral part of the second term is of course a constant depending only on the steady-state solutions. Denoting it by ν we have the equation for the wave shape

$$(\gamma+1) \lambda (\phi - \phi_m) \phi_\theta + |\phi|^{1/2} \nu = 0$$

For no value of ν can this equation provide a periodic solution which also satisfies the shock condition $\int_0^1 \phi d\theta = 0$. Integrating the above equation with respect to θ from 0 to 1 we get

$$\frac{\lambda(\gamma+1)}{2} \Delta [(\phi - \phi_m)^2] + \nu \int_0^1 |\phi|^{1/2} d\theta = 0 \quad (2.14)$$

where $\Delta f = f(1, \xi) - f(0, \xi)$

Now $\Delta [(\phi - \phi_m)^2] = 0$ from the definition of ϕ_m .

$$\therefore \int_0^1 |\phi|^{1/2} d\theta = 0$$

which has the

solution $\phi = 0$.

Therefore any wave with the square root driving term (i.e. case for $v' \gg u_2 - \bar{u}$) tends to decay to zero. Of course as soon as the perturbation amplitude decreases somewhat the square root driving term is no longer valid and a linear driving term has to be used. (The details of this case are still being worked out. For $v' \approx u_2 - \bar{u}$ it is found that the driving term can be approximated by a linear

function). Thus the 3 ranges of v' and $u_x - \bar{u}$ considered do present us with a reasonable picture of the phenomena. For $v' \ll u_x - \bar{u}$ the dependence of the driving term (the combustion rate) on v' is quadratic. As shown by Crocco²² instability can exist (i.e., periodic solutions can be found). These periodic solutions constitute a triggering limit for instability - any perturbation ultimately leading to an indefinite amplification. Of course this is quite unrealistic and we should expect to reach a limit cycle. The reason of course is that as the amplitude increases the quadratic driving term is no longer valid - for large amplitudes we have seen that the driving term only increases as the square root of the v' and leads to decaying solutions. Thus the limit cycle mentioned seems to exist for amplitudes lower than where the square root dependence holds. Thus the third range ($v' \approx u_x - \bar{u}$) where the driving term is linear in v' is expected to provide a stable limit cycle solution. As mentioned before work on this case is progressing rapidly and is expected to be completed in the near future.

B. NEW EXPANSION TECHNIQUE FOR THE CASE $v' \ll \bar{u} - \bar{u}_e$

The purpose of this article is to discuss the nonlinear instability in an annular combustion chamber for the case when the transverse velocity is much smaller than the difference of liquid drop and gas velocities using simplified vaporization model. Two objectives will be sought: 1) The final oscillatory conditions; 2) the triggering limit, above which the amplitude of oscillations becomes amplified and below which it decays.

Let us start with the gas-dynamic equations derived in Section A of this chapter and reproduced below for convenience.

$$\begin{aligned} (f-v) \frac{p_\alpha}{\delta} + u \frac{p_x}{\delta} + p(u_x - v_\alpha) \\ = Q \left[1 - \frac{\delta-1}{2} (2u_e u - u^2 - v^2) \right] \end{aligned} \quad (1)$$

$$\begin{aligned} (f-v) u_\alpha + u u_x + p^{-\frac{1}{\delta}} e^\sigma \frac{p_x}{\delta} \\ = p^{-\frac{1}{\delta}} e^\sigma Q (u_e - u) \end{aligned} \quad (2)$$

$$\begin{aligned} (f-v) v_\alpha + u v_x - p^{-\frac{1}{\delta}} e^\sigma \frac{p_x}{\delta} \\ = - p^{-\frac{1}{\delta}} e^\sigma Q v \end{aligned} \quad (3)$$

$$\begin{aligned} (f-v) \sigma_\alpha + u \sigma_x \\ = Q \left[\frac{1}{p} - p^{-\frac{1}{\delta}} e^\sigma - \frac{\delta-1}{2p} (2u_e u - u^2 - v^2) \right] \end{aligned} \quad (4)$$

with

$$\rho = p^{\frac{1}{\gamma}} e^{-\sigma}$$

this set of equations describes the flow phenomena in an annular rocket combustor. Discussion of the assumptions for these equations will not be given here. (See Part A). With the short nozzle approximation which gives the boundary condition at the end of the combustor, our main objective is to seek a periodic solution for spinning waves. At the nozzle end, the boundary condition is

$$\frac{u}{a} = \text{const} \left[1 + \frac{\gamma-1}{2} \left(\frac{u^2+v^2}{a^2} \right) \right]^{\frac{\gamma+1}{2(\gamma-1)}} \quad (5)$$

The steady-state solution can be obtained simply by integration:

$$\bar{\rho} \bar{u} = \int_0^x \bar{Q} dx \quad (6)$$

$$\frac{\bar{p}-1}{\gamma} = \bar{\rho} \bar{u} (\bar{u}_e - \bar{u}) \quad (7)$$

$$\bar{p} = \bar{p} \left(1 - \frac{\gamma-1}{2} \bar{u}^2 \right) \quad (8)$$

The injection rate is expressed by

$$\mu = \int_0^l \bar{Q} dx \quad (9)$$

The source term Q is being evaluated by assuming a vaporization model, i.e., the combustion process immediately follows the propellant vaporization. A simplified model has been suggested²⁵ (also see Part A)

$$Q = \frac{\mu}{u_e} c (V \rho g)^{\frac{1}{2}} \quad (10)$$

and the equation for the conservation of liquid drop mass is:

$$f V_x + u_e V_x = - \frac{u_e}{\mu} Q \quad (11)$$

where V is the drop volume.

The method of solving this problem is that of expansion in powers series in a small parameter ϵ , which is related to the perturbation amplitude of the physical quantities. After introducing such expansions in Equations (1) to (4) and (11), we obtain equations which correspond to different powers of ϵ and can be solved separately and successively. For small amplitude and vanishing gas source strength the steady-state conditions are uniform and the perturbations should satisfy the acoustic equations of which the general solution is known in some particular cases. In Refs. 22, 24 and 25 we see that choice of the expansion parameter ϵ is very critical and can lead to different results according to the different orders of the steady and perturbation quantities. It is the purpose of this discussion to show a proper way of selecting such a parameter which is based upon some essential requirements. We should not be mistaken that these requirements are the only ones, we could expect some modifications for other cases. However, the treatment below does have its own generality.

Let us assume that the unsteady parts of pressure, gas density, entropy, transverse velocity component and drop volume are of the same order, namely

$$p' = O(v') \quad (12)$$

$$\rho' = O(v') \quad (13)$$

$$s' = O(v') \quad (14)$$

$$V' = O(v') \quad (15)$$

the relation between v' and ϵ has not been established yet, but will be determined later.

From the expression of the combustion source (10) where

$$g = [(u - u_e)^2 + v^2]^{\frac{1}{2}} \quad (16)$$

and with the assumptions

$$\left| \frac{u'}{g} \right| \ll \left(\frac{v'}{g} \right)^2 \ll 1 \quad (17)$$

$$\left| \frac{\rho'}{\rho} \right| \ll 1, \quad \left| \frac{V'}{V} \right| \ll 1, \quad \left| \frac{Q'}{Q} \right| \ll 1 \quad (18)$$

We obtain the perturbation of Q

$$\frac{Q'}{Q} = \frac{1}{2} \left(-\frac{\rho'}{\rho} + \frac{V'}{V} + \frac{g'}{g} \right) \quad (19)$$

where
$$\frac{g'}{g} = \frac{1}{2} \left(-\frac{v'}{g} \right)^2 \quad (20)$$

the first relation of (17) indicates the fact that we shall consider the transverse mode only and (17) and (18) are the small perturbation assumptions.

The most important point here is we expect that $\frac{\rho'}{\rho}$, $\frac{V'}{V}$ and $\frac{g'}{g}$ will give the same contribution on $\frac{Q'}{Q}$, it is therefore necessary that they be of the same order

$$\frac{\rho'}{\rho} = O\left(\frac{g'}{g}\right) \quad (21)$$

$$\frac{V'}{V} = O\left(\frac{g'}{g}\right) \quad (22)$$

$$\frac{Q'}{Q} = O\left(\frac{g'}{g}\right) \quad (23)$$

since $\bar{\rho} = O(1)$, $\bar{V} = O(1)$, so we have

$$\rho' = O\left(\frac{g'}{g}\right) = O\left(\frac{v'}{g}\right)^2 \quad (24)$$

$$V' = O\left(\frac{v'}{g}\right)^2 \quad (25)$$

$$\frac{Q'}{Q} = O\left(\frac{v'}{\bar{v}}\right)^2 \quad (26)$$

with the use of (20). From (13) and (24), we obtain

$$v' = O(\bar{v}^2) \quad (27)$$

substituting in (13), (14), (15), (21) and (23) we have

$$p' = O(\bar{v}^2) \quad (28)$$

$$p' = O(\bar{v}^2) \quad (29)$$

$$v' = O(\bar{v}^2) \quad (30)$$

$$q' = O(\bar{v}^3) \quad (31)$$

and
$$\frac{Q'}{Q} = O(\bar{v}^2) \quad (32)$$

If we assume that the derivatives of all perturbation quantities with respect to α and χ are of the same order as the quantities themselves, i.e.,

$$p'_\alpha = O(p'), \quad p'_\chi = O(p')$$

$$v'_\alpha = O(v')$$

since
$$f = O(1), \quad p = O(1), \quad u = O(\mu)$$

after separating the steady-state part from Equation (1), the left-handed side of the unsteady equation is of the order

$$\text{LHS} = O(v')$$

and the right-handed side is

$$\text{RHS} = O(Q')$$

If we expect that the first order equation of the unsteady quantity be the acoustic equation (it should be realized here that the first order does not mean the term of power ϵ , rather, it is the first leading term of the unsteady quantity), clearly Q' should not appear at this order, the necessary condition would be that Q' is of higher order than v' .

Since ϵ is the actual expansion parameter, if we choose

$$Q' = O(v'\epsilon) \quad (33)$$

the above condition can be satisfied. Of course, the cases with $Q' = O(v'\epsilon^n)$ for any $n \geq 1$ would serve the same purpose but obviously will give different results. We shall not discuss other possibilities in this article.

The above argument for getting an acoustic type equation can also be applied to the drop volume equation. With the assumption

$$V'_d = O(V') \quad , \quad V'_x = O(V')$$

we obtain the unsteady-state equation from (11). The left-handed side is of order

$$\text{LHS} = O(V') = O(v')$$

and the right-handed side

$$\text{RHS} = O\left(\frac{u_e}{\mu} Q'\right)$$

In order to obtain an acoustic type equation, we choose

$$\frac{u_e}{\mu} Q' = O(v'\epsilon) \quad (34)$$

From (33) and (34), u_e should be the same order as μ

$$u_e = O(\mu) \quad (35)$$

this is what we observe in many practical rocket engines. Some of the former analyses^{22,25} require that u_e and μ be of different order,

applicability of those results is quite questionable.

Because $\bar{q} = \bar{u} - \bar{u}_e$, so

$$\bar{q} = O(\mu) \tag{36}$$

We also assume combustion zone is distributed along the axial distance, that means

$$\bar{V}_x = O(1) \tag{37}$$

from the drop volume equation we have

$$\bar{Q} = \mu \bar{V}_x \tag{38}$$

therefore

$$\bar{Q} = O(\mu) \tag{39}$$

Substituting (36) and (39) into (27) to (32), we have

$$v' = O(\mu^2) \tag{40}$$

$$\rho' = O(\mu^2) \tag{41}$$

$$\sigma' = O(\mu^2) \tag{42}$$

$$q' = O(\mu^3) \tag{43}$$

$$Q' = O(\mu^3) \tag{44}$$

and with (10), the order of C is

$$C = O(\mu^{\frac{1}{2}}) \tag{45}$$

since $Q' = O(v'\epsilon)$ (33)

it is seen that

$$\epsilon = O(\mu) \quad (46)$$

For convenience, we take $\epsilon = \mu$. The final result indicates that the expansion parameter should be the injection rate which is approximately the Mach number at the nozzle entrance.

Since we have obtained a proper expansion parameter, we can proceed to expand every variable into a power series of μ and substitute into the equations. After separation of terms of different powers in μ , the equations can be solved separately and successively. In many nonlinear problems, it is found that method of coordination stretching is very useful. Besides expanding the dependent variables, we also expand f, α, χ in power series of μ and a set of independent variables ξ and θ is introduced to replace χ and α . The following expansions have been taken

$$C = \mu^{\frac{1}{2}} D$$

$$\bar{p} = 1 + \mu \bar{p}_1 + \mu^2 \bar{p}_2 + \mu^3 \bar{p}_3$$

$$p' = \mu^2 p'_2 + \mu^3 p'_3$$

$$\bar{\rho} = 1 + \mu \bar{\rho}_1 + \mu^2 \bar{\rho}_2 + \mu^3 \bar{\rho}_3$$

$$\rho' = \mu^2 \rho'_2 + \mu^3 \rho'_3$$

$$\bar{\sigma} = \mu \bar{\sigma}_1 + \mu^2 \bar{\sigma}_2 + \mu^3 \bar{\sigma}_3$$

$$\sigma' = \mu^2 \sigma'_2 + \mu^3 \sigma'_3$$

$$\bar{V} = \bar{V}_0 + \mu \bar{V}_1 + \mu^2 \bar{V}_2 + \mu^3 \bar{V}_3$$

$$V' = \mu^2 V'_2 + \mu^3 V'_3$$

$$\bar{u} = \mu \bar{u}_1 + \mu^2 \bar{u}_2 + \mu^3 \bar{u}_3 + \mu^4 \bar{u}_4$$

$$u' = \mu^4 u'_4$$

$$\bar{v} = 0$$

$$v' = \mu^2 v'_2 + \mu^3 v'_3$$

$$\bar{u}_e = \mu \bar{u}_{e1}$$

$$\bar{Q} = \mu \bar{Q}_1 + \mu^2 \bar{Q}_2 + \mu^3 \bar{Q}_3$$

$$Q' = \mu^3 Q'_3$$

$$\bar{q} = \mu \bar{q}_1 + \mu^2 \bar{q}_2 + \mu^3 \bar{q}_3$$

$$q' = \mu^3 q'_3$$

with

$$\bar{q}_1 = \bar{u}_1 - \bar{u}_{e1} \quad (47)$$

$$\bar{Q}_1 = \frac{D}{u_{R1}} (\bar{V}_0 \bar{q}_1)^{\frac{1}{2}} \quad (48)$$

The coordinate stretching

$$\xi = x + \mu \xi_1 + \mu^2 \xi_2 + \mu^3 \xi_3 \quad (49)$$

$$\theta = \alpha + \mu \theta_1 + \mu^2 \theta_2 + \mu^3 \theta_3 \quad (50)$$

$$f = 1 + \mu f_1 + \mu^2 f_2 + \mu^2 f_3 \quad (50)$$

ξ, θ are the independent variables.

From (1), (2) and (11), we obtain the first order equations

$$\bar{u}_{1\xi} = \bar{Q}_1 \quad (51)$$

$$\bar{p}_{1\xi} = 0 \quad (52)$$

$$\bar{V}_{0\xi} (\xi_{10} + \bar{u}_{e_1}) = -\bar{u}_{e_1} \bar{Q}_1 \quad (53)$$

Since $\bar{p}_1(\xi=0) = 0$, from (52) we conclude that \bar{p}_1 should vanish, i.e.

$$\bar{p}_1 = 0 \quad (54)$$

the steady part of (53) is

$$\bar{V}_{0\xi} = -\bar{Q}_1 \quad (55)$$

the expression of \bar{Q}_1 is

$$\bar{Q}_1 = \frac{D}{\bar{u}_{e_1}} (\bar{V}_0 \bar{g}_1)^{\frac{1}{2}} = 2h (\bar{V}_0 \bar{g}_1)^{\frac{1}{2}} \quad (56)$$

where

$$h = \frac{D}{2\bar{u}_{e_1}}$$

The differential equations (51) and (55), combined with (56) and also with the boundary conditions that $\bar{V}_0(0) = 1$, $\bar{u}_1(0) = 0$, yield the following results:

For $0 \leq \bar{u}_1 \leq \bar{u}_{e1}$, $0 \leq \xi \leq \xi_0$

$$\bar{V}_0 = [\cosh(k\xi) - \sqrt{\bar{u}_{e1}} \sinh(k\xi)]^2 \quad (57)$$

$$\bar{u}_1 = 1 - [\cosh(k\xi) - \sqrt{\bar{u}_{e1}} \sinh(k\xi)]^2 \quad (58)$$

ξ_0 is determined by the condition that at $\xi = \xi_0$, $\bar{u}_1 = \bar{u}_{e1}$.

For $\bar{u}_{e1} \leq \bar{u}_1 \leq 1$, $\xi_0 \leq \xi \leq l$

$$\bar{V}_0 = \frac{1 - \bar{u}_{e1}}{2} \{ 1 + \cos[2k(\xi - \xi_0)] \} \quad (59)$$

$$\bar{u}_1 = \frac{1}{2} \{ (1 + \bar{u}_{e1}) + (1 - \bar{u}_{e1}) \cos[2k(\xi - \xi_0)] \} \quad (60)$$

where l is the end of the combustion zone, namely, $\bar{V}_0(l) = 0$, and $\bar{u}_1(l) = 1$.

$$l = \frac{\pi}{2k} + \xi_0 \quad (61)$$

The unsteady-state equation of (53) is

$$\bar{V}_{0\xi} \xi_{10} = 0 \quad (62)$$

since $\bar{V}_{0\xi}$ is not identically zero, so it is necessary that

$$\xi_{10} = 0 \quad (63)$$

that means ξ_1 is function of ξ only or $\xi_1 = \bar{\xi}_1$.

Since there are no unsteady terms in μ , we conclude that f_1 must be zero because this is the frequency correction to that order

Now we go to the second order equations. They are:

$$\bar{u}_{2\xi} + \bar{Q}_1 \bar{\xi}_{1\xi} = \frac{\bar{Q}_1}{2} \left[\frac{\bar{V}_1}{V_0} + \frac{\bar{u}_2}{\bar{g}_1} \right] \quad (64)$$

$$\frac{p_{2\xi}}{\delta} + \bar{Q}_1 \bar{u}_1 = -\bar{Q}_1 \bar{g}_1 \quad (65)$$

$$\frac{p'_{20}}{\delta} - v_{20}' = 0 \quad (66)$$

$$\sigma'_{20} + \bar{u}_1 \bar{\sigma}'_{1\xi} = -\bar{Q}_1 \bar{\sigma}_1 \quad (67)$$

$$\begin{aligned} [V'_{20} - \bar{Q}_1 \bar{\xi}_{20}] + \bar{u}_{e1} [\bar{V}_{1\xi} - \bar{Q}_1 \bar{\xi}_{1\xi}] \\ = -\bar{u}_{e1} \frac{\bar{Q}_1}{2} \left[\frac{\bar{V}_1}{V_0} + \frac{\bar{u}_2}{\bar{g}_1} \right] \end{aligned} \quad (68)$$

The steady-state equation of (67) reads

$$\bar{\sigma}'_{1\xi} + \frac{\bar{Q}_1}{\bar{u}_1} \bar{\sigma}_1 = 0 \quad (69)$$

the solution is

$$\begin{aligned} \bar{\sigma}_1 &= A \exp \left[-\int_0^\xi \frac{\bar{Q}_1 d\xi}{\bar{u}_1} \right] \\ &= \frac{A}{\bar{u}_1} \end{aligned}$$

but at $\xi=0$, $\bar{\sigma}_1=0$ this implies that A should be zero, or

$$\bar{\sigma}_1 = 0 \quad (70)$$

The unsteady-state equation is

$$\sigma'_{20} = 0 \quad (71)$$

the solution should be

$$\sigma_2' = b = \text{const} \quad (72)$$

if there is any dependence on ξ at all, it can be included in $\bar{\sigma}_2$.

The steady part of equation (68)

$$\bar{V}_{1\xi} - \bar{Q}_1 \bar{\xi}_{1\xi} = -\frac{\bar{Q}_1}{2} \left[\frac{\bar{V}_1}{V_0} + \frac{\bar{U}_2}{\delta_1} \right] \quad (73)$$

and (64) can be solved simultaneously. Rewriting these two equations, we have

$$\bar{V}_{1\xi} + \frac{\bar{Q}_1}{2} \left[\frac{\bar{V}_1}{V_0} + \frac{\bar{U}_2}{\delta_1} \right] = \bar{Q}_1 \bar{\xi}_{1\xi} \quad (74)$$

$$\bar{U}_{2\xi} - \frac{\bar{Q}_1}{2} \left[\frac{\bar{V}_1}{V_0} + \frac{\bar{U}_2}{\delta_1} \right] = -\bar{Q}_1 \bar{\xi}_{1\xi} \quad (75)$$

Adding these two equations and integrating, we get the result after applying the boundary condition that $\bar{V}_1(0) = \bar{U}_2(0) = 0$.

$$\bar{V}_1 + \bar{U}_2 = 0 \quad (76)$$

so (74) becomes

$$\left(\frac{\bar{V}_1}{V_0} \right)_{\xi} - \frac{\bar{Q}_1}{2} \left[\frac{1}{V_0} + \frac{1}{\delta_1} \right] \left(\frac{\bar{V}_1}{V_0} \right) = -\frac{\bar{Q}_1}{V_0} \bar{\xi}_{1\xi} \quad (77)$$

The general solution is

$$\begin{aligned} \frac{\bar{V}_1}{V_0} = & A \exp \left[\int_0^{\xi} \frac{\bar{Q}_1}{2} \left(\frac{1}{V_0} + \frac{1}{\delta_1} \right) d\xi \right] \\ & + \exp \left[\int_0^{\xi} \frac{\bar{Q}_1}{2} \left(\frac{1}{V_0} + \frac{1}{\delta_1} \right) d\xi \right] \\ & \times \int_0^{\xi} \left\{ \exp \left[-\int_0^{\xi'} \frac{\bar{Q}_1}{2} \left(\frac{1}{V_0} + \frac{1}{\delta_1} \right) d\xi' \right] \left(-\frac{\bar{Q}_1}{V_0} \bar{\xi}_{1\xi'} \right) \right\} d\xi' \end{aligned}$$

The boundary condition requires that $A = 0$.

The choice of $\bar{\xi}_{1\xi}$ should be such that the power series expansion of \bar{V} converges everywhere, i.e., $\frac{\bar{V}_1}{\bar{V}_0}$ should be finite. Hence, we see that if we take $\bar{\xi}_{1\xi} = 0$, the solution would be

$$\bar{V}_1 = 0 \quad (78)$$

also
$$\bar{u}_2 = 0 \quad (79)$$

(65) yields a steady-state equation:

$$\frac{\bar{p}_{2\xi}}{\delta} = -\bar{Q}_1 (2\bar{u}_1 - \bar{u}_{e1}) \quad (80)$$

which gives the result

$$\frac{\bar{p}_2}{\delta} = -\delta \bar{u}_1 (\bar{u}_1 - \bar{u}_{e1}) \quad (81)$$

with the boundary condition $\bar{p}_2(0) = 0$.

The unsteady-state term of (65) is

$$p'_{2\xi} = 0 \quad (82)$$

From (66) and (82), we get

$$\frac{p'_2}{\delta} = \phi(\theta) \quad (83)$$

$$v'_2 = \phi(\theta) + C(\xi) \quad (84)$$

where ϕ is function of θ only and C is function of ξ only and they will be determined by the higher order equations.

We now consider the third order equations:

From (4), we obtain

$$\sigma'_3 \theta + \bar{u}_1 \sigma'_{2\xi} = \bar{Q}_1 \left[\frac{1-\delta}{\delta} p_2 - \sigma_2 - \frac{\delta-1}{2} (2\bar{u}_{e1}\bar{u}_1 - \bar{u}_1^2) \right] \quad (85)$$

the steady-state relation is

$$\bar{\sigma}_{2\xi} + \frac{\bar{Q}_1}{\bar{u}_1} \bar{\sigma}_2 = \bar{Q}_1 \left(\frac{\delta-1}{2} \right) (3\bar{u}_1 - 4\bar{u}_{e1}) \quad (86)$$

With the boundary condition $\bar{\sigma}_2(0) = 0$, the solution is

$$\bar{\sigma}_2 = \frac{\delta-1}{2} (\bar{u}_1 - 2\bar{u}_{e1}) \bar{u}_1 \quad (87)$$

The unsteady-state equation is

$$\bar{\sigma}'_{30} = \bar{Q}_1 \left(\frac{1-\delta}{\delta} \tau_2' - \sigma_2' \right)$$

or

$$\bar{\sigma}'_{30} = \bar{Q}_1 [(1-\delta)\phi - b] \quad (88)$$

From (1), we have

$$\begin{aligned} & \left[\frac{\tau_{30}}{\delta} - \nu_{30} \right] + \left[\bar{u}_{3\xi} - \frac{\bar{Q}_1}{2} \left(\frac{\bar{V}_2}{V_0} + \frac{\bar{u}_3}{\bar{\delta}_1} \right) \right] \\ & = \bar{Q}_1 \left[\frac{5(\delta+1)}{4} \bar{u}_1^2 - \frac{3\delta}{2} \bar{u}_1 \bar{u}_{e1} - \bar{\xi}_{2\xi} \right] \\ & + \bar{Q}_1 \left[\frac{1-2\delta}{2} \phi - \frac{1}{2} b + \frac{1}{2} \left(\frac{V_2'}{V_0} \right) + \frac{1}{4} \left(\frac{\phi+c}{\bar{\delta}_1} \right)^2 \right] \end{aligned} \quad (89)$$

after substitution of the results from the first and second order solutions.

The steady-state equation is

$$\begin{aligned} & \bar{u}_{3\xi} - \frac{\bar{Q}_1}{2} \left(\frac{\bar{V}_2}{V_0} + \frac{\bar{u}_3}{\bar{\delta}_1} \right) \\ & = \bar{Q}_1 \left[\frac{5(\delta+1)}{4} \bar{u}_1^2 - \frac{3\delta}{2} \bar{u}_1 \bar{u}_{e1} - \bar{\xi}_{2\xi} \right] \end{aligned} \quad (90)$$

and the unsteady-state equation is

$$\frac{p'_{30}}{\delta} - v'_{30} = \bar{Q}_1 \left[\frac{1-2\delta}{2} \phi - \frac{b}{2} + \frac{1}{2} \left(\frac{V'_2}{V_0} \right) + \frac{1}{4} \left(\frac{\phi+c}{\delta} \right)^2 \right] \quad (91)$$

We obtain the following equation from (2)

$$\frac{1}{\delta} (p'_{33} + p'_{20} \theta_{13}) + \bar{Q}_1 \xi_{20} = 0 \quad (92)$$

The steady-state part is

$$\bar{p}_{33} = 0 \quad (93)$$

which gives

$$\bar{p}_3 = 0 \quad (94)$$

because of the boundary condition.

The unsteady-state equation is

$$\frac{p'_{33}}{\delta} + \phi_0 \theta_{13} + \bar{Q}_1 \xi_{20} = 0 \quad (95)$$

From (11), we have

$$\begin{aligned} & \left[(V'_{30} - \bar{Q}_1 \xi_{30}) + \bar{u}_{e1} V'_{23} \right] \\ & + \bar{u}_{e1} \left[\bar{V}_{23} + \frac{\bar{Q}_1}{2} \left(\frac{\bar{V}_2}{V_0} + \frac{\bar{u}_3}{\delta_1} \right) \right] \\ & = -\bar{u}_{e1} \bar{Q}_1 \left\{ -\frac{\delta+1}{4} \bar{u}_1^2 + \frac{\delta}{2} \bar{u}_{e1} \bar{u}_1 - \bar{\xi}_{23} \right\} \\ & - \bar{u}_{e1} \bar{Q}_1 \left\{ -\frac{1}{2} (b-\phi) + \frac{1}{2} \frac{V'_2}{V_0} + \frac{1}{4} \left(\frac{\phi+c}{\delta} \right)^2 - \xi'_{23} \right\} \end{aligned} \quad (96)$$

The steady-state equation:

$$\begin{aligned} \bar{V}_{2\xi} + \frac{\bar{Q}_1}{2} \left(\frac{\bar{V}_2}{V_0} + \frac{\bar{u}_3}{\delta_1} \right) \\ = -\bar{Q}_1 \left\{ -\frac{\delta+1}{4} \bar{u}_1^2 + \frac{\delta}{2} \bar{u}_e \bar{u}_1 - \bar{\xi}_{2\xi} \right\} \end{aligned} \quad (97)$$

and the unsteady-state

$$\begin{aligned} (V_{30}' - \bar{Q}_1 \xi_{30}) + \bar{u}_e V_{2\xi}' \\ = -\bar{u}_e \bar{Q}_1 \left\{ -\frac{1}{2} (b-\phi) + \frac{1}{2} \left(\frac{V_3'}{V_0} \right) + \frac{1}{4} \left(\frac{\phi+c}{\delta_1} \right)^2 \right. \\ \left. - \xi_{2\xi}' \right\} \end{aligned} \quad (98)$$

We add (90) and (97) together and use the boundary condition that $\bar{V}_2(0) = 0$ and $\bar{u}_3(0) = 0$, we obtain

$$\bar{u}_3 + \bar{V}_2 = \left(\frac{\delta+1}{2} \bar{u}_1 - \delta \bar{u}_e \right) \bar{u}_1^2 \quad (99)$$

Substituting this result into (96) and (97), we have the following two equations:

$$\begin{aligned} \left(\frac{\bar{u}_3}{\delta_1} \right)_{\xi} + \frac{\bar{Q}_1}{2} \left(\frac{1}{V_0} + \frac{1}{\delta_1} \right) \left(\frac{\bar{u}_3}{\delta_1} \right) \\ = \frac{\bar{Q}_1}{\delta_1} \left\{ \left(3 + \frac{\bar{u}_1}{V_0} \right) \left(-\frac{\delta+1}{4} \bar{u}_1^2 - \frac{\delta}{2} \bar{u}_e \bar{u}_1 \right) \right. \\ \left. + \frac{\delta+1}{2} \bar{u}_1^2 - \bar{\xi}_{2\xi} \right\} \end{aligned} \quad (100)$$

$$\begin{aligned} \left(\frac{\bar{V}_2}{V_0} \right)_{\xi} - \frac{\bar{Q}_1}{2} \left(\frac{1}{V_0} + \frac{1}{\delta_1} \right) \left(\frac{\bar{V}_2}{V_0} \right) \\ = -\frac{\bar{Q}_1}{V_0} \left\{ \left(1 - \frac{\bar{u}_1}{\delta_1} \right) \left(-\frac{\delta}{2} \bar{u}_e \bar{u}_1 - \frac{\delta+1}{4} \bar{u}_1^2 \right) \right. \\ \left. - \bar{\xi}_{2\xi} \right\} \end{aligned} \quad (101)$$

The solutions of these two equations present some difficulties here because of the singularities at $\bar{\xi}_1 = 0$ and $\bar{V}_0 = 0$. By taking $\bar{\xi}_2 = 0$ (no stretching), straight forward integration yields the results that $\frac{\bar{V}_2}{\bar{V}_0}$ and $\frac{\bar{U}_3}{\bar{\xi}_1}$ tend to infinity at the singular points and this is not acceptable because the requirement for the validity of series expansions, $\frac{\bar{V}_2}{\bar{V}_0}$ and $\frac{\bar{U}_3}{\bar{\xi}_1}$ should be finite everywhere. Also the singularities are the causes of difficulties to solve the unsteady equations. Although no final results can be concluded at the moment, we have been able to show the correct approach to this problem. It is believed that the technique or ordering in this article can be extended to other similar situations. Work has been progressing and will be completed soon.

REFERENCES

1. Crocco, L., Harrje, D.T., Sirignano, W.A., et al, "Nonlinear Aspects of Combustion Instability in Liquid Propellant Rocket Motors", Department of Aerospace and Mechanical Sciences Report 553-g, 1 June 1967.
2. Ibid, Report 553-f, 1 June 1966.
3. Ibid, Report 553-e, 1 June 1965.
4. Ibid, Report 553-d, 1 June 1964.
5. Crocco, L., and Cheng, S.I., Theory of Combustion Instability in Liquid Propellant Rocket Motors, AGARD Monograph No. 8, Butterworths Scientific Pub., Ltd., London, 1956.
6. Crocco, L., "Theoretical Studies on Liquid Propellant Rocket Instability", 10th Symposium (International) on Combustion, Combustion Institute, Pittsburgh, Penn., June 1965, pg. 1101.
7. Mitchell, C.E., "Axial Mode Shock Wave Combustion Instability in Liquid Propellant Rocket Engines", Department of Aerospace and Mechanical Sciences Technical Report No. 798, July 1967, (Ph.D. Thesis) (NASA CR 72259).
8. Zimm, B.T., "A Theoretical Study of Nonlinear Transverse Combustion Instability in Liquid Propellant Rocket Motors", Technical Report No. 732, Department of Aerospace and Mechanical Sciences, Princeton University, May 1966 (Ph.D. Thesis).
9. Sirignano, W.A., "A Theoretical Study of Nonlinear Combustion Instability: Longitudinal Mode", Technical Report No. 677, Department of Aerospace and Mechanical Sciences, Princeton University, March 1964, (Ph.D. Thesis).
10. Strahle, W.C., "A Theoretical Study of Unsteady Droplet Burning: Transients and Periodic Solutions", Princeton University Aeronautical Engineering Laboratory Report No. 671, December 1963. (Ph.D. Thesis)
11. Reardon, F.H., "An Investigation of Transverse Mode Combustion Instability in Liquid Propellant Rocket Motors", Princeton University Aeronautical Engineering Report No. 550, 1 June 1961. (Ph.D. Thesis)
12. Crocco, L., Grey, J., and Harrje, D.T., "Theory of Liquid Propellant Rocket Combustion Instability and its Experimental Verification", ARS Journal, Vol. 30, No. 2, February 1960, pp. 159-168.
13. Crocco, L., Harrje, D.T., Reardon, F.H., and Strahle, W.C., "Combustion Instability in Liquid Propellant Rocket Motors", (Thirty-fifth Progress Report), Princeton University Aeronautical Engineering Report No. 216-ii, June 1961.

REFERENCES - continued

14. Harrje, D.T., "Heat Transfer in Oscillating Flow - Final Report", Princeton University Department of Aerospace and Mechanical Sciences Report 483-g, 15 October 1967.
15. Clayton, R.M. and Rogero, R.S., "Experimental Measurements on a Rotating Detonation-Like Wave Observed During Liquid Rocket Resonant Combustion", Jet Propulsion Laboratory Technical Report No. 32-788, 15 August 1965.
16. Prandtl, L., Essentials of Fluid Dynamics, Blackie and Son, London 1953, p. 54.
17. "Special Considerations for Combustion Instability Instrumentation and Data Representation", CPIA Publication No. 170, June 1968.
18. Nicholls, J.A., Debra, E.K., Ragland, K.W., Ranger, A.A., "Two Phase Detonations and Drop Shattering Studies", University of Michigan NASA CR 72225, April 1967.
19. Bowman, C.T., "Experimental Investigation of High-Frequency Longitudinal Combustion Instability in Gaseous Propellant Rocket Motors", AFOSR Report No. 66-2725 (Princeton University Department of Aerospace and Mechanical Sciences Technical Report 784), January 1967.
20. Crocco, L, Harrje, D.T., Reardon, F.H., "Transverse Combustion Instability in Liquid Propellant Rocket Motors, ARS Journal, Vol. 32, pg. 366, March 1962.
21. Branch, M., Undergraduate thesis performed on the flow reactor at Princeton during 1965 (unpublished).
22. Crocco, L., "Research on Combustion Instability in Liquid Propellant Rocket Motors", 12th International Combustion Symposium, Poitiers, France, July 1968 (to be published).
23. Priem, R.J. and Heidmann, M.F., "Propellant Vaporization as a Design Criterion for Rocket-Engine Combustion Chambers", NASA TR R-67, 1960.
24. Crocco, L., "Nonlinear Transversal Instability in a Thin Annular Chamber" (to be published).
25. Crocco, L., "Nonlinear Combustion Instability with Simplified Droplet Evaporation Model" (to be published).

DISTRIBUTION FOR THIS REPORT

NASA

NASA Headquarters
Washington, D.C. 20546
Attn: Mr. A. Gessow
Attn: Dr. R.S. Levine RPL (3)
Attn: Mr. A.O. Tischler RP

NASA
Universal North Building
Connecticut & Florida Avenues
Washington, D.C.
Attn: Dr. T.L. Smull, Director
Grants & Space Contracts (10)

NASA Scientific & Technical
Information Facility
P.O. Box 33
College Park, Maryland 20740 (15)

NASA Headquarters
Washington, D.C. 20546
Attn: Mr. E.L. Gray, Director
Advanced Manned Missions, MT
Office of Manned Space Flight

Attn: Mr. V.L. Johnson, Director
Launch Vehicles & Propulsion, SV
Office of Space Science

Ames Research Center
Moffett Field
California 94035
Attn: Technical Librarian

Goddard Space Flight Center
Greenbelt, Maryland 20771
Attn: Technical Librarian

Jet Propulsion Laboratory
California Institute of Technology
4800 Oak Grove Drive
Pasadena, California 91103
Attn: Mr. J.H. Rupe
Attn: Technical Librarian

John F. Kennedy Space Center, NASA
Cocoa Beach, Florida 32931
Attn: Technical Librarian

Langley Research Center
Langley Station
Hampton, Virginia 23365
Attn: Technical Librarian

NASA
Lewis Research Center
21000 Brookpark Road
Cleveland, Ohio 44135
Attn: Mr. M.F. Heidmann
(Technical Monitor)
Attn: Dr. R.J. Priem
Attn: Mr. E.W. Conrad
Attn: Report Control
Attn: Technical Librarian

NASA
Manned Spacecraft Center
Houston, Texas 77058
Attn: Tech. Info. Library Code BM6

Marshall Space Flight Center
R-P&VED
Huntsville, Alabama 35812
Attn: Mr. J. Thomson
Attn: Mr. R.J. Richmond
Attn: Technical Librarian

GOVERNMENT INSTALLATIONS

Headquarters, U.S. Air Force
Washington 25, D.C.
Attn: Technical Librarian

Aeronautical Systems Division
Air Force Systems Command
Wright-Patterson Air Force Base
Dayton, Ohio 45433
Attn: Technical Librarian

Air Force Missile Test Center
Patrick Air Force Base
Florida
Attn: Technical Librarian

AFOSR-Propulsion Division
1400 Wilson Boulevard
Arlington, Virginia 22209
Attn: Dr. B.T. Wolfson

Air Force Rocket Propulsion Laboratory
Research & Technology Division
Air Force Systems Command
Edwards, California 93523
Attn: Mr. R.R. Weiss, RPRR
Attn: Mr. B.R. Bornhorst
Attn: Technical Librarian

SAMSO (SMSDI-STINFO)
AF Unit Post Office
Los Angeles, California 90045
Attn: Technical Librarian

ARL (ARC)
Building 450
Wright-Patterson Air Force Base
Dayton, Ohio
Attn: Dr. K. Scheller

Arnold Engineering Development Center
Arnold Air Force Station
Tullahoma, Tennessee
Attn: Technical Librarian

Department of the Navy
Bureau of Naval Weapons
Washington, D.C. 20360
Attn: Technical Librarian

Department of the Navy
Office of Naval Research
Washington, D.C. 20360
Attn: Mr. R.D. Jackel

Defense Documentation Center Headquarters
Cameron Station, Building 5
5010 Duke Street
Alexandria, Virginia 22314
Attn: TISIA

Naval Ordnance Station
Research & Development Dept.
Indian Head, Maryland 20640
Attn: Dr. L.A. Dickinson

Picatinny Arsenal
Dover, New Jersey 07801
Attn: Mr. E. Jenkins
Attn: Technical Librarian

Redstone Scientific Information
Building 4484
Redstone Arsenal
Huntsville, Alabama
Attn: Technical Librarian

RTNT
Bolling Field
Washington, D.C. 20332
Attn: Dr. L. Green, Jr.

U.S. Army Missile Command
Redstone Arsenal
Huntsville
Alabama 35809
Attn: Mr. J. Connaughton
Attn: Technical Librarian

U.S. Atomic Energy Commission
Technical Information Services
Box 62
Oak Ridge, Tennessee
Attn: Technical Librarian

U.S. Naval Ordnance Test Station
China Lake
California 93557
Attn: Mr. T. Inouye
Attn: Technical Librarian

CPIA

Chemical Propulsion Information Agency
Applied Physics Laboratory
The John Hopkins University
8621 Georgia Avenue
Silver Spring, Maryland 20910
Attn: Mr. T.W. Christian
Attn: Technical Librarian

INDUSTRY CONTRACTORS

Aerojet-General Corporation
P.O. Box 296
Azusa, California 91702
Attn: Dr. R.J. Hefner
Attn: Technical Librarian

Aerojet-General Corporation
P.O. Box 1947
Sacramento, California 95809
Attn: Mr. J.M. McBride
Attn: Technical Librarian
Bldg. 2015, Dept. 2410

Aeronutronic
Philco Corporation
Ford Road
Newport Beach, California 92663
Attn: Technical Librarian

Aerospace Corporation
P.O. Box 95085
Los Angeles, California 90045
Attn: Mr. O.W. Dykema
Attn: Technical Librarian

Astrosystems International, Inc.
1275 Bloomfield Avenue
Fairfield, New Jersey 07007
Attn: Technical Librarian

Atlantic Research Corporation
Edsall Road and Shirley Highway
Alexandria, Virginia 22314
Attn: Technical Librarian

Autonetics
Div. of North American Aviation, Inc.
3370 Miraloma Avenue
Anaheim, California 92803
Attn: Dr. J.C. Chu

Battelle Memorial Institute
505 King Avenue
Columbus 1, Ohio 43201
Attn: Mr. C.E. Day,
Classified Rept. Librarian

Bell Aerosystems Company
P.O. Box 1
Buffalo 5, New York 14240
Attn: Dr. K. Berman
Attn: Mr. J.M. Senneff
Attn: Technical Librarian

Boeing Company
P.O. Box 3707
Seattle, Washington 98124
Attn: Technical Librarian

Bolt, Berenak & Newman, Inc.
Cambridge, Massachusetts
Attn: Dr. I. Dyer

Chrysler Corporation
Missile Division
P.O. Box 2628
Detroit, Michigan 48231
Attn: Technical Librarian

Curtiss-Wright Corporation
Wright Aeronautical Division
Wood-Ridge, New Jersey 07075
Attn: Technical Librarian

Defense Research Corporation
6300 Hollister Avenue
P.O. Box 3587
Santa Barbara, California 93105
Attn: Dr. C.H. Yang

Douglas Aircraft Company
Missile & Space Systems Division
3000 Ocean Park Boulevard
Santa Monica, California 90406
Attn: Technical Librarian

Douglas Aircraft Company
Astropower Laboratory
2121 Paularino
Newport Beach, California 92663
Attn: Technical Librarian

Dynamic Science Corporation
1900 Walker Avenue
Monrovia, California 91016
Attn: Mr. R.J. Hoffman

General Dynamics/Astronautics
Library & Information Services (128-00)
P.O. Box 1128
San Diego, California 92112
Attn: Technical Librarian

General Electric Company
Advanced Engine & Technology Dept.
Cincinnati, Ohio 45215
Attn: Technical Librarian

General Electric Company
Malta Test Station
Ballston Spa, New York 12020
Attn: Dr. A. Graham, Manager
Rocket Engines

General Electric Company
Re-Entry Systems Department
3198 Chestnut Street
Philadelphia, Pennsylvania 19101
Attn: Technical Librarian

Geophysics Corporation of America
Technical Division
Bedford, Massachusetts 01734
Attn: Mr. A.C. Toby

Grumman Aircraft Engineering Corp.
Bethpage
Long Island, New York 11714
Attn: Technical Librarian

Institute for Defense Analyses
RESD
400 Army-Navy Drive
Arlington, Virginia 22202
Attn: Dr. W.C. Strahle

Ling-Temco-Vought Corporation
Astronautics
P.O. Box 5907
Dallas, Texas 75222
Attn: Technical Librarian

Arthur D. Little, Inc.
20 Acorn Park
Cambridge, Massachusetts 02140
Attn: Technical Librarian

Lockheed Missiles & Space Co.
P.O. Box 504
Sunnyvale, California 94088
Attn: Technical Information Center

Lockheed Propulsion Company
P.O. Box 111
Redlands, California 91409
Attn: Technical Librarian

McDonnell Aircraft Corporation
P.O. Box 516
Municipal Airport
St. Louis, Missouri 63166
Attn: Technical Librarian

The Marquardt Corporation
16555 Saticoy Street
Van Nuys, California 91409
Attn: Technical Librarian

Martin Marietta Corporation
Denver Division
P.O. Box 179
Denver, Colorado 80201
Attn: Technical Librarian

Multi-Tech. Inc.
Box 4186 No. Annex
San Fernando, California
Attn: Mr. F.B. Cramer

Northrup Space Laboratories
3401 West Broadway
Hawthorne, California 90250
Attn: Technical Librarian

Rocket Research Corporation
520 South Portland Street
Seattle, Washington 98108
Attn: Technical Librarian

Rocketdyne
Division of North American Aviation
6633 Canoga Avenue
Canoga Park, California 91304
Attn: Mr. R. Fontaine
Attn: Dr. R.B. Lawhead
Attn: Technical Librarian
(Library 586-306)

Space & Information Systems Division
North American Aviation, Inc.
12214 Lakewood Boulevard
Downey, California 90241
Attn: Technical Librarian

Rohm & Haas Company
Redstone Arsenal
Huntsville, Alabama
Attn: Librarian

Stanford Research Institute
333 Ravenswood Avenue
Menlo Park, California 94025
Attn: Dr. G. Marxman

Thiokol Chemical Corporation
Huntsville Division
Huntsville, Alabama
Attn: Technical Librarian

Thiokol Chemical Corporation
Reaction Motors Division
Denville, New Jersey 07834
Attn: Mr. D. Mann
Attn: Technical Librarian

TRW Systems
One Space Park
Redondo Beach, California 90278
Attn: Mr. G.W. Elverum
Attn: Mr. D.H. Lee
Attn: Technical Librarian

United Technology Center
Division of United Aircraft Corporation
P.O. Box 358
Sunnyvale, California 94088
Attn: Mr. R.H. Osborn
Attn: Technical Librarian

Pratt & Whitney Aircraft Company
Division of United Aircraft Corp.
West Palm Beach
Florida
Attn: Mr. G. Lewis

Pratt & Whitney Aircraft Company
Division of United Aircraft Corp.
Engineering, Building 1-F
East Hartford, Connecticut
Attn: Mr. D.H. Utvik

Research Laboratories
Division of United Aircraft Corp.
400 Main Street
East Hartford, Connecticut 06108
Attn: Technical Librarian

Walter Kidde and Company
Aerospace Operations
567 Main Street
Belleville, New Jersey 07109
Attn: Technical Librarian

Warner-Swasey Company
Control Instrument Division
32-16 Downing Street
Flushing, New York 11354
Attn: Dr. R.H. Tourin

UNIVERSITIES

California Institute of Technology
204 Karman Laboratory
Pasadena, California 91109
Attn: Prof. F.E. Culick

Case Institute of Technology
Engineering Division
University Circle
Cleveland, Ohio 44106
Attn: Prof. C.R. Klotz

Dartmouth University
Hanover
New Hampshire 03755
Attn: Prof. P.D. McCormack

Georgia Institute of Technology
Aerospace School
Atlanta 13
Georgia 30332
Attn: Prof. B.T. Zinn
Prof. E.W. Price

Illinois Institute of Technology
10 W. 35th Street
Chicago, Illinois 60616
Attn: Dr. P.T. Torda

The Johns Hopkins University
Applied Physics Laboratory
8621 Georgia Avenue
Silver Spring, Maryland 20910
Attn: Dr. W.G. Berl

Massachusetts Institute of Technology
Cambridge 39
Massachusetts 02139
Attn: Prof. T.Y. Toong
Dept. of Mechanical Engineering
Attn: Gail E. Partridge, Librarian
Engineering Projects Laboratory

New York University
Dept. of Chemical Engineering
New York 53, New York
Attn: Prof. P.F. Winternitz

Ohio State University
Rocket Research Laboratory
Dept. of Aeronautical
and Astronautical Eng.
Columbus 10, Ohio 42310
Attn: Technical Librarian

Polytechnic Institute of Brooklyn
Graduate Center
Route 110
Farmingdale, New York 11735
Attn: Prof. V.D. Agosta

Purdue University
School of Mechanical Engineering
Lafayette, Indiana 47907
Attn: Prof. J.R. Osborn

Sacramento State College
Engineering Division
60000 J. Street
Sacramento, California 95819
Attn: Prof. F.H. Reardon

Sheffield University
Research Laboratories
Harpur Hill
Buxton, Derbyshire
England
Attn: Dr. V.J. Ibberson

University of California
Department of Chemical Engineering
6161 Etcheverry Hall
Berkeley, California 94720
Attn: Prof. A.K. Oppenheim

University of Wisconsin
Dept. of Mechanical Engineering
1513 University Avenue
Madison, Wisconsin 53705
Attn: Prof. P.S. Myers

University of Michigan
Aeronautical & Astronautical Eng. Labs.
Aircraft Propulsion Lab.
North Campus
Ann Arbor, Michigan 48104
Attn: Dr. J.A. Nicholls

Yale University
Dept. of Engineering & Applied Science
Mason Laboratory
400 Temple Street
New Haven, Connecticut
Attn: Prof. B.T. Chu

University of Southern California
Dept. of Mechanical Engineering
University Park
Los Angeles, California 90007
Attn: Prof. M. Gerstein

Colorado State University
Dept. of Mechanical Engineering
Fort Collins, Colorado 80521
Attn: Prof. C.E. Mitchell